Development of Modeling and Optimization Technologies for Vapor Compression Refrigeration Cycle

Zhao Lei

School of Electrical & Electronic Engineering

Nanyang Technological University

2013

Development of Modeling and Optimization Technologies for Vapor Compression Refrigeration Cycle

Zhao Lei

School of Electrical & Electronic Engineering

A thesis submitted to Nanyang Technological University
in partial fulfillment of the requirement for the degree of
Doctor of Philosohpy

2013

Acknowledgments

First and foremost, I would like to express my sincere gratitude to my supervisor, Associate Professor Dr. Cai Wenjian, for his tremendous support, and invaluable guidance throughout the course of my research work.

I wish to thank my wife, for her love, understanding and encouragement. Thanks also to my friends for their presence and help to complete this significant research.

I particularly thank Dr. Ding Xudong and Dr. Yan Jia for their continuous guidance and help that I have received from them throughout the duration of my research

I also thank my colleagues and seniors in the Process Instrumentation Laboratory and the laboratory supervisor, Mr. Yock, for their help during the course of my study.

The work was funded by National Research Foundation of Singapore: NRF2008EWT-CERP002-010. The other project partners are also acknowledged.

Summary

This thesis presents the research results on the new modeling for vapor compression cycle (VCC) based on single layer feed-forward neural network (SLFN) trained with extreme learning machine (ELM), and the development and implementation of a novel optimization approach based on SLFN model. Furthermore, the centralized and decentralized optimization problems of VCC are formulated, the corresponding solution methodology are then developed. The details of these methodologies are as follows:

1. A single hidden layer feed-forward neural network (SLFN) is used to model the VCC, and an optimal system model, associated with cooling load, environment and system operating states, is developed. The SLFN model is then combined with a grid search algorithm to compute the system optimal set points for different cooling loads. Simulation and experiment results show that the SLFN trained with ELM achieves higher prediction accuracy than the ones with the back-propagation and support vector learning machines.

2. The model-based centralized optimization for VCC is developed based on a modified genetic algorithm, which is capable of minimizing the system energy consumption under cooling load, hybrid models and physical constraints, achieving the accurate estimates of the operating states and the global optimal set point.

3. The decentralized methodology is proposed with application to the VCC, by decomposing the complex global optimization of VCC into the local evaporator, condenser and compressor optimizations based on component hybrid models and interactive constraints. The decentralized optimization method is then further simplified to the unconstrained subsystem optimization with gradient based search methods with the result that the time cost can be efficiently reduced compared with the centralized optimization.

The main contribution of this thesis is to propose three systematic approaches in optimizing the vapor compression refrigeration cycle. In practice, these approaches can be chosen accordingly to balance the energy saving and speed requirements. These

approaches offer significant advantages versus traditional VCC control and optimization methods.

Table of Contents

Figure List

Table List

Nomenclatures

A_v	opening percentage of electronic expansion valve
c	coefficients of hybrid models
d	coefficients of cost functions
f	function
F	frequency of compressor
K	penalty
H	enthalpy
$H_{c,fg}$	enthalpy difference of gas and liquid saturated refrigerant in condenser
$H_{c,r,i}$	condenser inlet refrigerant enthalpy
$H_{c,r,o}$	condenser outlet refrigerant enthalpy
$H_{com,r,i}$	compressor inlet refrigerant enthalpy
$H_{com,r,o}$	compressor outlet refrigerant enthalpy
$H_{e,g}$	enthalpy of saturated refrigerant in evaporator
$H_{e,r,i}$	evaporator inlet refrigerant enthalpy
$H_{e,r,o}$	evaporator outlet refrigerant enthalpy
$H_{i,s}$	compressor outlet refrigerant enthalpy under isentropic compression
H_k	Cholesky factorization of Hessian Matrix of the cost function in step k
M	Cholesky factorization of Hessian Matrix of the cost function
$\dot{m}_{c,air}$	air flow rate of condenser
$\dot{m}_{c,air,max}$	upper bound of air flow rate of condenser
$\dot{m}_{c,air,min}$	lower bound of air flow rate of condenser
$\dot{m}_{c,air,nom}$	nominal air flow rate of condenser
$\dot{m}_{e,air}$	air flow rate of evaporator
$\dot{m}_{e,air,max}$	upper bound of air flow rate of evaporator
$\dot{m}_{e,air,min}$	lower bound of air flow rate of evaporator

$\dot{m}_{e,air,nom}$	nominal air flow rate of evaporator
$\dot{m}_r$	refrigerant mass flow rate
$\dot{m}_{r,max}$	maximal refrigerant mass flow rate
$\dot{m}_{r,min}$	minimal refrigerant mass flow rate
P_c	refrigerant saturated pressure in condenser
$P_{c,max}$	maximal condenser saturated pressure allowed
$P_{c,min}$	minimal condenser saturated pressure allowed
P_e	refrigerant saturated pressure in evaporator
$P_{e,max}$	maximal evaporator saturated pressure allowed
$P_{e,min}$	minimal evaporator saturated pressure allowed
$\dot{Q}_c$	heat transfer rate in condenser
$\dot{Q}_e$	heat transfer rate in evaporator
$\dot{Q}_{com}$	heat transfer rate in compressor
$\dot{Q}_{req}$	cooling load requirement
SC	subcool temperature
SH	superheat temperature
$T_{c,air,i}$	condenser inlet air temperature
$T_{c,max}$	maximal refrigerant saturation temperature in condenser
$T_{c,min}$	minimum refrigerant saturation temperature in condenser
$T_{c,r,i}$	condenser inlet refrigerant temperature
$T_{c,r,o}$	condenser outlet refrigerant temperature
$T_{c,sc}$	condenser subcool temperature
$T_{c,r,sat}$	condenser refrigerant saturated temperature
$T_{com,r,i}$	compressor inlet refrigerant temperature
$T_{com,r,o}$	compressor outlet refrigerant temperature

$\boldsymbol{T_{e,air,i}}$	evaporator inlet air temperature
$\boldsymbol{T_{e,r,i}}$	evaporator refrigerant inlet temperature
$\boldsymbol{T_{e,r,o}}$	evaporator refrigerant outlet temperature
$\boldsymbol{T_{e,r,sat}}$	refrigerant saturated temperature in evaporator
$\boldsymbol{T_{e,max}}$	maximal refrigerant saturation temperature in evaporator
$\boldsymbol{T_{e,min}}$	minimal refrigerant saturation temperature in evaporator
$\boldsymbol{T_{e,sh}}$	evaporator superheat temperature
$\boldsymbol{T_{e,max}}$	upper bound of superheat
$\boldsymbol{T_{e,min}}$	lower bound of superheat
$\boldsymbol{\dot{W}_{c,fan}}$	condenser fan power
$\boldsymbol{\dot{W}_{c,fan,nom}}$	condenser fan power when air flow rate is $m_{c,air,nom}$
$\boldsymbol{\dot{W}_{com}}$	electricity power consumption of compressor
$\boldsymbol{\dot{W}_{c,fan}}$	evaporator fan power
$\boldsymbol{\dot{W}_{e,fan,nom}}$	evaporator fan power when air flow rate is $m_{e,air,nom}$
$\boldsymbol{\dot{W}_{total}}$	total power
$\boldsymbol{x}$	state vector of subsystem
$\boldsymbol{\eta_{com}}$	enthalpy delivery efficiency of compressor
$\boldsymbol{\rho}$	inlet refrigerant density
$\boldsymbol{\beta}$	coefficients of energy consumption terms
$\boldsymbol{\gamma}$	updating coefficient of β

Subscripts

air	feature of air
c	condenser
com	compressor
e	evaporator
ev	expansion valve
fan	evaporator or condenser fan

i	inlet
k	number of current cycle
m	mass flow rate
r	refrigerant
o	outlet
$\boldsymbol{\eta}$	enthalpy delivery efficiency

Chapter 1 Introduction

1.1 Overview of vapor compression cycle

It is well known that the primary goal of refrigeration and air-conditioning systems is to move heat from one physical location to another. It is because of such a remarkable characteristic that, nowadays, a large amount of refrigeration and air-conditioning systems have been widely used for food production and distribution, chemical and industry processes, air conditioning for comfort, and special applications [1, 2]. The considerable energy consumption of refrigeration and air-conditioning systems has also attracted a great deal of attentions. For instance, in the warm and non-humid areas of the US, as shown in statistical data, the air conditioners and refrigerators consume about 28% of electrical energy per year. Moreover, in tropical regions of the world, such as Singapore, the electricity consumption of air conditioning systems is more than 52% of the total electric energy generated according to BCA's Green Mark program [3]. Although the electrical VCCs have the advantages of high efficiency and low cost, and are currently dominant among all types of cooling systems in market, how to further reduce the energy consumption in vapor compression refrigeration systems and relieve both energy shortage and global warming effects are still the challenging topics of the engineers and scientists in this area.

A vapor compression cycle has basically four components – Evaporator, Compressor, Condenser, and Expansion Valve, respectively, as shown in Figure 1, that are connected in a closed loop such that the working fluid is continuously circulated in the cycle. Its working principle is briefly stated as follows [1]:

1. Refrigerant starts from state 1, the inlet of the compressor, in gas phase at a low pressure and a low temperature. As the refrigerant exits the compressor at state 2, it is still in gas phase but with high pressure (saturation pressure) and high temperature.

   The superheated vapor refrigerant enters the condenser at state 2, where the heat from the working fluid is transferred to secondary fluid as the secondary fluid has relatively lower temperature. Inside the condenser, the refrigerant is in two phases (liquid mixed with gas). When the refrigerant exits the condenser after transferring

the heat to the secondary fluid, the temperature is below the condensation temperature to ensure the fully liquidated refrigerant.

2. The refrigerant in liquid phase enters the expansion valve at the state 3 where the pressure of the fluid is decreased through the throttling effect of the expansion valve. The sudden decrease in the pressure of the refrigerant causes it to partially evaporate which in turn reduces the saturation temperature. Thus, when the refrigerant exits the valve it is in low pressure, low temperature and two phases (liquid mixed with gas).
3. At state 4, the refrigerant enters the evaporator at low temperature and low pressure condition. Since the refrigerant temperature is lower than the temperature of cold reservoir, the refrigerant completely evaporates at a constant temperature with the help of evaporator fan to increase the heat transfer rate. At the exit of the evaporator, the temperature is slightly above the evaporating temperature for the safe operation of compressor.

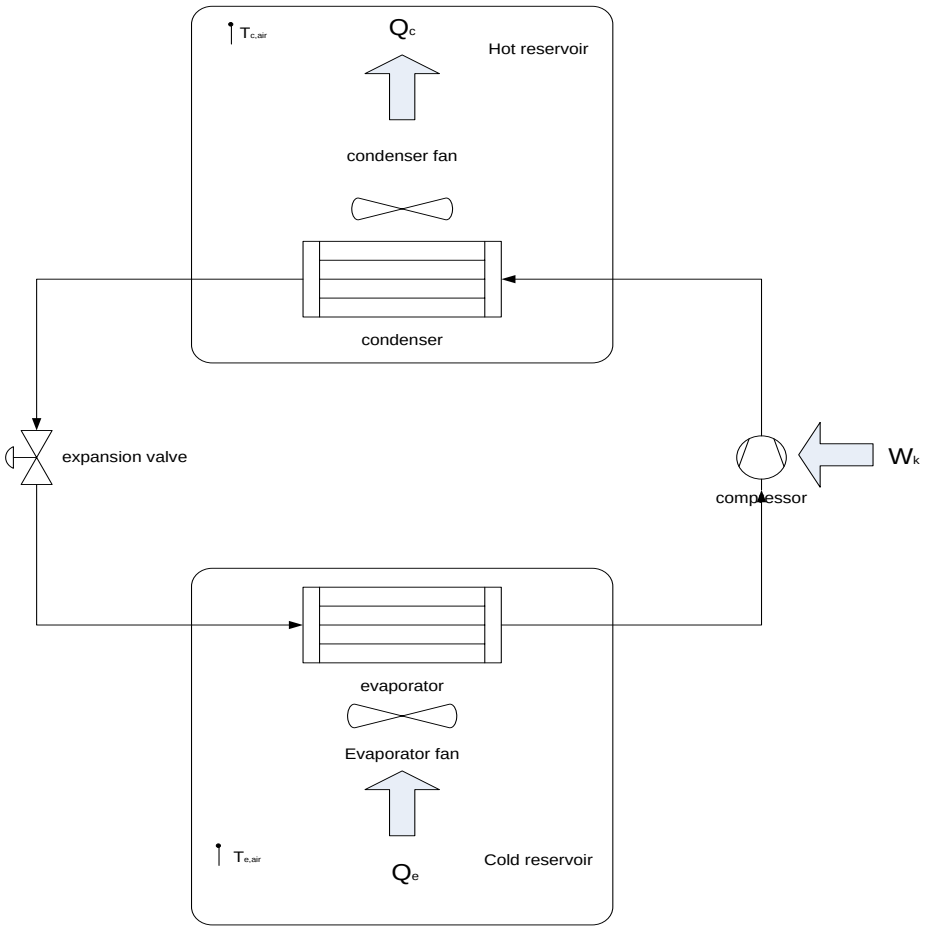

Figure 1 Vapor compression refrigeration cycle

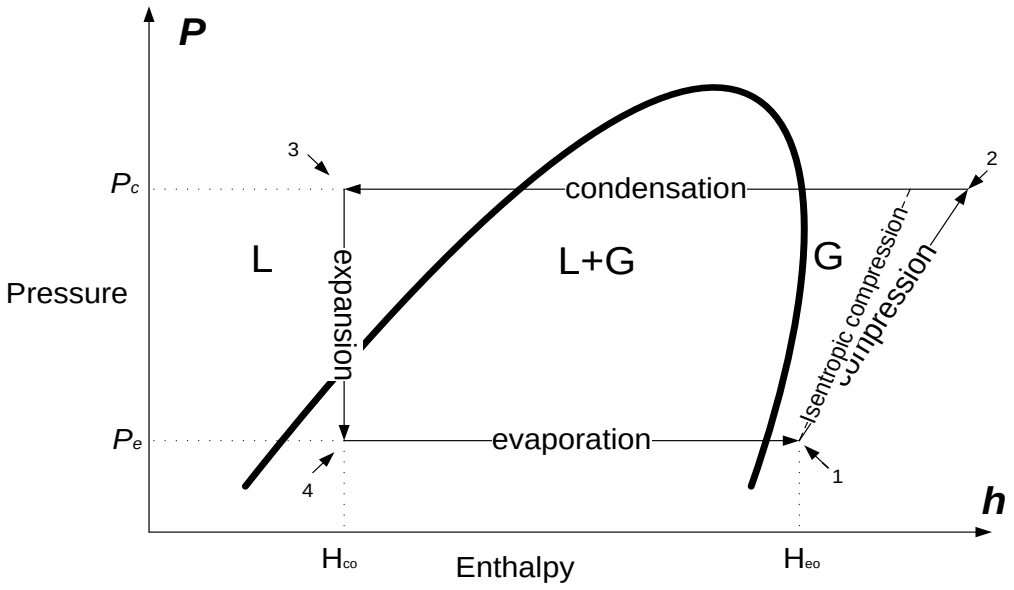

Figure 2 P-h chart of vapor compression cycle

1.2 Motivations and objectives

Singapore is a tropical country with an average annual ambient temperature of 29.40℃ and an average annual ambient relative humidity of 85%. The electricity consumption in building HVAC systems is very high. According to BCA's Green Mark program, more than 52% of the total electric energy of the country is used for running air conditioning systems. Survey data shows that the energy consumption of a middle size commercial building can even reach about 1,000,000 kWh per month. Considering that the current electricity bill in Singapore is around 23 cents per kWh, the energy cost solely for air conditioning is about 230, 000 SGD. It is estimated that, in Singapore, there are more than 10,000 large commercial and industrial buildings that are equipped with central air conditioning systems. Running these systems may cost several million to tens of million dollars per building per year. In an effort to reduce energy costs, currently superheat is usually controlled to the minimal acceptable level to decrease the specific volume of refrigerant, therefore to increase compressor efficiency [4]. Its drawback is that it doesn't consider the energy saving potential of all components and does rely on experience to determine the minimal acceptable superheat and control scheme of compressor and expansion valve. Some classical methods for air conditioning system optimization based on gradient are proposed, however, since system states of vapor compression refrigeration

cycle are severely interacted, these methods usually converge to a local minimum which could be quite far from the global optimal solution. System effective optimization techniques for HVAC (heating, ventilation and air conditioning) based on genetic algorithm have been proposed, but these research focused on the whole system, the vapor compression cycle (named chiller in HVAC system) is simply modeled by a polynomial function, the important components interactions inside the cycle are neglected. Therefore, the optimal designs of VCC is essential for reducing the energy consumption, and the optimization methodologies developed in this thesis for VCCs will significantly advance the research and manufacturing in the area of refrigeration and air-conditioning systems in the near future.

1.3 Major contributions

The major contributions in this study include

- Development of cooling tower hybrid models with fouling effect;
- Development of the optimal SLFN system model with the extreme learning machine;
- Formulation of the centralized optimization methodology for VCCs;
- Development of a genetic algorithm-based centralized optimization algorithm for VCCs with experiment validation;
- Development of a decentralized optimization algorithm for VCC with experiment validation;

1.4 Organization of the thesis

The rest of the thesis is organized as follows: In Chapter 2, the fundamentals of neural networks, the basic training methods, the genetic algorithms, the SLFNs, and the ELM, used for the modeling and optimization of VCCs in this thesis, are briefly presented. Chapter 3 describes the hybrid model of the individual components in air conditioning systems. Chapter 4 develops an optimal SLFN model for VCCs, where the SLFN is trained with the extreme learning machine, and the excellent performance is validated with the experimental data. The energy consumption and system stability are modeled with SLFN trained by ELM for optimization in Chapter 5. In Chapter 6, a centralized

optimization technique based on the genetic algorithm is proposed with the consideration of the system energy consumption and constraints. Chapter 7 focuses on the development of a novel decentralized optimization scheme aiming at performing fast system optimization for VCCs. Chapter 8 gives the conclusion and future work.

Chapter 2 Neural Modeling and Optimization Methods

2.1 Introduction to Neural Networks

2.1.1 Biological neuron

The artificial neural network is originally inspired by the examination of human central nervous system and the neuron that is the basic computational unit in the system. Statistical data show that a human brain consists of 10 billion neurons with interconnections [5].

The biological neuron is shown in Figure 3, which consists of three regions: Dendrites that represents inputs, soma which is the cell body, and axon. Normally the neuron's dendrite tree connects to thousands of surrounding neurons. When the neighboring neuron is stimulated, the corresponding positive or negative charges will reach the neuron's dendrite tree and be received. When the charge level exceeds a critical valve, the neuron will generate an electrical pulse that transmits from cell body to axon, then down to the next neuron [6].

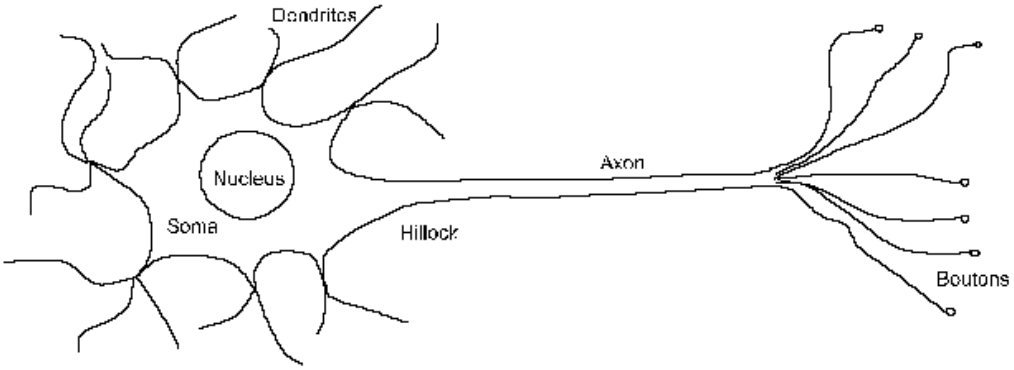

Figure 3 Schematic of biological neuron

2.1.2 Models of an artificial neuron

Similar to the human brain neuron cell, an artificial neuron is the basic unit for information processing in artificial neural network. Two most widely used neuron models are additive neuron and radial basis function (RBF) neuron.

The block diagram for the model of an additive neuron is shown in Figure 4. An additive neuron is made up of three basic elements:

A set of links (or called synapses): Each link (or synapse) is characterized by a weight or strength, which is different from the synapse of human brain, and the weight or strength may lie in a range with both positive and negative values. The synaptic weight w_{kj} means the weight between the input element j and the neuron k.

An adder: The adder is used for calculating the sum of input signals that are weighted by the respective synaptic weights.

An activation function: The function aims to limit the amplitude of the signals from the adder and keeps the output of the neuron in some range. Typically, the normalized amplitude of the output signal of a neuron is in the range of [0, 1] or alternatively [-1, 1].

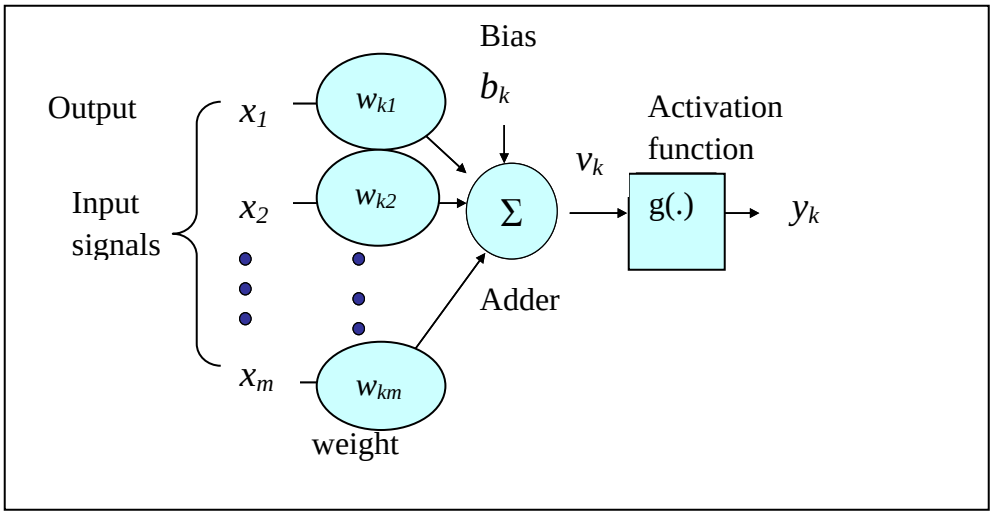

Figure 4 Model of a neuron (Additive neuron)

The mathematical model of artificial neuron is as follows [7]:

$$y_k = g\left(\sum_{j=1}^{m} w_{kj} x_j + b_k\right) \tag{1}$$

where x_j is the input signals; w_{kj} is the weight of connection k; b_k is the bias; $g(.)$ is the activation function; and y_k is the output signal of the neuron k.

Three typical activation functions are as follows:

Threshold function

$$g(x) = \begin{cases} 1 & if\ x \geq 0 \\ 0 & if\ x < 0 \end{cases} \tag{2}$$

Piecewise-Linear function

$$g(x)=\begin{cases}1 & if\ x\geq 1\\ v & if\ 0<x<1\\ 0 & if\ x\leq 0\end{cases} \tag{3}$$

Sigmoid function

$$g(x)=\frac{1}{1+\exp(-ax)} \tag{4}$$

where a is a slope parameter of the sigmoid function.

The block diagram for the model of an RBF neuron is shown in Figure 5. An RBF neuron model consists of three major elements: a set of links, a distance calculator, and activation function. The synaptic weights of the links are usually defaulted as 1. A new parameter called the center of the neuron $\boldsymbol{c}_k$ is introduced in the model. Euclidean distance is taken between the input vector and center of the neuron [8].

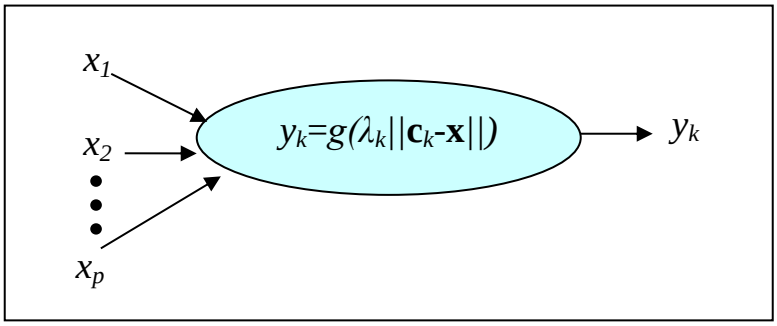

Figure 5 Model of a neuron (RBF neuron)

For RBF neurons, the mathematical model is as follows:

$$y_k = g(\lambda_k \,\|\, \mathbf{c}_k - \mathbf{x} \,\|) \tag{5}$$

where $\mathbf{x}$ is the input vector; $\boldsymbol{c_k}$ is the center vector of RBF neuron k; $g(.)$ is the activation function; and y_k is the output signal of the neuron k.

Several commonly activation functions for RBF neuron are listed as follows:

$$
\begin{aligned}
g(\mathbf{x}) &= \exp\left(-\frac{\|\mathbf{c}-\mathbf{x}\|^2}{2\lambda^2}\right); \\
g(\mathbf{x}) &= \sqrt{\|\mathbf{c}-\mathbf{x}\|^2+\lambda^2} \\
g(\mathbf{x}) &= \|\mathbf{c}-\mathbf{x}\|^2 \log(\|\mathbf{c}-\mathbf{x}\|^2); \\
g(\mathbf{x}) &= -\sqrt{\|\mathbf{c}-\mathbf{x}\|^2+\lambda^2}
\end{aligned}
\tag{6}
$$

2.1.3 Network structures

Two fundamental neuron network architectures are presented in this section. In neural networks, there are three basic layers: input layer, hidden layers, and output layer. According to the number of hidden layers, the feed forward neural network can be classified into:

Single-Layer Feedforward Networks

There is only one hidden layer in single-layer feed-forward networks. An illustration for the network is shown in Figure 6.

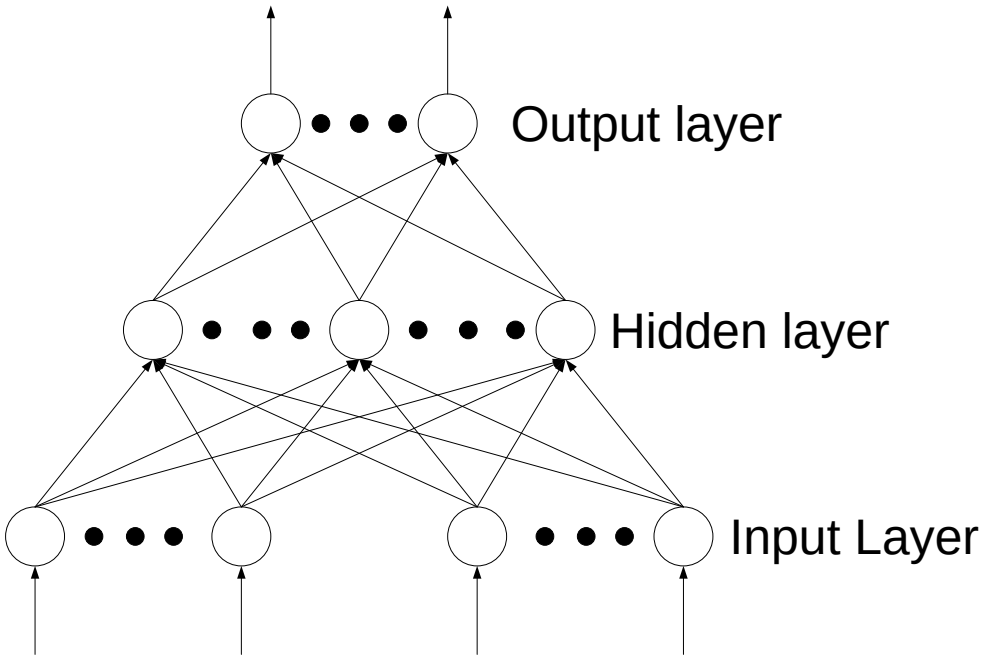

Figure 6 Single Layer Feed-forward Neural Network

Multi-Hidden Layer Neural Networks

The second fundamental neural network architecture has more than one hidden layers. The introduction of more hidden layers aims to provide higher network capacity, which

can manage higher-dimensional nonlinear classification. Signals travel from input layer of source nodes to the first hidden layer, and the output signals of the first hidden layer are used as the input of the second hidden layer, and so on. The output of output layer reflects the overall response of the network by applying the input signals. Figure 7 shows a multi hidden layer feed-forward network.

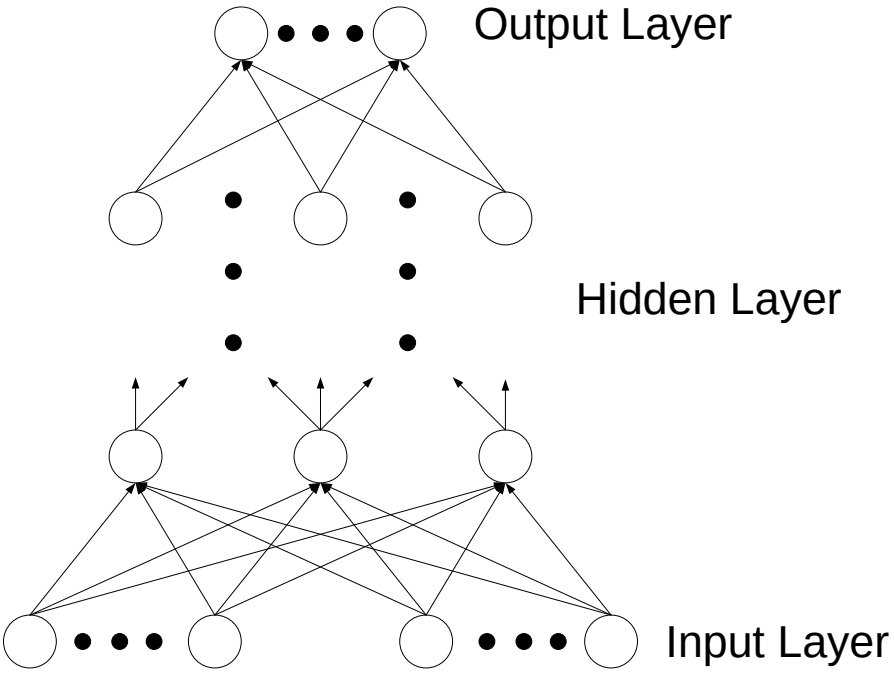

Figure 7 Multilayer Feed-Forward Neural Network

Gradient-descent learning algorithms are commonly used to train the multilayer neural networks in classic neural network theory. Back-propagation (BP) algorithm is one of the most popular algorithms among all the gradient-descent learning algorithms. It is used in supervised learning and based on the error correction learning rule, the learning process can be divided to a forward process and a backward process. In the forward process, input vectors are provided to the input layer of neural networks, inputs propagates through networks layer by layer to the output layer and produces the corresponding outputs. During the backward process, the actual output of the network is compared with the desired output to calculate the error. The weights are adjusted in backward process following the back propagation rule to reduce the error. This process continues until the stop criterion is satisfied.

The squared errors are summed up to generate the cost function of network, then the weights are updated using the formula below [8].

$$\mathbf{W}(n+1) = \mathbf{W}(n) + \eta \triangle \mathbf{E}(n) = \mathbf{W}(n) - \eta \frac{\partial \mathbf{E}(n)}{\partial \mathbf{W}} \tag{7}$$

where the parameter η is learning rate, **W**(n) is the weight vector at the *n*th iteration, and Δ**E**(n) indicates the cost function gradient at the *n*th iteration.

The BP algorithm needs to compute the gradient of cost function repeatedly, so its convergence speed is usually quite slow, especially when the number of hidden neurons is large. Furthermore, BP is highly possible to converge to local minima for nonlinear optimization problem, or the convergence rate may be slow for flat regions, or even never terminate.

2.2 Support Vector Machine (SVM)

The Support Vector Machine (SVM) of statistical learning theory proposed by Vapnik [9, 10] was developed based on the structural risk minimization principle. Nowadays, SVMs and the derived kernel methods attract more and more researchers due to their excellent performance in data mining tasks such as classification, regression, and novelty detection [11].

Basically, a SVM aims at distinguishing different patterns. The main idea under SVM is to construct a hyperplane that maximizes the margin of separation between different classes. In other words, the hyperplane performs as the decision maker that gives the largest distance between two different patterns. The mathematical description of SVM is as follows:

Linearly separable case

For a two-class classification problem, given *m* training pairs $\{(\mathbf{x}_i, t_i)\}_{i=1}^{m}$, where $\mathbf{x}_i \in \mathbf{R}^d$ is an input vector labeled by $t_i \in \{-1, +1\}$ for *i*=1, …, *m*. A decision hyperplane should follow

$$\boldsymbol{w}^T \boldsymbol{x} + b = 0 \tag{8}$$

where **w** is the weight vector and *b* is the bias. The function of the input pattern can be expressed as follows:

$$f(x) = \mathrm{sgn}\left(\boldsymbol{w}^T \boldsymbol{x} + b\right) \tag{9}$$

where

$$\mathrm{sgn}\left(k\right) = \begin{cases} 1 & if \quad k \geq 0 \\ -1 & if \quad k < 0 \end{cases} \tag{10}$$

To maximize the margin for linearly separable case, the problem becomes finding the solution of following optimization problem:

$$\begin{aligned} &\min \frac{1}{2}\|\boldsymbol{w}\|^2 \\ &s.t. \quad t_i\left(w^T x_i + b\right) \geq 1 \quad \forall i = 1, \ldots, m \end{aligned} \tag{11}$$

Linearly non-separable case

For some practical problem, the hyperplane which can successfully classifies the pattern set without error thus no longer exists, these problems are classified as nonseparable. As a result, a soft margin of separation is defined which allows small amount of wrong classification. A non-negative slacking variable set $\{\xi_i\}_{i=1}^m$ is introduced to the inequality. The non-zero $\xi_i > 0$ are those training patterns that do not satisfy the constraints in Eq. (11). The optimal hyper-plane for non-separable problem could be found by solving the quadratic programming problem shown as follows:

$$\begin{aligned} &\min \frac{1}{2}\|\boldsymbol{w}\|^2 + C\sum_{i=1}^{m} \xi_i \\ &s.t. \quad t_i\left(w^T x_i + b\right) \geq 1 - \xi_i \quad \forall i = 1, \ldots, m \\ &\xi_i \geq 0 \end{aligned} \tag{12}$$

The problem is usually posed in its *Wolfe dual form* with respect to Lagrange multipliers $\alpha_i \in [0, C],\ i = 1, ..., m,$ which can be solved by standard quadratic optimization package. The bias b can be easily calculated from any margin vector x_i satisfying $0<\alpha_i<C$. The discriminative function is therefore given by

$$f\left(x\right) = \mathrm{sgn}\left(\boldsymbol{w}^T \boldsymbol{x} + b\right) = \mathrm{sgn}\left(\sum_{i=1}^{m} \alpha_i t_i \boldsymbol{x}_i^T \boldsymbol{x} + b\right) \tag{13}$$

In typical classification task, only a small number of the Lagrange multipliers α_i tends to be greater than zero. The respective training vectors are called *support vectors*, and ***f(*x*)*** depends on them exclusively.

For some problems, nonlinear SVMs can be used to achieve better results[9]. The method can map the input vectors from low to a high dimensional feature space using a nonlinear mapping Φ, this mapping transfer the original problem into a linear separable problem that can be solved using linear SVMs. The nonlinear mapping Φ is performed by employing kernel function *K*, the commonly used kernel functions include the Gaussian kernel $\exp\left(-\|\boldsymbol{x}-\boldsymbol{x}_i\|^2/2\delta^2\right)$ and the polynomial kernel $\left(\boldsymbol{x}^T\boldsymbol{x}_i+1\right)^p$. The corresponding function is

$$f\left(x\right)=\operatorname{sgn}\left(\sum_{i=1}^{m}\alpha_i t_i K\left(\boldsymbol{x}_i^T\boldsymbol{x}\right)+b\right) \tag{14}$$

2.3 The SLFN and ELM

Consider *N* distinct sample data vector pairs $\left(X_i,t_i\right)$ that are the collected measurements from a vapor compression cycle. The *i*th input pattern vector and the desired *i*th output vector are respectively defined as $X_i=\left[x_{i1}\quad x_{i2}\quad\cdots\quad x_{in}\right]^T$ and $t_i=\left[t_{i1}\quad t_{i2}\quad\cdots\quad t_{im}\right]^T$, for $i=1,2,\cdots N$. The structure of SLFN to be used to learn the given input and output pairs is shown in Figure 8[12]:

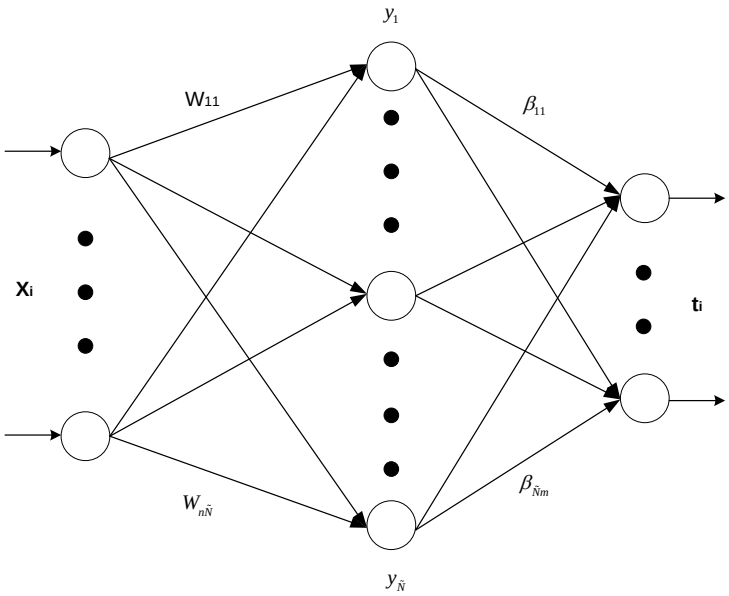

Figure 8 Single hidden layer feedforward neural network

where the nodes in the input and output layer are linear, and the nodes in hidden layer are with the nonlinear activation functions, described by

$$y_{ki} = \varphi(W_k^T x_i) \tag{15}$$

W_k in (15) is the input weight vector to the *k*th hidden neuron, defined as:

$$W_k = \begin{bmatrix} W_{1k} & W_{2k} & \cdots & W_{nk} \end{bmatrix}^T \tag{16}$$

for $k = 1, 2, \cdots \tilde{N}$, and values of the input weights in W_k are all randomly selected based on ELM [13, 14].

The hidden layer output vector Y_i, corresponding the input vector X_i, can then be expressed as:

$$\begin{aligned} Y_i &= \begin{bmatrix} y_{1i} & y_{2i} & \cdots & y_{\tilde{N}i} \end{bmatrix}^T \\ &= \begin{bmatrix} \varphi(W_1^T X_i) & \varphi(W_2^T X_i) & \cdots & \varphi(W_{\tilde{N}}^T X_i) \end{bmatrix}^T \end{aligned} \tag{17}$$

Using (17), the *j*th output of the SLFN can be obtained as:

$$O_{ji} = \sum_{l=1}^{\tilde{N}} \beta_{lj} \varphi(W_l^T X_i) \qquad j = 1, 2, \cdots m \tag{18}$$

and the *i*th output vector of the SLFN is of the form:

$$
\begin{aligned}
O_i &= \begin{bmatrix} O_{1i} & O_{2i} & \cdots & O_{mi} \end{bmatrix}^T \\
&= \left[\sum_{l=1}^{\tilde{N}} \beta_{l1} \varphi(W_l^T X_i) \quad \sum_{l=1}^{\tilde{N}} \beta_{l2} \varphi(W_l^T X_i) \quad \cdots \quad \sum_{l=1}^{\tilde{N}} \beta_{lm} \varphi(W_l^T X_i) \right]^T
\end{aligned} \tag{19}
$$

Then all N output vectors of the SLFN, corresponding to the N distinct input vectors $X_1, X_2 \cdots X_N$, can be written in the following matrix form:

$$
\begin{aligned}
O &= [O_1 \quad O_2 \cdots O_N] \\
&= \begin{bmatrix} \sum_{l=1}^{\tilde{N}} \beta_{l1} \varphi(W_l^T X_1) & \sum_{l=1}^{\tilde{N}} \beta_{l1} \varphi(W_l^T X_2) & \cdots & \sum_{l=1}^{\tilde{N}} \beta_{l1} \varphi(W_l^T X_N) \\ \vdots & \vdots & \cdots & \vdots \\ \sum_{l=1}^{\tilde{N}} \beta_{lm} \varphi(W_l^T X_1) & \sum_{l=1}^{\tilde{N}} \beta_{lm} \varphi(W_l^T X_2) & \cdots & \sum_{l=1}^{\tilde{N}} \beta_{lm} \varphi(W_l^T X_N) \end{bmatrix} \\
&= \begin{bmatrix} \beta_1^T \phi_1 & \beta_1^T \phi_2 & \cdots & \beta_1^T \phi_N \\ \beta_2^T \phi_1 & \beta_2^T \phi_2 & \cdots & \beta_2^T \phi_N \\ \vdots & \vdots & \vdots & \vdots \\ \beta_m^T \phi_1 & \beta_m^T \phi_2 & \cdots & \beta_m^T \phi_N \end{bmatrix} = \beta^T \phi
\end{aligned} \tag{20}
$$

with

$$
\beta_i = \begin{bmatrix} \beta_{1i} & \beta_{2i} & \cdots & \beta_{\tilde{N}i} \end{bmatrix}^T \qquad i = 1, 2, \cdots m \tag{21}
$$

$$
\phi_i = \begin{bmatrix} \varphi(W_1^T X_i) & \varphi(W_2^T X_i) & \cdots & \varphi(W_{\tilde{N}}^T X_i) \end{bmatrix}^T \qquad i = 1, 2, \cdots N \tag{22}
$$

$$
\beta = \begin{bmatrix} \beta_1 & \beta_2 & \cdots & \beta_m \end{bmatrix} \tag{23}
$$

$$
\phi = \begin{bmatrix} \phi_1 & \phi_2 & \cdots & \phi_N \end{bmatrix} \tag{24}
$$

$$
t = \begin{bmatrix} t_1 & t_2 & \cdots & t_N \end{bmatrix} \tag{25}
$$

The matrix H is square and invertible if and only if the number of hidden nodes is equal to the number of distinct training samples and all the training samples are linearly unrelated, the linear independence can be derived from random choice of hidden layer weights, as a result, ELM can approximate these training samples with zero error. However, in practice the number of hidden nodes is usually smaller than training sample number, thus H is non-square. In linear algebra, the smallest norm least squares solution of the above linear system is given by:

$$\hat{\beta} = \phi^{+} t^{T} \tag{26}$$

where ϕ^{+} is the Moore Penrose generalized inverse of matrix H [15]. The definition of the Moore–Penrose generalized inverse, its definition and characteristics are given in Appendix C:

According to the discussion above, the algorithm ELM are as following:

Given a training set and hidden node number,

Step 1 Randomly generate weights and bias of hidden nodes

Step 2 Calculate the hidden layer output matrix based on step 1

Step 3 Calculate the output weight based on Eq. (27):

$$\beta = \phi^{+} t^{T} \tag{27}$$

2.4 Genetic Algorithm

Genetic algorithms (also called evolutionary algorithm) are adaptive heuristic search method which finds solutions for problems within a defined search space. The genetic algorithm was first proposed by Holland [16] and consolidated and developed by Goldberg[17, 18]. It has been widely studied and used in the fields of engineering and management for complex problems such as planning and automatic programming.

The terminology used in genetic algorithm is explained as following.

Chromosome: Chromosome matrix consists of the variables to be modified in the program. They are represented in gray code in a specified number of bits. All the variables are included in a single row of the matrix. Each row indicates a new individual of the population.

Population: Chromosome matrix is called a population. Defined by the user, in fact, it indicates the number of rows of the chromosome matrix.

Variables in chromosome: These are the variables that can be changed, i.e. manipulated by the user, which affects the fitness function/ objective function of a system. One row of the chromosome matrix contains the binary value (in gray code) of all the variables.

Characteristics of Genetic Algorithms

a. Genetic algorithms can handle highly non-linear complex set of equations and constraints also. The reason is that the algorithm does not try to solve the equations to find the variables. Instead it searches the entire variable range, evaluates the equations, calculates the fitness values, and decides on the variable value with the maximum fitness value as the optimum solution. All this is done without disobeying the constraints.
b. GA is simple and easy to implement and provides a fast robust solution over a wide and probably unclear search space for difficult high-dimensional problems.
c. Genetic algorithms can tend to settle to a local optimum value. This can be avoided by increasing the mutation rate, so that solutions outside the local range will also be considered.
d. For a dynamic set of equations e.g. dynamic constraints, the result of the algorithm might not be optimal if it is not rapid enough to adapt to the changing equations.
e. For the optimization of vapor compression cycle, GA would suffice. For the complexity of the equations involved, GA would serve the purpose of finding an optimal solution without much difficulty.

A basic genetic algorithm can be explained as a series of steps using the genetic operators, which searches for an optimal value of an objective within the search space specified. Before describing the evolutionary process, the initialization of genetic algorithm is as follows.

Initialization and Encoding

The potential solution of an optimization problem is an individual which can be represented by a set of variables or chromosomes. A chromosome is a binary string of variable values as defined earlier.

Binary string encoding [19] is used for its simplicity. But the use of Gray coding is preferred for overcoming the hidden representative bias in binary representation. The hamming distance between adjacent values in Gray coding is always constant. For example,

Table 1 Comparison of Binary and Gray Code

Real value	0	1	2	3	4	5	6	7	8

Binary	0000	0001	0010	0011	0100	0101	0110	0111	1000
Gray code	0000	0001	0011	0010	0110	0111	0101	0100	1100

Table 1 shows that binary coding of real numbers is in a regular sequence. Gray coding is such that adjacent real values differ by only one bit in the gray code interpretation.

A random of population of chromosomes, is generated such that, when decoded to real values, the variable values lie within their limitations. The whole generation should possibly try to include the entire range of values.

Objective Function and Fitness Function

From this population an initial objective function is created, which indicates the fitness of the individuals in the population array. This is the most important connection between genetic algorithm and its practical optimization application. For minimization, the individual with the lowest numerical value of objective function is fitter. The fitness function is used to transform the objective function into a linear array of individuals with varying rankings. Mathematically,

$$Fit(x) = g(f(x)) \tag{28}$$

where, *f(x)* is the objective function, and *Fit(x)* is the fitness function. *g(.)* operator transforms the objective function to fitness function.

For transformation, linear ranking method with selective pressure of 2 can be used. The Selective pressure denotes the rank range of each individual in the population. Linear ranking denotes that if the population has *N* elements, then the rank is equally distributed from 0-2, for *N* elements.

$$\begin{aligned} &for\ i\ =\ 0\ to\ N,? \\ &Rank(i)\ =\ 2*i/(N-1) \\ &end \end{aligned}$$

Each element in *Rank* differs from the successor element by a value of *(Selective Pressure*(1/N-1))*. The first element in the array *Rank* is 0, and the last element is 2(for a selective pressure of 2). The lower ranks are assigned to higher objective valued individuals and higher ranks to lower objective valued individuals.

Genetic Algorithm Methodology and Flowchart

The evolutionary process of GA for a population with corresponding fitness values is described as below.

Selection: Selection is the process of estimating the number of times an individual is selected as a proportion of the whole population according to the respective fitness value. The ratio of amount of individuals that have to be selected from the parent generation is called as Generation Gap.

The genetic operator in the scope of this thesis is the Roulette wheel selection. In this type of selection, individuals with higher fitness value have more probability of getting selected than individuals with low fitness value. This method can be explained with an example as shown in Figure 9. A random number is generated using the outer circle sector. The number generated should be from 1 to 16. Similarly, the inner circle consists of the individuals (*N* elements from *I1* to *I6*) of the population such that, the fitter individuals will get a proportionally greater portion of the inner circle. This does not rule out the weaker individuals or chromosomes, which get smaller quantities of the circle than the stronger individuals. The number generated randomly is matched to the sector of the inner circle on which it falls; thus the corresponding individual is selected.

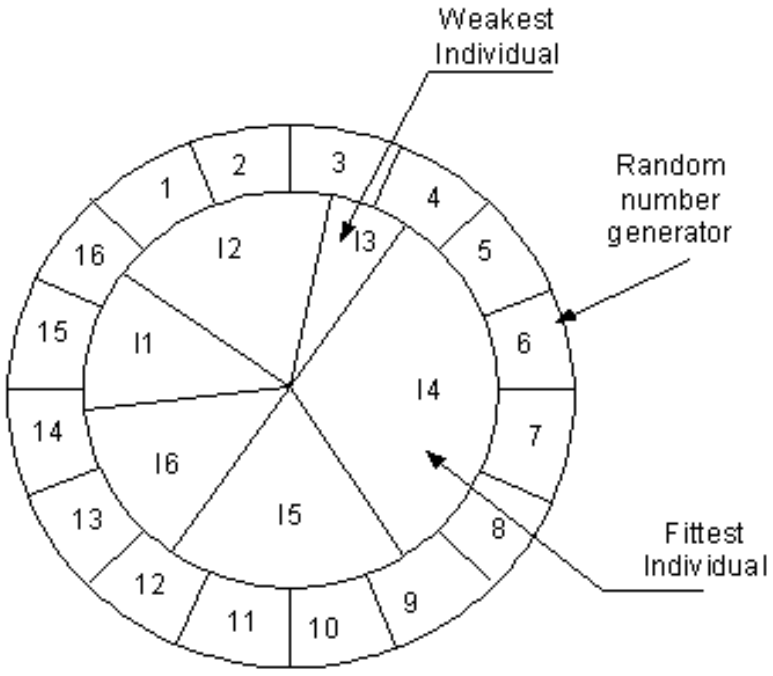

Figure 9 Example of Roulette Wheel Selection

Reproduction (Crossover): From the selected population, a new population of same size is generated, so that some characteristics of the parent population are absorbed by the new generation. The new population will try to converge in the range where the fitness values will be higher. The types of crossover that are generally used are one-point, two-point and uniform crossover[17]. An example of 2-point crossover is shown in Table 2 for individuals with length of 12. The crossover points are at the 5^{th} bit and the 8^{th} bit. Thus the string in-between is exchanged between the two parents to form new in dividuals (child 1 and child 2).

Table 2 Example of two point crossover

Parent 1	0000 0101 1001
Parent 2	0010 1100 0111
Child 1	0000 1100 1001
Child 2	0010 0101 0111

Mutation: To avoid the algorithm to get trapped in a local optimum value, this step is required to be performed on the population. A completely random change is made in the new population, so that a very small percentage of the individuals are mutated. The individual should be totally different than its previous form and preferably not in the range of values that the current population set is in.

The mutation process can be done by changing any bit in the individual of the parent generation. For more complex types of mutation, random binary values can be added to very few individuals from the parent population. An example of the simpler type of mutation can be shown as,

Parent individual: 0 0 1 1 1 1 0 0 (Mutation at 6^{th} bit in parent individual)

New individual: 0 0 0 1 1 1 0 0

The bit which has to be mutated is randomly selected throughout the chromosomes. If the amount of individuals that are mutated is higher, the probability of converging to an optimal value of fitness function becomes lesser, because the mutation probability

increases the chances of destroying a fit individual. The mutation probability has to be kept at an optimal low value so as to make the population diverse while not destroying good individuals [20].

Reinsertion: In this step, fitness values of the new population (offspring) after reproduction and mutation are calculated. Based on the fitness values, the offspring are then reinserted into parent population such that, they replace the weaker individuals in the parent population.

Termination: The termination of genetic algorithm can be done in two ways.

1) If the population converges to a minimum value, and stays near the minimum value for a predefined number of iterations, the genetic algorithm can be terminated.
2) If the maximum generation number is reached.

2.5 Summary

The basics of neural networks, supporting vector machine, SLFN, extreme learning machine, and genetic algorithm to be used for the modeling and optimization of VCCs have been briefly studied in this chapter. It will be seen later that all of these intelligent methods are essential for developing the SLFN optimal model and the optimization methodologies for VCCs. Also, the detailed discussions on the application of these new neural model and optimization techniques to air conditioning systems will be explored in next few chapters.

Chapter 3 Hybrid Models

3.1 Mathematical modeling of VCC components

The major components of an air conditioning system are compressor, evaporator, condenser and expansion valve, respectively. The operation of each component has significant influence on the system operating states as well as the system energy consumption. Many models have been developed either for the separate components or for the whole systems. It has been noted that, although the modeling of compressors, expansion valves as well as the overall systems has been studied [20-22], the works in this area is mainly focused on the heat exchanger models, such as the distributed models, the NTU models, the black box models, and the hybrid models, respectively.

Distributed models: The heat exchanger is usually divided into a number of segments. Because the segments can be sized according to the required accuracy, the distributed models are capable of providing complete heat exchanger information, such as the refrigerant pressures and temperatures at different locations as well as their dynamic responses. Wang and Touber [23] derived dynamic equations of direct expansion evaporator based on the mass and energy balance functions, where the mass transport in air cooler is computed by using a simple propagation equation. Meanwhile, some advanced computer packages are utilized to solve the momentum one-dimensional two-phase flow for studying the steady state slip effect. An efficient and stable two-level iteration method was proposed in [24] to numerically calculate the model solution with the result that the dynamic behavior of the evaporator with a step change in the inlet refrigerant flowrate is discussed in detail. A further study on the distributed modeling was proposed in [24] that takes account of the non-homogeneous flows of the liquid and vapor in the two-phase evaporating flow region with the cocurrent-flow or counterflow configurations. Furthermore, Tso et.al [25] provided the details of distributed dynamic model that describes the behavior of the frost evaporator, including frost growth variation and densification along the coil at different positions. However, the drawbacks of these distributed models are that the void fraction and two phase flow cannot be accurately described, the iterative computing of the parameters and states with these models is time consuming, and it is very hard to use these models for online optimization.

e-NTU models: Kays and London proposed the concept of e-NTU method in [27] where a scalar parameter, called the heat transfer effectiveness *e*, was first defined, which is the ratio of the amount of the transferred heat to the maximum amount of heat that could be transferred for an infinitely long heat exchanger. Since the number of iterative steps is reduced in the e-NTU models, the heat exchanger analysis is greatly simplified. The e-NTU method was further developed by Browne and Bansal in [26], where an elemental approach is utilized to analyze the heat exchanger and the difference in heat transfer coefficients through the heat exchanger is involved in the analysis with the result that the higher prediction accuracy and better performance are achieved. In [27-31], the e-NTU method was applied to the different types of heat exchangers, such as cooling tower, regenerator and tube in tank, with excellent performance. However, the limitations of the e-NTU in practice are that (i) it is hard to measure the accurate geometric information that is used for determining the product of heat transfer coefficient and air; (ii) it is difficult to use the e-NTU method for online optimization; (iii) as the capacity ratio of the heat exchanger is close to zero, the e-NTU method can nor perform well.

Black-box model: Generally, polynomial functions and artificial intelligent networks are often used to approximate the complex relationship between system states. A heat exchanger can be represented by a set of transfer functions whose coefficients are calculated through fitting experiment data. This approach is particularly useful when the information of heat exchanger is limited or the experiment data is abundant. Xie et.al[32] employed Artificial Neural Network (ANN) to analyze the heat transfer of shell-and-tube heat exchangers, and studied the effect of different network configurations on modeling accuracy. Hao and Xiang [33] applied neural networks to predict the thermal performance as well as Colburn factor and friction factor of different type fin-tube heat exchangers, based on the data obtained under various experimental conditions. Tan et.al [34] employed artificial neural network models to simulate compact heat exchanger thermal performance with water/ethylene glycol mixtures as the working fluids, and also discussed the possibility of using the self-organizing-map for heat exchanger condition monitoring. However, it is noticeable that the prediction accuracy usually degrades when the estimated condition is beyond the training data scope.

Hybrid model: In order to construct a simple yet accurate model for online optimization, Cai et al. in [35, 36] proposed a hybrid modeling approach to model single phase fluid heat exchangers, e.g. cooling coils and cooling towers, the simulation and experiment results verified the model accuracy and robustness. Ding et.al [37, 38] proposed hybrid modeling approach for two-phase flow evaporators and condensers based on the energy and material balance, and thermodynamic principles to formulate the process fundamental governing equations. The hybrid model takes advantages of both physical and empirical modeling approaches as it is based on material characteristics and thermodynamic principles, while using experiment data to fit the coefficients which are hard to measure directly. Specifically, a hybrid model can be constructed as follows: (i) Determining the energy and material balance relations, and thermodynamic principles of heat exchanger to formulate the process fundamental governing equations in another format; (ii) Selecting the measureable and controllable input/output variables that influence system performance significantly; (iii) Representing the unmeasureable variables in the original equations with constants of variables in step (2); (iv) Deriving a single equation which uncovers inputs and outputs relations; and (v) Identifying the approximated constants by curve fitting method based on experiment data. In this thesis, we will extend this technique to develop a hybrid model for cooling towers with fouling effect.

3.2 Evaporators

An evaporation process mainly consists of an expansion valve and an evaporator, its schematic is shown as in Figure 10, including two loops: the working fluid loop and the secondary fluid loop.

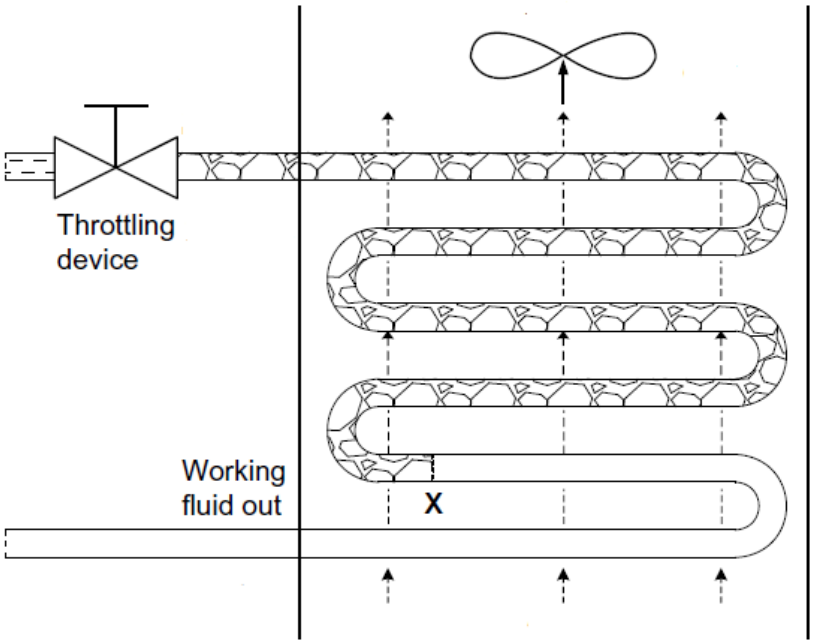

Figure 10 Schematic of evaporation process

The working principle of evaporation has been introduced in Chapter 1. Based on mass and energy balance, a simple hybrid model to describe the heat transfer properties in evaporator is given as [37]

$$\dot{Q}_e = \frac{\left(H_{e,g} - H_{e,r,i}\right)\dot{m}_r + c_{e,1}\dot{m}_r^{c_{e,3}}\left(T_{e,air,i} - T_{e,r,sat}\right)}{1 + c_{e,2}\left(\frac{\dot{m}_r}{\dot{m}_{e,air}}\right)^{c_{e,3}}} \tag{29}$$

where $c_{e,1}$,$c_{e,2}$ and $c_{e,3}$ are constants obtained by catalog or experiment data, $H_{e,g}$, $H_{e,r,i}$, $\dot{m}_r$, $\dot{m}_{e,air}$, $T_{e,air,i}$, $T_{e,r,sat}$ and $\dot{Q}_e$ are the enthalpy of saturated gas phase refrigerant in evaporator, refrigerant enthalpy at evaporator inlet, refrigerant mass flow rate, air outside evaporator, temperature of inlet air and saturated refrigerant of evaporator, heat exchanging rate of evaporator, respectively (see Appendix A for the calculations of $H_{e,g}$, $H_{e,r,i}$ and $T_{e,r,sat}$). This hybrid model of evaporator will be applied to centralized optimization.

In Eq. (29), the fluid property factors and evaporator geometric factors are lumped into the coefficients, the specific relations are

$$c_{e,1} = b_{r,sh}A_{sh} \tag{30}$$

$$c_{e,2} = \frac{b_{r,sh} A_{sh}}{b_{a,dp} A_{dp}} \tag{31}$$

and *e* is the power of Reynold number in Dittus-Boelter equation.

The rule of thumb value $c_{e,3}$ = 0.8 is often adopted in practice. If it is reckoned as unknown, The system identification problem can be solved with the nonlinear least-squares method, widely known as Levenberg–Marquardt method, the specific format is as follows:

$$\begin{aligned} f(c) &= \sum_{i=1}^{N} r_i^2(c) \\ &= \sum_{i=1}^{N} \left(\frac{\left(H_{g,i} - H_{WFi,i}\right)\dot{m}_{WF,i} + c_{e,1}\dot{m}_{WF,i}^{c_{e,3}}\left(T_{SFi,i} - T_{sat,i}\right)}{1 + c_{e,2}\left(\frac{\dot{m}_{WF,i}}{\dot{m}_{SF,i}}\right)^{c_{e,3}}} - Q_i \right)^2 \end{aligned} \tag{32}$$

where *f(c)* is the sum of the squares of the residuals between evaluated and experiment data, N is the number of samples; Q_i is the measured heat transfer rate from experiment. The optimal coefficients can be solved with Levenberg-Marquart [39, 40] (Its details can be found in Appendix B)

The fitting results for evaporator hybrid model are shown in Figure 11 and Figure 12,

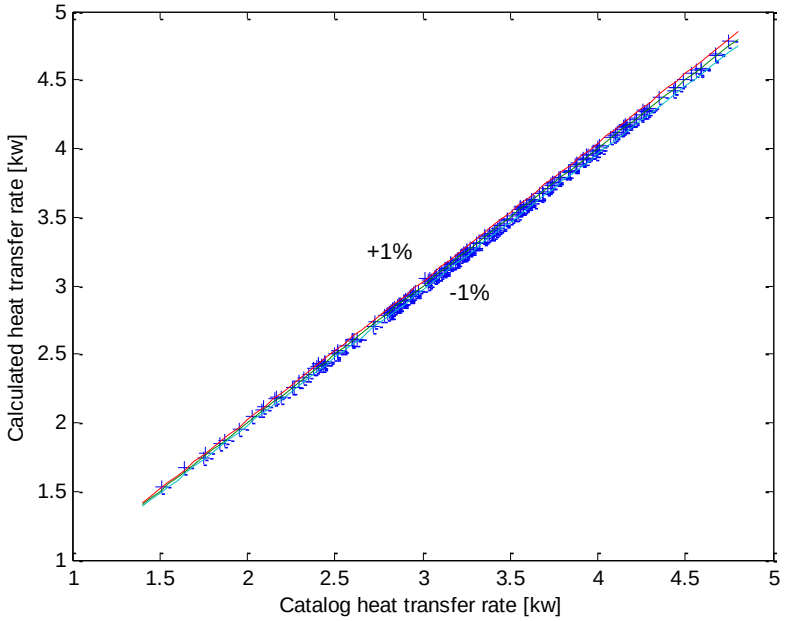

Figure 11 Experiment fitting by evaporator hybrid model

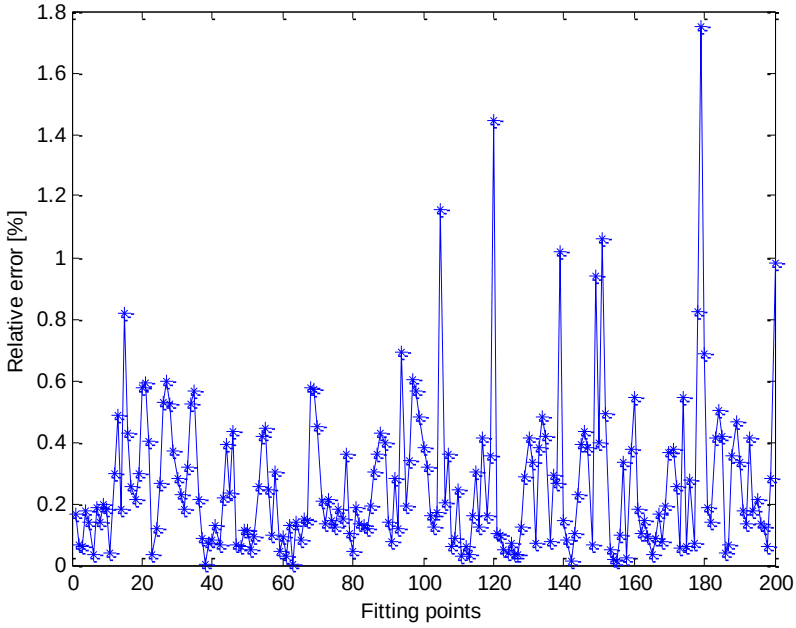

Figure 12 Relative error of evaporator hybrid model

It can be seen from the experimental results, the predicting errors of both models are all within ±2%. There are two key causes of the predicting errors: the sensor errors in

measurement and the fluid properties variations due to temperature change which is not considered in the model.

3.3 Condensers

The schematic of condenser has been introduced in the introduction part, whose chart is shown in Figure 13, which consists of two loops: the working fluid loop and the secondary fluid loop.

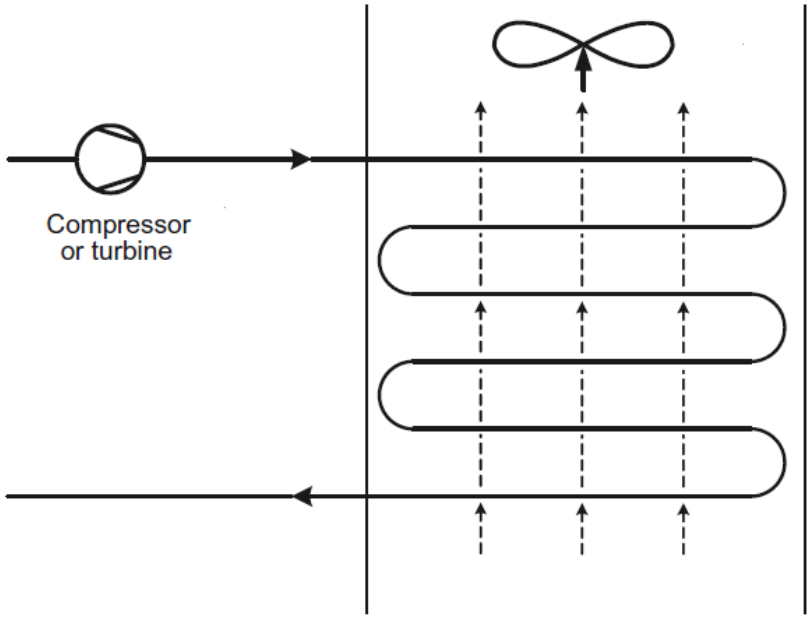

Figure 13 Schematic chart of condenser

Similar to the evaporator, condenser heat transfer properties can also be represented by a hybrid model [38]:

$$\dot{Q}_c = \frac{c_{c,1}\dot{m}_r^{c_{c,4}}\left(T_{c,r,sat} - T_{c,air,i}\right) + c_{c,2}\dot{m}_r\left(T_{c,r,i} - T_{c,r,sat}\right) + H_{c,fg}\dot{m}_r}{1 + c_{c,3}\left(\frac{\dot{m}_r}{\dot{m}_{c,air}}\right)^{c_{c,4}}} \tag{33}$$

where $c_{c,1}$,$c_{c,2}$, $c_{c,3}$ and $c_{c,4}$ are constants calculated by catalog or experiment data, $H_{c,fg}$ is enthalpy difference between saturated liquid and gas phase refrigerant in condenser, $\dot{m}_{c,air}$ is the mass flow rate of air outside condenser. $T_{c,r,sat}$, $T_{c,r,i}$, $T_{c,air,i}$ are temperature of saturated refrigerant, inlet refrigerant and inlet air of condenser, respectively, $\dot{Q}_c$ is the heat transferring rate of condenser (see Appendix A for the calculations of $H_{c,fg}$ and $T_{c,r,sat}$).

The fitting results of condenser hybrid model are shown in Figure 14 and Figure 15:

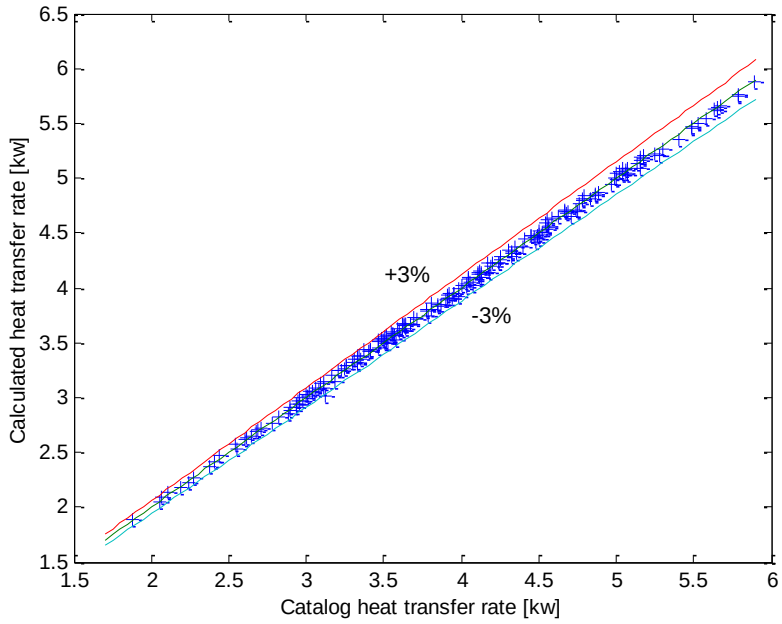

Figure 14 Experiment fitting by condenser hybrid model

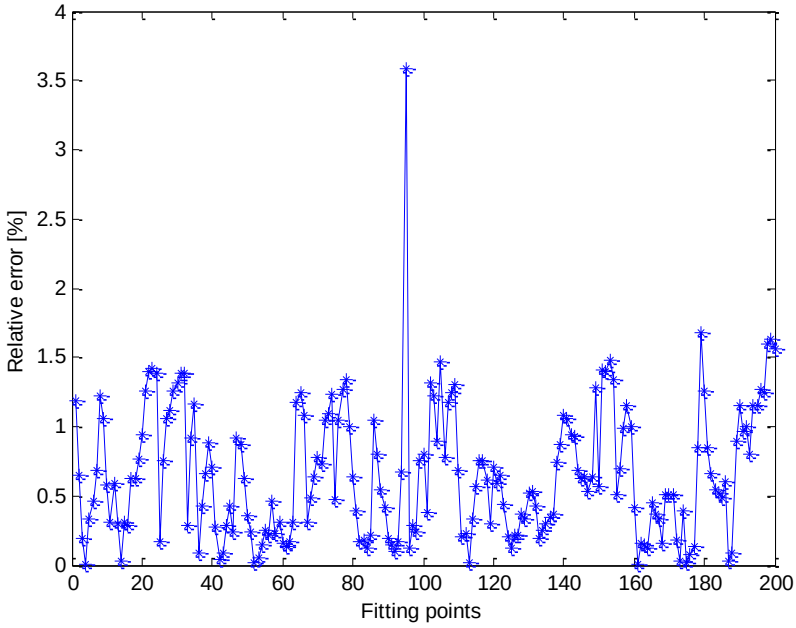

Figure 15 Relative error of condenser hybrid model

The predicting errors of hybrid models are all within ±3%. Furthermore, most of the predicting errors locate within ±2%, validating the accuracy of hybrid modeling approach.

The time cost of hybrid model is also significant reduced compared with the recursive approaches such as distributed model and e-NTU method.

3.4 Compressors and expansion valves

In a compressor, the mass flow rate and the refrigerant energy change during compression stroke can be expressed by [41]:

$$\dot{m}_r = \left(c_{com,m,1} - c_{com,m,2} \left(\frac{P_c}{P_e} \right)^{c_{com,m,3}} \right) F_{com} \tag{34}$$

and

$$\dot{Q}_{com} = \frac{n}{n-1}(V_a - V_d) P_e \left[\left(\frac{P_c}{P_e} \right)^{\frac{n-1}{n}} - 1 \right] F_{com} \dot{m}_r \tag{35}$$

respectively, where $c_{com,m,1}$, $c_{com,m,2}$ and $c_{com,m,3}$ are constants decided by curve-fitting, P_c, P_e, F_{com}, n, V_a, V_d, and $\dot{Q}_{com}$ are condensing temperature, evaporating pressure, compressor frequency, polytropic exponent, volume at bottom dead center, volume when suction valve open and mechanical work input to refrigerant by compressor, respectively. Since the parameters n, V_a and V_d are constants for a given compressor and at a specified working environment, Eq. (35) can be further simplified to a hybrid model form:

$$\dot{Q}_{com} = c_{com,q,1} F_{com} \dot{m}_r P_e \left(\left(\frac{P_c}{P_e} \right)^{c_{com,q,2}} - 1 \right) \tag{36}$$

where $c_{com,q,1} = \frac{n}{n-1}(V_a - V_d)$ and $c_{com,q,2} = \frac{n-1}{n}$

The fitting results for compressor are shown in Figure 16, 17, 18 and 19.

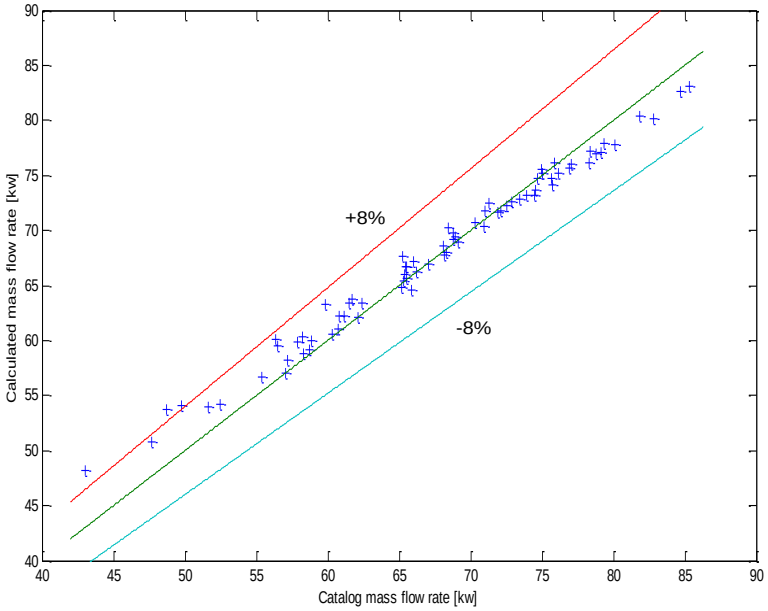

Figure 16 Fitting results of compressor mass flow rate

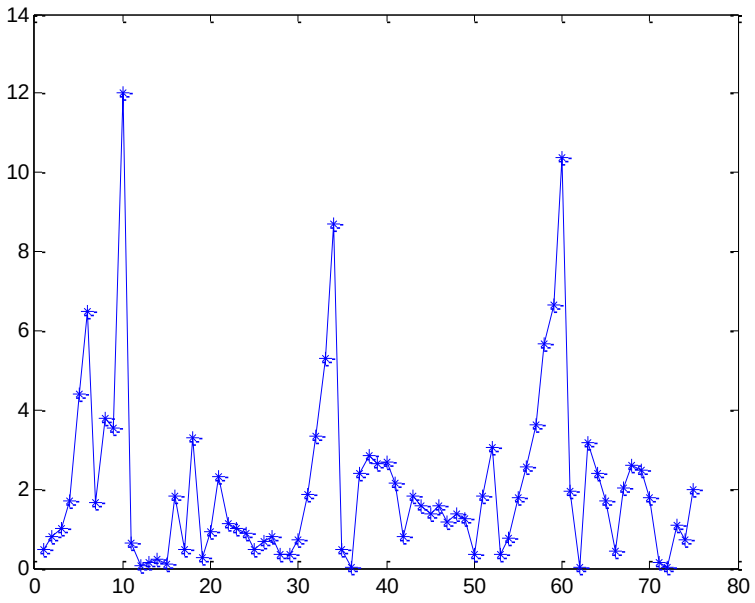

Figure 17 Relative error of fitting result of compressor mass flow rate

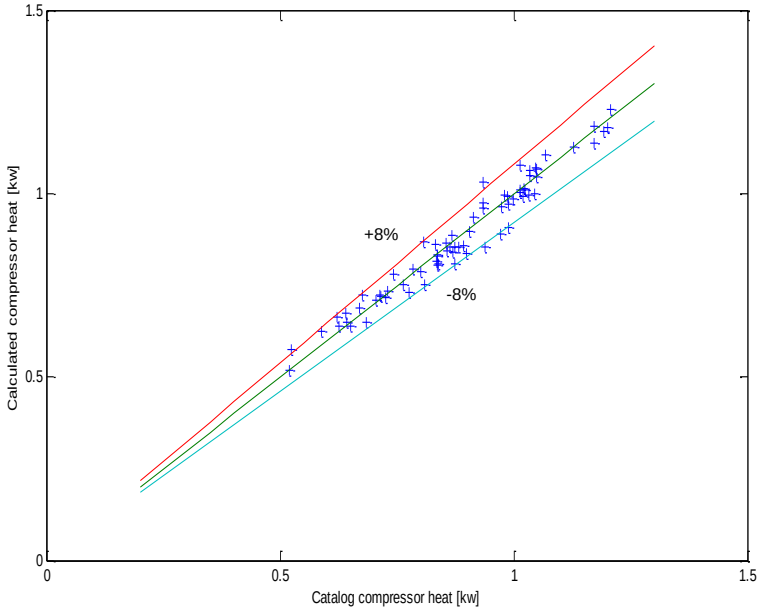

Figure 18 Fitting results of compressor energy

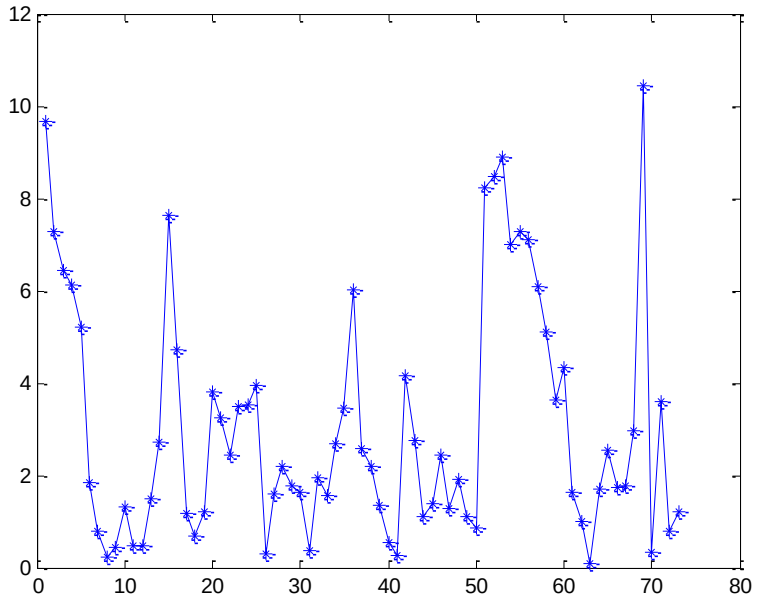

Figure 19 Relative error of compressor heat

The mass flow rate of expansion valve is determined by valve opening percentage, pressure difference and inlet refrigerant density. Its mass flow rate is given by [42, 43]

$$\dot{m}_r = (c_{ev,1} + c_{ev,2} A_v)\sqrt{\rho(P_c - P_e)} \tag{37}$$

where $c_{ev,1}$ and $c_{ev,2}$ are constants, A_v and ρ are opening percentage of electronic expansion valve and density of inlet refrigerant, respectively (see Appendix A for the calculation of ρ).

Furthermore, the mechanical characteristics of expansion valve determines that the inlet and outlet enthalpy should be equal, consequently refrigerant enthalpy is constant which implies

$$\dot{Q}_{ev} = 0 \tag{38}$$

3.5 Hybrid model with fouling effect

3.5.1 Model development

In the hybrid model, the basic principle is the heat transfer balance of working and secondary fluid corresponding to the flow inside and outside the heat exchanger tube. It is well known that [44]:

$$Q = U(T_o - T_i) \tag{39}$$

where T_o, T_i, U and Q are external and internal fluid temperature, overall thermal conductance and cooling load respectively.

The thermal conductance of heat exchanger can be divided into three major parts: thermal conductance of working fluid convection, of secondary fluid convection and of coil metal conductance. These three thermal conductance are connected in series, so the overall thermal conductance can be calculated by

$$U = \frac{1}{(\frac{1}{U_i} + \frac{1}{U_c} + \frac{1}{U_e})} \tag{40}$$

where U_i, U_e and U_c represent thermal conductance of internal and external fluid, heat exchanger coil metal, respectively. Thermal conductance of coil metal is normally much larger than that of working and secondary fluid, which means that the term in the middle of denominator is negligible, so the overall thermal conductance becomes

$$U = \frac{1}{(\frac{1}{U_i} + \frac{1}{U_e})} = \frac{1}{(\frac{1}{h_e A_e} + \frac{1}{h_i A_i})} \tag{41}$$

For steady working and secondary flow, the film coefficient of internal fluid follows Dittus-Boelter equation [45]:

$$h = C\left(\frac{4\dot{m}}{\pi\mu D}\right)^{e}\left(\frac{c_p\mu}{k}\right)^{f}\frac{k}{D} \tag{42}$$

where *C, e, f* are constants determined by system characteristics, *D* is coil diameter and c_p specific heat of working fluid, *k* thermal conductivity, μ viscosity.

The equation corresponding to secondary flow is as follows [46]:

$$h = C\left(\frac{\dot{m}D}{\mu S}\right)^{e}\left(\frac{c_p\mu}{k}\right)^{f}\frac{k}{D} \tag{43}$$

where *S* is the air passing area, c_p, *k* and μ are specific heat, thermal conductivity and viscosity of secondary flow, respectivly.

When temperature fluctuation is small, $\left(\frac{c_p\mu}{k}\right)$ and $\frac{k}{D}$ can be considered as constants, so film coefficient can be simplified as:

$$h = b\dot{m}^{e} \tag{44}$$

where

$$b = \frac{C4^{e}c_p^{f}k^{1-f}\mu^{f-e}}{\pi^{e}D^{1+e}} \tag{45}$$

After combining (39), (42), (43) and (45), we obtain the following equation:

$$Q = \frac{c_1\dot{m}_e^{e}}{1+c_2\left(\dot{m}_e/\dot{m}_i\right)^{e}}\left(T_e - T_i\right) \tag{46}$$

where $c_1 = b_e A_e$ and $c_2 = b_e A_{e_i}/b_i A$

It should be noted that the original hybrid model is accurate only for clean heat exchanger. However, the heat exchanger in chemical industry usually suffers from fouling effect, resulting in the decrease of the thermal conductance and the coefficients drift. Therefore, it is essential to modify the original hybrid model for improving its accuracy under fouling condition. Considering the fouling effect on heat exchanger thermal conductance, we express Eq. (40) as follows:

$$U = \frac{1}{(\frac{1}{U_i} + \frac{1}{U_c(U_i, U_e, t)} + \frac{1}{U_e})} \tag{47}$$

Considering the fact that the thermal conductance drift of coil is influenced by the working and secondary fluid, we rewrite Eq. (47) in the following form:

$$U = \frac{1}{f(U_i, U_e, t)(\frac{1}{U_i} + \frac{1}{U_e})} \tag{48}$$

Then equation (46) becomes

$$Q = \frac{c_1 \dot{m}_e^e}{f(U_i, U_e, t)\left(1 + c_2 \left(\dot{m}_e / \dot{m}_i\right)^e\right)} \left(T_e - T_i\right) \tag{49}$$

where $f(U_i,U_e,t)$ is a nonlinear function that depends on time, working, secondary fluid characteristics, environment and coil material, and whose detailed expression is determined by the prevailing fouling effect.

Based on the above analysis, several existing fouling models are listed as follows:

Linear fouling model

This fouling model describes the resistance change of heat exchanger with crystallization of a well-formed deposit consisting of a substantially pure salt [47-49].

$$U = U_c \Big/ \left[1 - \sqrt{\alpha} \Phi^{-1}(p)\right] \left(t / M\right) \tag{50}$$

where U_c is the heat conductance of clean heat exchanger, α scatter parameter, Φ risk function, p risk level, M median time.

Combining Eq. (49) and (50), we have

$$Q = \frac{c_1 \dot{m}_e^e}{\left(1 + c_3 t\right)\left(1 + c_2 \left(\dot{m}_e / \dot{m}_i\right)^e\right)} \left(T_e - T_i\right) \tag{51}$$

Where $c_3 = \left[1 - \sqrt{\alpha} \Phi^{-1}(p)\right] \Big/ M$

Power-law fouling model

The power-law fouling model is based on the deposition of $CaCO_3$ under high temperature, its equation version is like linear fouling model [50, 51].

$$U = U_c \Big/ \left(\left[1 - \sqrt{\alpha} \Phi^{-1}(p) \right] t^n / M^n \right) \tag{52}$$

For the heat exchanger following power law fouling, the hybrid model becomes

$$Q = \frac{c_1 \dot{m}_e^e}{\left(1 + c_3 t^{c_4}\right)\left(1 + c_2 \left(\dot{m}_e / \dot{m}_i\right)^e\right)} \left(T_e - T_i\right) \tag{53}$$

Where $c_3 = \left[1 - \sqrt{\alpha} \Phi^{-1}(p) \right] \Big/ M^n$ and $c_4 = n$

Falling-rate fouling model

This model simulates the situation when the deposition rate is always greater than the removal rate, it is normally observed in particulate fouling [52, 53]. The resistance of heat exchanger of falling-rate fouling model under risk *p* is

$$U = U_c \Big/ \left(\left[1 - \sqrt{\alpha} \Phi^{-1}(p) \right] \ln(t) / \ln(M) \right) \tag{54}$$

Thus

$$Q = \frac{c_1 \dot{m}_e^e}{\left(1 + c_3 \ln(t)\right)\left(1 + c_2 \left(\dot{m}_e / \dot{m}_i\right)^e\right)} \left(T_e - T_i\right) \tag{55}$$

where $c_3 = \left[1 - \sqrt{\alpha} \Phi^{-1}(p) \right] \Big/ \ln(M)$

Asymptotic fouling model

Asymptotic fouling usually occurs in cooling water exchangers. It is caused by simultaneous crystallization of salts or suspended particles [54]. The thermal conductance under this condition is of the form:

$$U = U_f^* \Big/ \left[1 - \exp\left\{ -\ln\left[1 / \left(1 - U_f^* / U_c \right) \right] \left[1 - \sqrt{\alpha} \Phi^{-1}(p) \right] t / M \right\} \right] \tag{56}$$

With Eq. (56), the hybrid model becomes

$$Q = \frac{c_1 \dot{m}_e^e}{\left(c_4 + c_3 \exp(c_5 t)\right)\left(1 + c_2 \left(\dot{m}_e / \dot{m}_i\right)^e\right)} \left(T_e - T_i\right) \tag{57}$$

where $c_3 = -U_c / U_f^*$, $c_4 = 1 + U_c / U_f^*$, $c_5 = \left\{ -\ln\left[1 / \left(1 - U_f^* / U_c \right) \right] \left[1 - \sqrt{\alpha} \Phi^{-1}(p) \right] \Big/ M \right\}$

In power or chemical industry, the heat transfer efficiency is a decisive factor. The long term fouling effect on heat transfer is considerable, to maintain heat transfer task, the cleaning process should be performed periodically based on the fouling model. However, it is hard to determine the heat exchanger follows which type of fouling effect in practice. Direct application of time related hybrid model seems infeasible. Therefore, it is suggested to use the following model for fouling heat exchangers.

$$Q = \frac{c_1 \dot{m}_e^{c_3}}{\left(c_4 + c_5 t + c_6 t^2 + c_7 t^3\right)\left(1 + c_2 \left(\dot{m}_e / \dot{m}_i\right)^{c_3}\right)} \left(T_e - T_i\right) \tag{58}$$

The reason of choosing three-order polynomial to represent fouling effect is that it balances precision and over-fitting risk.

3.5.2 Model validation

To identify the coefficients in the modified hybrid model (MHM), we construct the following cost function:

$$f(c) = \sum_{i=1}^{N} r_i^2(c) = \sum_{i=1}^{N} (Q_m - Q_{cal})^2 \tag{59}$$

where Q_m and Q_{cal} are the measured and calculated heat transfer rate, respectively. According to the proposed hybrid model of cooling tower, calculated heat transfer equals to the right side of Eq. (58), thus the cost function becomes

$$f(c) = \left(\frac{c_1 \dot{m}_e^{e}}{\left(c_4 + c_5 t + c_6 t^2 + c_7 t^3\right)\left(1 + c_2 \left(\dot{m}_e / \dot{m}_i\right)^{e}\right)} \left(T_e - T_i\right) - Q_m \right)^2 \tag{60}$$

To obtain the optimal coefficients, Levenberg-Marquadt method is adopted (Details are given in Appendix B)[55]. In MHM, the coefficients are identified in two steps. Firstly, the measured data of clean heat exchanger are used to identify c_1, c_2 and c_3, respectively. The other four coefficients are then identified with the measured fouling condition.

The raw data are processed according to the following procedures:

- Filtering the white noise in the measured data to ensure the stability of identification process.

- Heat transfer is calculated indirectly with the change of enthalpy of working fluid.

$$Q = \dot{m}_w (h_{w,i} - h_{w,o}) \tag{61}$$

where $h_{r,i}$ and $h_{r,o}$ are working fluid enthalpies at input and output point.

- The flow rate of secondary is estimated from following equation:

$$\dot{m}_s = Q_m / (h_{s,i} - h_{s,o}) \tag{62}$$

where $h_{s,i}$ and $h_{s,o}$ are enthalpies of the input and output external fluid.

All the enthalpies of internal and external fluid are then calculated with the measurements of the temperatures, pressures and humidity.

The experiment has been conducted on a pilot centralized HVAC system that consists of three sets of chillers, zones, AHUs and cooling towers, with the controlled cooling load, the measured water flow rates, inlet and outlet water temperatures, dry/wet bulb air temperatures and pressures.

In this experiment, the cooling capacity is controlled through setting air and water flow rates as their inlet temperature are fixed during the whole experiment. The water in experiment system is polluted to show the fouling effect on hybrid model. To research the effect of coefficient drifting, the system ran more than 100 hours for 100 consecutive data groups under fouling effect.

The relative error R_e, used as the main criterion for accuracy evaluation in this experiment, is defined as:

$$R_e = \frac{|Measured\ data - Calculated\ data|}{Calculated\ data} \times 100\% \tag{63}$$

For identifying the coefficients, ten sets of data are measured immediately after cleaning. As the time is too short for heat exchanger to be fouled, the heat exchanger can be considered as clean, thus c_1, c_2 and c_3 are calculated through fitting these data sets. The rest of the coefficients are obtained through fitting the other measured data sets by considering fouling effect.

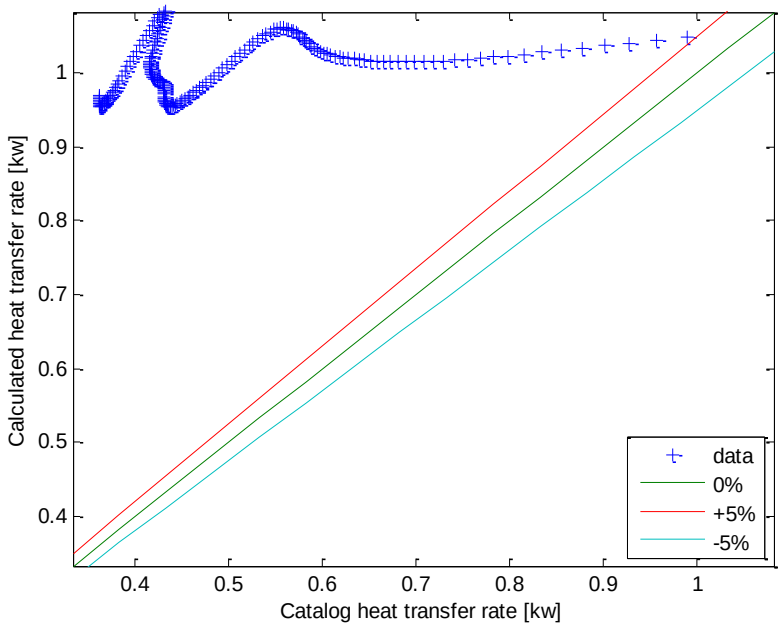

Figure 20 Fitting results of original hybrid model under fouling effect

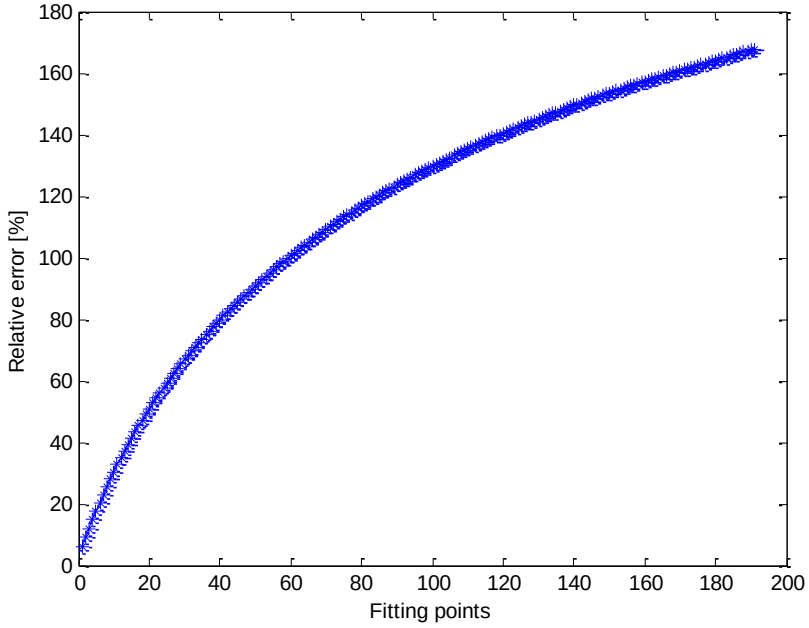

Figure 21 Relative error of original hybrid model under fouling effect

It is seen from Figure 20 and Figure 21 that the hybrid model tends to give a larger heat transfer prediction since it neglects the increasing heat resistance of coil surface, resulting

in a significant coefficients drift from the original hybrid model. Figure 22 illustrates the difference between the calculated and measured heat transfers.

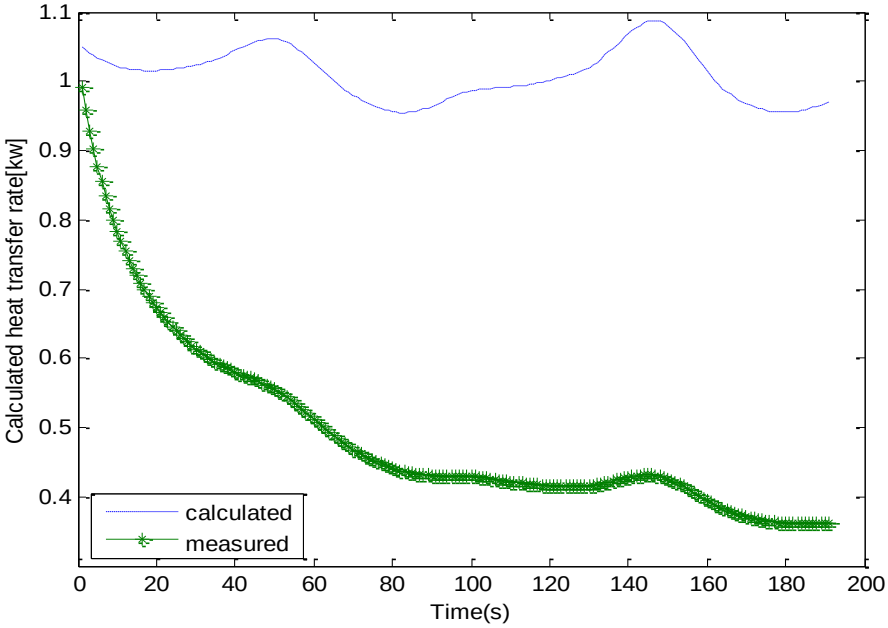

Figure 22 Calculated and measured heat transfer rate by original model

For the MHM, the prediction results are as follows:

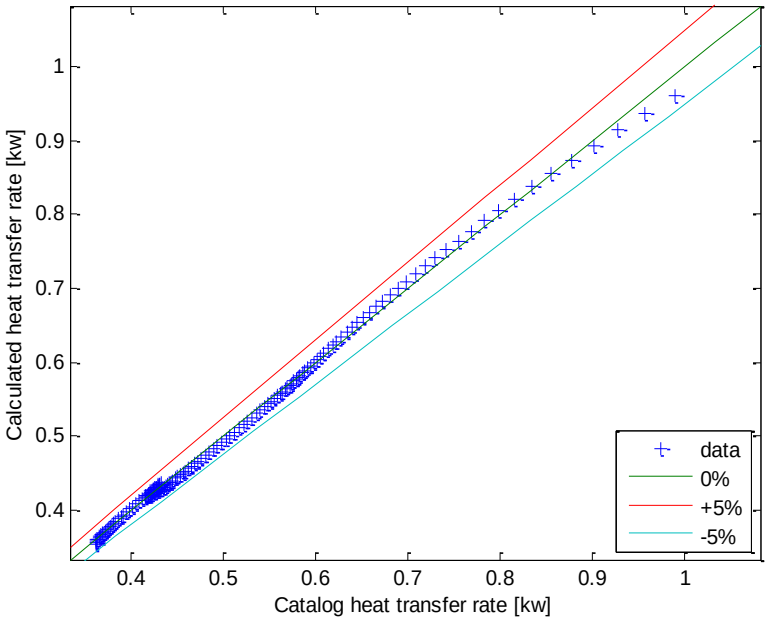

Figure 23 Fitting results of modified hybrid model

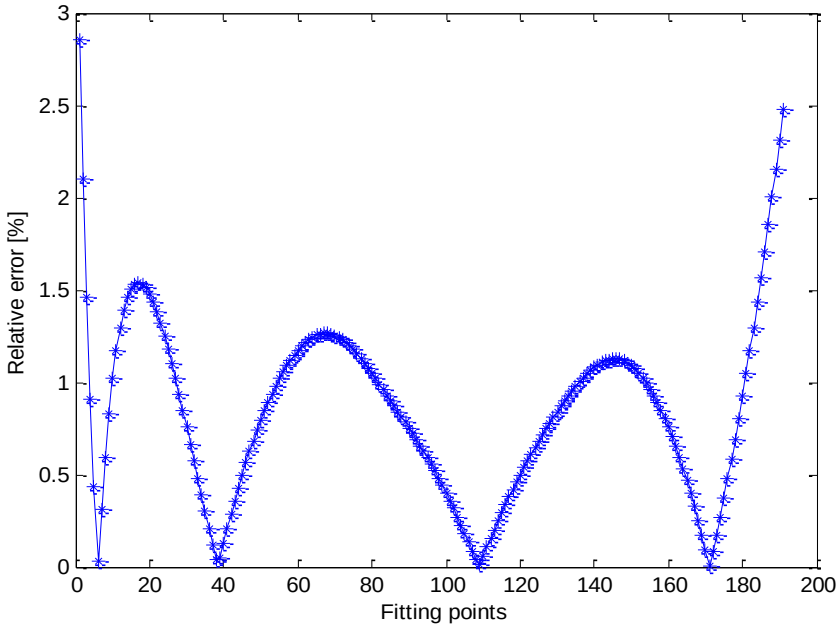

Figure 24 Relative error of modified hybrid model

From Figure 23 and Figure 24, it can be seen that the fitting result is much better than that of original hybrid model. All fitting points are close to the 1:1 line and within ±3% range compared with ±160% of original model. The precision improvement is significant.

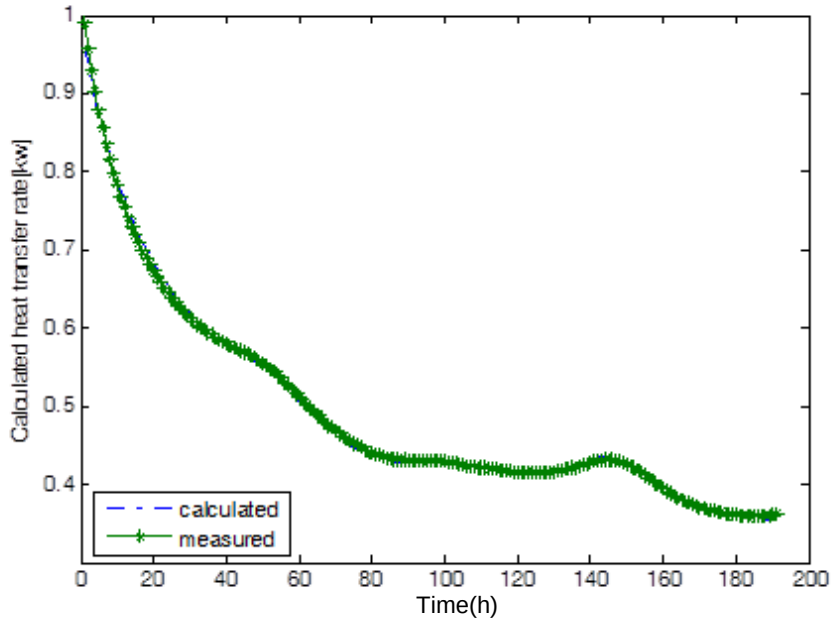

Figure 25 Calculated and measured heat transfer rate of modified model

With the developed MHM, the time for heat exchanger to achieve critical heat transfer efficiency can be calculated. The following figure illustrates the heat transfer decay ratio.

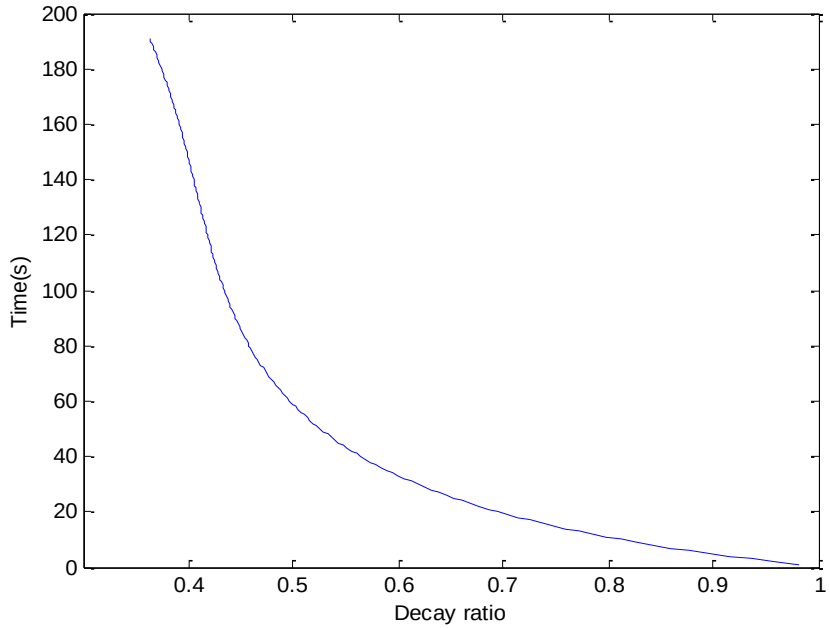

Figure 26 Relationship between time and decay ratio

3.6 Summary

The hybrid models of the major components of VCCs and air conditioning systems, including evaporators, condensers, compressors, expansion valves and cooling towers, have been presented in this chapter. It has been seen that (i) the models of heat exchangers such as evaporators and condensers can be deduced through the heat transfer mechanism and the energy balance principle; (ii) the hybrid models of compressors and evaporators are derived from the volumetric and adiabatic efficiency; (iii) the hybrid model of cooling tower considering fouling effect can be deduced based on the foul modeling of cooling tower. Experimental results have shown that all these models are capable of accurately predicting the system states over a wide operating range.

In practice, the model coefficients can be obtained through fitting the available experiment data or performance data from the manufacturers' catalogue. The high speed and accuracy of hybrid models have confirmed the suitability of the models for online optimization. It will be seen that the developed hybrid models in this chapter, including

condenser, evaporator and compressor, play an important role for developing the optimization methodologies in the following chapters.

Chapter 4 Modeling and Optimization of VCCs based on ELM

4.1 Background of ELM and VCC modeling with the SLFN

The modeling of air conditioning systems has attracted a great deal of attentions recently. Many engineering techniques have been employed for modeling vapor compression cycle (VCC) systems [23, 24]. Because of the complexity of vapor compression systems with nonlinearities and uncertainties, it is very difficult to obtain a perfect mathematical model to sufficiently describe the dynamics of vapor compression systems. Facing such a challenge, some researchers have attempted to model VCC with the data obtained from experimental studies [26, 37, 38, 41, 56]. In addition, neural networks [5, 8], due to their excellent performance in approximating complex nonlinear functions, have been introduced for modeling and optimizing air conditioning systems. Hosoz and Ertunc [57] developed a neural network model with five neurons in input layer for predicting condenser load, mass flow rate of refrigerant, compressor power absorbed by the refrigerant, electric power consumed by the compressor motor, and coefficient of performance (COP) of a refrigeration system with an evaporative condenser. Its simulation results demonstrated the effectiveness of the neural models. Yilmaz and Atik [58] proposed a feed-forward neural network with condenser water flow rate as the input to predict the performance of a variable cooling capacity mechanical cooling system. Navarro et.al [59] developed a radiant based function neural network model for predicting the performance parameters (such as cooling capacity, power consumption and chiller water outlet temperature) of a variable speed compression based refrigeration systems with reference to speed, chill water temperature inlet, condensing water temperature inlet and refrigerant evaporator temperature. Saiduret. al [60] proposed a more comprehensive neural model to predict the energy performance of refrigerator by considering both the system parameters such as capacity, loading , number of units and the occupants' parameters such as door opening, age, income, location and number of occupants.

Recently, a novel learning algorithm for single-hidden-layer feed-forward neural networks (SLFN), called extreme learning machine (ELM), has been developed in [13, 14, 61-64] by Huang et. al. The main characteristics of the ELM are that both the input-weights and hidden biases are randomly chosen, and the output weights are analytically determined by

using the Moore–Penrose (MP) generalized inverse [65]. It has been further shown in [66] that ELM achieves the better generalization performance for equality constrained optimization problems, the extremely fast speed of convergence, and the easy conversion of complex learning into simple linear fitting. Most importantly, the ELM avoids many difficulties brought by gradient-based learning methods such as choosing stopping criteria, learning rate, learning epochs, local minima, and the over-tuned problems.

ELM has been widely used in various fields due to its excellent speed and high accuracy. Nizar et.al [67]employed both ELM and online ELM to analyze the nontechnical loss. They used customer load-profile information to expose abnormal behavior and extracted customer behavior patterns with ELM as data mining techniques. Sun et.al [68] applied ELM to investigate the relationship between sales amount and some significant factors which affect demand. The experiment results show that ELM outperforms back propagation in accuracy and speed. Kim et.al [69] proposed to use morphology filter and principle component analysis for feature extraction, and then used ELM to classify the ECG signal to six beat types, experiment results prove that its performance is better than that of BP, RBF and SVM. Minhas et.al [70] used ELM to classify human actions based on spatio-temporal and local static features that are extracted using motion-selectivity techniques, and claimed more than 10 times speed improvement compared with conventional method.

In this chapter, we will choose SLFN to model the vapor compression cycle for four reasons: 1) SLFN is a universal black box model with no requirement on prior knowledge; 2) it is the best black box model which can balance the model accuracy and complexity for VCC modeling; 3) its flexibility simplifies further development for future research or advanced applications; 4) It can be directly trained by ELM algorithm. It will be shown that, with the ELM, the input weights are randomly assigned and the output weights are globally trained with the batch learning type least squares. In addition to the standard constraint used in the ELM, the constraint that satisfies the cooling load requirement in a vapor compression system is included in the global optimization for deriving the optimal output weights of the SLFN. In the experimental section, all training data pairs are obtained from the experiments, and the SLFN model is tested and compared with the ones trained with the BP, the SVR (support vector regression) and the RBF, respectively, with

the results that the developed SLFN model behaves with excellent robustness against high frequency noises involved in the testing data and provides the high accuracy for the prediction of the system states in the vapor compression cycle, then an optimization methodology based on the SLFN model is proposed. The SLFN aims at classifying system stability and predicting its energy consumption, ELM is selected for training the SLFN with experiment data of the testing system and shows significant reduction of training time and computational burden compared with other intelligent methods.

4.2 Black box-like neural model trained with the ELM

Consider *N* distinct sample data vector pairs (x_i, t_i) that are collected measurements from a vapor compression cycle. The i*th* input pattern vector X_i is defined as:

$$\begin{aligned} X_i &= \begin{bmatrix} x_{i1} & x_{i2} & \cdots & x_{i6} \end{bmatrix}^T \\ &= \begin{bmatrix} F_{com,i} & F_{e,a,i} & F_{c,a,i} & A_{v,i} & T_{out,i} & T_{in,i} \end{bmatrix}^T \end{aligned} \tag{64}$$

and the desired *i*th output vector:

$$t_i = \begin{bmatrix} t_{i1} & t_{i2} & t_{i3} & t_{i4} & t_{i5} \end{bmatrix}^T = \begin{bmatrix} P_{c,i} & P_{e,i} & SC_i & SH_i & W_{sy,i} \end{bmatrix}^T \tag{65}$$

for $i = 1, 2, \cdots N$

In the thesis, the following SLFN in Figure 27 will be used to model the relationship between the input pattern vectors and the desired output vectors described in Eq. (64) and (65), respectively:

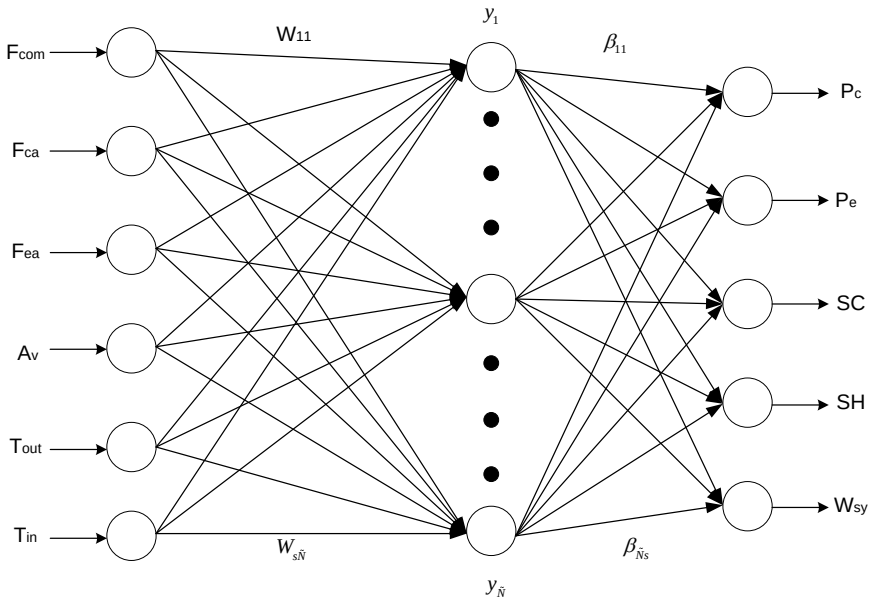

Figure 27 The SLFN for modeling of VCC dynamics

where the nodes in the input and output layer are linear, and the nodes in hidden layer are nonlinear with the nonlinear activation functions, described by

$$y_{ki} = \varphi(W_k^T x_i) \tag{66}$$

W_k in (66) is the input weight vector to the k*th* hidden neuron, defined as:

$$W_k = \begin{bmatrix} W_{1k} & W_{2k} & \cdots & W_{6k} \end{bmatrix}^T \tag{67}$$

for $k = 1, 2, \cdots \tilde{N}$, and values of the input weights in W_k are all randomly selected based on ELM [13, 14].

The hidden layer output vector Y_i, corresponding the input vector X_i, can then be expressed as:

$$\begin{aligned} Y_i &= \begin{bmatrix} y_{1i} & y_{2i} & \cdots & y_{\tilde{N}i} \end{bmatrix}^T \\ &= \begin{bmatrix} \varphi(W_1^T X_i) & \varphi(W_2^T X_i) & \cdots & \varphi(W_{\tilde{N}}^T X_i) \end{bmatrix}^T \end{aligned} \tag{68}$$

Using (68), the *j*th output of the SLFN can be obtained as:

$$O_{ji} = \sum_{l=1}^{\tilde{N}} \beta_{lj} \varphi(W_l^T X_i) \qquad j = 1, 2, \cdots 5 \tag{69}$$

and the *i*th output vector of the SLFN is of the form:

$$O_i = \begin{bmatrix} O_{1i} & O_{2i} & O_{3i} & O_{4i} & O_{5i} \end{bmatrix}^T$$
$$= \left[\sum_{l=1}^{\tilde{N}} \beta_{l1} \varphi(W_l^T X_i) \quad \sum_{l=1}^{\tilde{N}} \beta_{l2} \varphi(W_l^T X_i) \quad \cdots \quad \sum_{l=1}^{\tilde{N}} \beta_{l5} \varphi(W_l^T X_i) \right]^T \tag{70}$$

Then all N output vectors of the SLFN, corresponding to the N distinct input vectors $X_1, X_2 \cdots X_N$, can be written in the following matrix form:

$$O = [O_1 \quad O_2 \cdots O_N]$$
$$= \begin{bmatrix} \sum_{l=1}^{\tilde{N}} \beta_{l1} \varphi(W_l^T X_1) & \sum_{l=1}^{\tilde{N}} \beta_{l1} \varphi(W_l^T X_2) & \cdots & \sum_{l=1}^{\tilde{N}} \beta_{l1} \varphi(W_l^T X_N) \\ \vdots & \vdots & \cdots & \vdots \\ \sum_{l=1}^{\tilde{N}} \beta_{l5} \varphi(W_l^T X_1) & \sum_{l=1}^{\tilde{N}} \beta_{l5} \varphi(W_l^T X_2) & \cdots & \sum_{l=1}^{\tilde{N}} \beta_{l5} \varphi(W_l^T X_N) \end{bmatrix} \tag{71}$$
$$= \begin{bmatrix} \beta_1^T \phi_1 & \beta_1^T \phi_2 & \cdots & \beta_1^T \phi_N \\ \beta_2^T \phi_1 & \beta_2^T \phi_2 & \cdots & \beta_2^T \phi_N \\ \vdots & \vdots & \vdots & \vdots \\ \beta_5^T \phi_1 & \beta_5^T \phi_2 & \cdots & \beta_5^T \phi_N \end{bmatrix} = \beta^T \phi$$

with

$$\beta_i = \begin{bmatrix} \beta_{1i} & \beta_{2i} & \cdots & \beta_{\tilde{N}i} \end{bmatrix}^T \tag{72}$$

and

$$\phi_i = \begin{bmatrix} \varphi(W_1^T X_i) & \varphi(W_2^T X_i) & \cdots & \varphi(W_{\tilde{N}}^T X_i) \end{bmatrix}^T \tag{73}$$

$$\beta = [\beta_1 \quad \beta_2 \quad \cdots \quad \beta_5] \tag{74}$$

$$\phi = [\phi_1 \quad \phi_2 \quad \cdots \quad \phi_N] \tag{75}$$

It is seen from the above descriptions that, after the input weights are randomly initialized, the accuracy of the modeling of the VCC dynamics largely depends on the values of the output weights of the SLFN. For this purpose, we formulate the optimization of the output weight matrix β as follows:

$$\min \left\{ \frac{1}{2} \|\varepsilon\|^2 + \frac{d}{2} \|\beta\|^2 \right\} \tag{76}$$

subject to

$$\varepsilon = O - T = \beta^T \phi - T \tag{77}$$

and

$$\dot{Q}_{e,i} = \dot{Q}_{req,i} = f(T_{out,i}, T_{in,i}) \qquad i = 1, 2, \cdots N \tag{78}$$

where matrix O in Eq. (77) contains all output data of the SLFN, corresponding the N input pattern vectors, as described in Eq. (64)

Remark 3.1: The optimization constraint in (78) indicates the VCC system must meet the cooling load requirement, which is a function of indoor and outdoor temperature [71, 72].

Based on the system dynamics, we can express $\dot{Q}_{ei}$ as follows:

$$\begin{aligned}\dot{Q}_{ei} &= \dot{m}_r * \left(H_{e,r,o} - H_{c,r,o}\right) \\ &= F_{com,i}\left(c_{com,m,1} - c_{com,m,2}\left(\frac{P_{c,i}}{P_{e,i}}\right)^{c_{com,m,3}}\right)\left(b_{he,1} + b_{he,2}P_{e,i} + b_{he,3}SH_i - \left(b_{hc,1} + b_{hc,2}P_{c,i} + b_{hc,3}SC_i\right)\right)\end{aligned} \tag{79}$$

Eq. (79) stands since the enthalpies of Eq. (79) can be calculated by linear functions of pressure and temperature.

Defining

$$\gamma_i = F_{com,i}\left(c_{com,m,1} - c_{com,m,2}\left(\frac{P_{ci}}{P_{ei}}\right)^{c_{com,m,3}}\right) \tag{80}$$

we can then rewrite $\dot{Q}_{ei}$ as follows:

$$\begin{aligned}\dot{Q}_{ei} &= \gamma_i \bullet \left(\left(b_{he,1} - b_{hc,1}\right) - b_{hc,2}P_{ci} + b_{he,2}P_{ei} - b_{hc,3}SC_i + b_{he,3}SH_i\right) \\ &= d_{0i} + \begin{bmatrix} d_{1i} & d_{2i} & d_{3i} & d_{4i} & 0 \end{bmatrix} \begin{bmatrix} P_{ci} \\ P_{ei} \\ SC_i \\ SH_i \\ W_{ei} \end{bmatrix} \\ &= d_{0i} + d_i^T O_i\end{aligned} \tag{81}$$

where

$$\begin{cases} d_{0i} = \gamma_i (b_{he,1} - b_{hc,1}) \\ d_{1i} = -\gamma_i b_{hc,2} \\ d_{2i} = \gamma_i b_{he,2} \\ d_{3i} = -\gamma_i b_{hc,3} \\ d_{4i} = \gamma_i b_{he,3} \\ d_{5i} = 0 \end{cases}, \beta_k = \begin{bmatrix} \beta_{1k} \\ \beta_{2k} \\ \vdots \\ \beta_{\tilde{N}k} \end{bmatrix} \qquad \phi_p = \begin{bmatrix} \varphi\left(W_1^T X_p\right) \\ \varphi\left(W_2^T X_p\right) \\ \vdots \\ \varphi\left(W_{\tilde{N}}^T X_p\right) \end{bmatrix} = \begin{bmatrix} \phi_{1p} \\ \phi_{2p} \\ \vdots \\ \phi_{\tilde{N}p} \end{bmatrix} \tag{82}$$

For the minimization of (76), the following Lagrange function is constructed:

$$L = \frac{1}{2}\sum_{i=1}^{5}\sum_{j=1}^{N}\varepsilon_{ij}^2 + \frac{d}{2}\sum_{i=1}^{5}\sum_{j=1}^{\tilde{N}}\beta_{ij}^2 + \sum_{k=1}^{5}\sum_{p=1}^{N}\lambda_{kp}\left(\beta_k^T\phi_p - t_{kp} - \varepsilon_{kp}\right) + \sum_{p=1}^{N}\bar{\lambda}_p\left(Q_{ep} - f(T_{out,p}, T_{in,p})\right) \tag{83}$$

It is noted from (81) that

$$\begin{aligned} \sum_{p=1}^{N}\bar{\lambda}_p\left(\dot{Q}_{ep} - \dot{Q}_{rqp}\right) &= \sum_{p=1}^{N}\bar{\lambda}_p\left(d_{0p} + d_p^T O_p - f(T_{out,p}, T_{in,p})\right) \\ &= \begin{pmatrix} \bar{\lambda}_1 & \bar{\lambda}_2 & \cdots & \bar{\lambda}_N \end{pmatrix} \begin{bmatrix} d_{01} + d_1^T O_1 - f(T_{out,1}, T_{in,1}) \\ d_{02} + d_2^T O_2 - f(T_{out,2}, T_{in,2}) \\ \vdots \\ d_{0N} + d_N^T O_N - f(T_{out,N}, T_{in,N}) \end{bmatrix} \\ &= \bar{\lambda}^T d_0 + \sum_{p=1}^{N}\bar{\lambda}_p d_p^T O_p - \bar{\lambda}^T f(T_{out}, T_{in}) \\ &= \bar{\lambda}^T d_0 + \sum_{p=1}^{N}\bar{\lambda}_p \sum_{k=1}^{5} d_{kp}\beta_k^T\phi_p - \bar{\lambda}^T f(T_{out}, T_{in}) \end{aligned} \tag{84}$$

where

$$d_0 = \begin{bmatrix} d_{01} & d_{02} & \cdots & d_{05} \end{bmatrix}^T$$

$$d_p = \begin{bmatrix} d_{1p} & d_{2p} & \cdots & d_{5p} \end{bmatrix}^T$$

$$f(T_{out}, T_{in}) = \begin{bmatrix} f(T_{out,1}, T_{in,1}) & f(T_{out,2}, T_{in,2}) & \cdots & f(T_{out,N}, T_{in,N}) \end{bmatrix}^T$$

$$\bar{\lambda}^T = \begin{bmatrix} \bar{\lambda}_1 & \bar{\lambda}_2 & \cdots & \bar{\lambda}_N \end{bmatrix}$$

$$\lambda = \begin{bmatrix} \lambda_1 \\ \lambda_2 \\ \vdots \\ \lambda_5 \end{bmatrix} = \begin{bmatrix} \lambda_{11} & \lambda_{12} & \cdots & \lambda_{1N} \\ \lambda_{21} & \lambda_{22} & \cdots & \lambda_{2N} \\ \vdots & \vdots & \vdots & \vdots \\ \lambda_{51} & \lambda_{52} & \cdots & \lambda_{5N} \end{bmatrix} \tag{85}$$

Differentiating Eq. (84) with respect to β_{ij}, we have

$$\begin{aligned}\frac{\partial L}{\partial \beta_{ij}} &= d\beta_{ij} + \sum_{p=1}^{N} \lambda_{jp}\phi_{ip} + \sum_{p=1}^{N} d_{jp}\phi_{ip}\bar{\lambda}_p \\ &= d\beta_{ij} + \begin{bmatrix} \lambda_{j1} & \lambda_{j2} & \cdots & \lambda_{jN} \end{bmatrix} \begin{bmatrix} \phi_{i1} \\ \phi_{i2} \\ \vdots \\ \phi_{iN} \end{bmatrix} + \begin{bmatrix} \bar{\lambda}_1 & \bar{\lambda}_2 & \cdots & \bar{\lambda}_N \end{bmatrix} \begin{bmatrix} d_{j1}\phi_{i1} \\ d_{j2}\phi_{i2} \\ \vdots \\ d_{jN}\phi_{iN} \end{bmatrix} \\ &= d\beta_{ij} + \begin{bmatrix} \lambda_{j1} & \lambda_{j2} & \cdots & \lambda_{jN} \end{bmatrix} \begin{bmatrix} \phi_{i1} \\ \phi_{i2} \\ \vdots \\ \phi_{iN} \end{bmatrix} + \begin{bmatrix} \bar{\lambda}_1 & \bar{\lambda}_2 & \cdots & \bar{\lambda}_N \end{bmatrix} d_{j1} K \begin{bmatrix} \phi_{i1} \\ \phi_{i2} \\ \vdots \\ \phi_{iN} \end{bmatrix} \\ &= d\beta_{ij} + \tilde{\lambda}_j \bullet \tilde{\phi}_i^T + d_{j1}\bar{\lambda}^T K \tilde{\phi}_i^T = 0\end{aligned} \tag{86}$$

where

$$K = \begin{bmatrix} K_1 & 0 & \cdots & \cdots \\ 0 & K_2 & \ddots & \cdots \\ \cdots & \ddots & \ddots & 0 \\ \cdots & \cdots & 0 & K_N \end{bmatrix}_{N \times N} \tag{87}$$

$$K_i = \frac{d_{ji}}{d_{j1}} = \frac{\gamma_i}{\gamma_1} \tag{88}$$

$$\tilde{\phi}_i = \begin{bmatrix} \phi_{i1} & \phi_{i2} & \cdots & \phi_{iN} \end{bmatrix} \tag{89}$$

and

$$\tilde{\lambda}_j = \begin{bmatrix} \lambda_{j1} & \lambda_{j2} & \cdots & \lambda_{jN} \end{bmatrix} \tag{90}$$

Thus,

$$d\beta_{ij} = -\left(\tilde{\lambda}_j + d_j \bar{\lambda}^T K\right)\phi_i^T \tag{91}$$

$$d\beta_j^T = d\begin{bmatrix} \beta_{1j} & \beta_{2j} & \cdots & \beta_{\tilde{N}j} \end{bmatrix} = -\left(\tilde{\lambda}_j + d_j \bar{\lambda}^T K\right)\phi^T \tag{92}$$

$$d\beta^T = \begin{bmatrix} \beta_1^T \\ \beta_2^T \\ \vdots \\ \beta_5^T \end{bmatrix} = -\begin{bmatrix} \tilde{\lambda}_1 + d_1\bar{\lambda}^T K \\ \tilde{\lambda}_2 + d_2\bar{\lambda}^T K \\ \vdots \\ \tilde{\lambda}_5 + d_5\bar{\lambda}^T K \end{bmatrix}\phi^T = -\lambda\phi^T - \begin{bmatrix} d_1\bar{\lambda}^T K \\ d_2\bar{\lambda}^T K \\ \vdots \\ d_5\bar{\lambda}^T K \end{bmatrix}\phi^T$$
$$= -\left[\lambda + \begin{bmatrix} d_1\bar{\lambda}^T K \\ d_2\bar{\lambda}^T K \\ \vdots \\ d_5\bar{\lambda}^T K \end{bmatrix}\right]\phi^T = -\left[\lambda + \begin{bmatrix} d_1 \\ d_2 \\ \vdots \\ d_5 \end{bmatrix}\bar{\lambda}^T K\right]\phi^T \tag{93}$$

$$d\beta = -\phi\left[\lambda^T + K\bar{\lambda}\begin{bmatrix} d_1 & d_2 & \cdots & d_5 \end{bmatrix}\right] \tag{94}$$

In addition,

$$\sum_{p=1}^{N}\bar{\lambda}_p\left(\dot{Q}_{ep} - f(T_{out,p}, T_{in,p})\right) = \sum_{p=1}^{N}\bar{\lambda}_p\left(d_{0p} + d_p^T O_p - f(T_{out,p}, T_{in,p})\right)$$
$$= \begin{pmatrix} \bar{\lambda}_1 & \bar{\lambda}_2 & \cdots & \bar{\lambda}_N \end{pmatrix}\begin{bmatrix} d_{o1} + d_1^T O_1 - f(T_{out,1}, T_{in,1}) \\ d_{o2} + d_2^T O_2 - f(T_{out,2}, T_{in,2}) \\ \vdots \\ d_{oN} + d_N^T O_N - f(T_{out,N}, T_{in,N}) \end{bmatrix}$$
$$= \bar{\lambda}^T d_0 + \sum_{p=1}^{N}\bar{\lambda}d_p^T O_p - \bar{\lambda}^T f(T_{out}, T_{in})$$
$$= \bar{\lambda}^T d_0 + \sum_{p=1}^{N}\bar{\lambda}\sum_{k=1}^{5} d_{kp}\left(\varepsilon_{kp} + t_{kp}\right) - \bar{\lambda}^T f(T_{out}, T_{in}) \tag{95}$$

Thus,

$$L = \frac{1}{2}\sum_{i=1}^{5}\sum_{j=1}^{N}\varepsilon_{ij}^2 + \frac{d}{2}\sum_{i=1}^{5}\sum_{j=1}^{\tilde{N}}\beta_{ij}^2 + \sum_{k=1}^{5}\sum_{p=1}^{N}\lambda_{kp}\left(\beta_k^T\phi_p - t_{kp} - \varepsilon_{kp}\right)$$
$$+\bar{\lambda}^T d_0 - \bar{\lambda}^T f(T_{out}, T_{in}) + \sum_{p=1}^{N}\bar{\lambda}_p\sum_{k=1}^{5} d_{kp}\left(\varepsilon_{kp} + t_{kp}\right) \tag{96}$$

Also,

$$\frac{\partial L}{\partial \varepsilon_{ij}} = \varepsilon_{ij} + \lambda_{ij} + \bar{\lambda}_j d_{ij} = 0 \tag{97}$$

Correspondingly, the value of ε_{ij} is

$$\varepsilon_{ij} = -\left(\lambda_{ij} + \bar{\lambda}_j d_{ij}\right) \tag{98}$$

$$\varepsilon_j = \begin{bmatrix} \varepsilon_{1j} \\ \varepsilon_{2j} \\ \vdots \\ \varepsilon_{5j} \end{bmatrix} = -\begin{bmatrix} \lambda_{1j} + \bar{\lambda}_j d_{1j} \\ \lambda_{2j} + \bar{\lambda}_j d_{2j} \\ \vdots \\ \lambda_{5j} + \bar{\lambda}_j d_{5j} \end{bmatrix} \tag{99}$$

$$\varepsilon = \begin{bmatrix} \varepsilon_1 & \varepsilon_2 & \cdots & \varepsilon_N \end{bmatrix} = -\lambda - \begin{bmatrix} \bar{\lambda}_1 d_{11} & \bar{\lambda}_2 d_{12} & \cdots & \bar{\lambda}_N d_{1N} \\ \bar{\lambda}_1 d_{21} & \bar{\lambda}_2 d_{22} & \cdots & \bar{\lambda}_N d_{2N} \\ \vdots & \vdots & \cdots & \vdots \\ \bar{\lambda}_1 d_{51} & \bar{\lambda}_2 d_{52} & \cdots & \bar{\lambda}_N d_{5N} \end{bmatrix} = -\lambda - \begin{bmatrix} \begin{bmatrix} d_1 \\ d_2 \\ \vdots \\ d_5 \end{bmatrix} \bar{\lambda} K \end{bmatrix} \tag{100}$$

Thus

$$d\beta = -\phi\varepsilon^T = \phi\left(\beta^T\phi - T\right)^T = \phi\phi^T\beta - \phi T^T \tag{101}$$

$$\left(\phi\phi^T - dI\right)\beta = \phi T^T \Rightarrow \beta = \left(\phi\phi^T - dI\right)^{-1}\phi T^T \tag{102}$$

The optimal estimate of the output weight matrix β derived in (102) can then be used in the SLFN in Figure 27 for the prediction of the system state defined in the output vector in (65)

4.3 Model validation

To illustrate the SLFN modeling for VCC dynamics proposed in this paper, we consider an SLFN with 50 hidden nodes, five output nodes and six input nodes, to model the measured system states with high frequency noise. The input data vectors to the SLFN are operating states under different cooling loads. The desired output values of the SLFN, providing with the desired values of the model, for all input data vectors, are measure by using the pressure, temperature sensors and power meter, respectively.

For comparison purpose, we have implemented the trainings of the SLFNs with the BP, the SVR and constraint ELM, respectively, with the training data pairs measured with the high frequency noises due to the density wave instability [73-75]. To evaluate the generalization performance after training, the SLFN models are tested with 1000 groups of measured data disturbed with high frequency noises.

Both the training and testing results for evaporating and condensing pressures are depicted in Figure 28 to Figure 35, where the predicted values are provided by the SLFNs trained with the BP, the SVR and the ELM, respectively. It is seen that the prediction deviations

of these two pressures obtained from the SLFN with the ELM are the smallest, the corresponding points are closer to the middle line. Its prediction errors of P_c and P_e are almost within $\pm 4.5\%$ and $\pm 7\%$, respectively. The prediction errors of SVR, on the other hand, are within $\pm 6\%$ and $\pm 10\%$, respectively, which are slightly larger than that of ELM. It is also noticeable that the deviations of the predicted value obtained from the SLFN with the BP are much larger than the other two algorithms, the maximum deviation of condensing and evaporating predictions can even reach 12% and 17%, respectively.

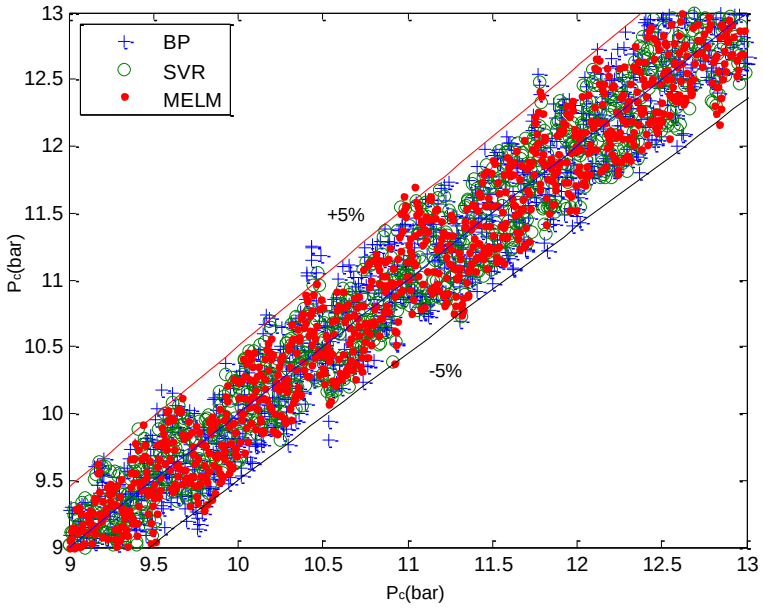

Figure 28 P_c Training Accuracy

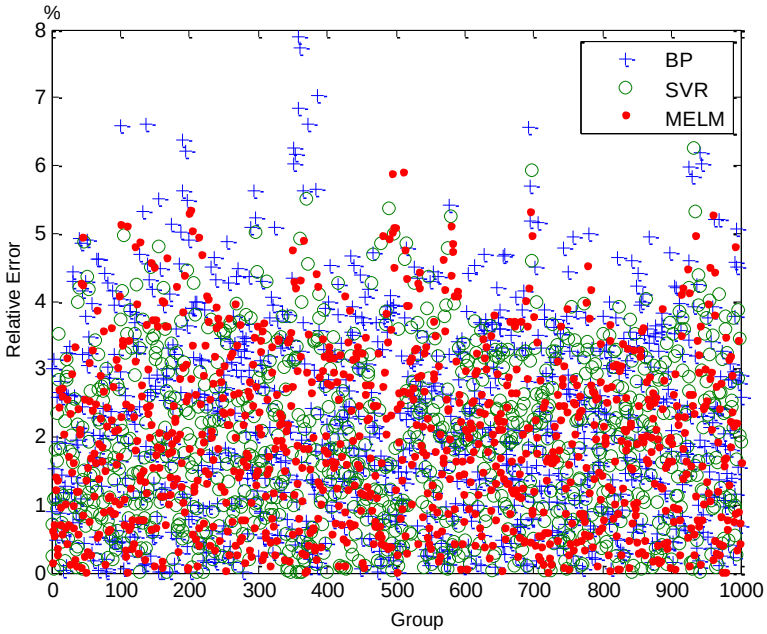

Figure 29 RME of P_c Training

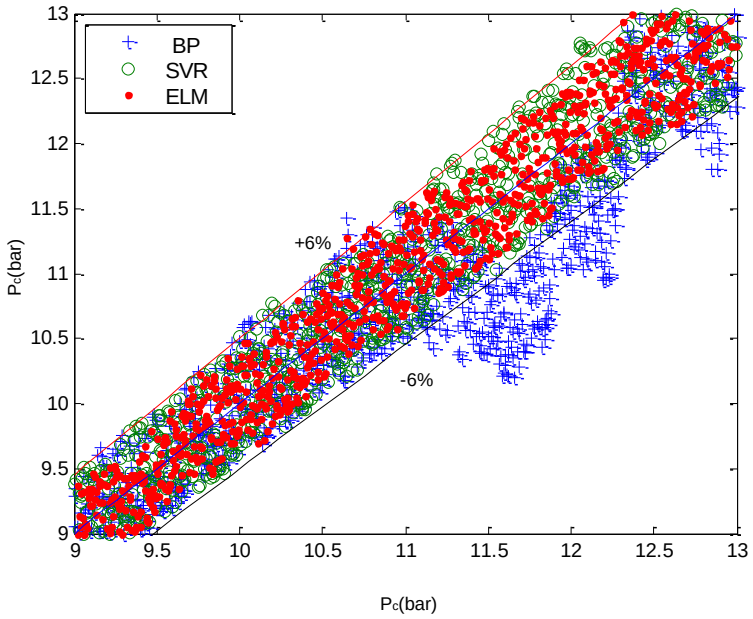

Figure 30 P_c Testing Accuracy

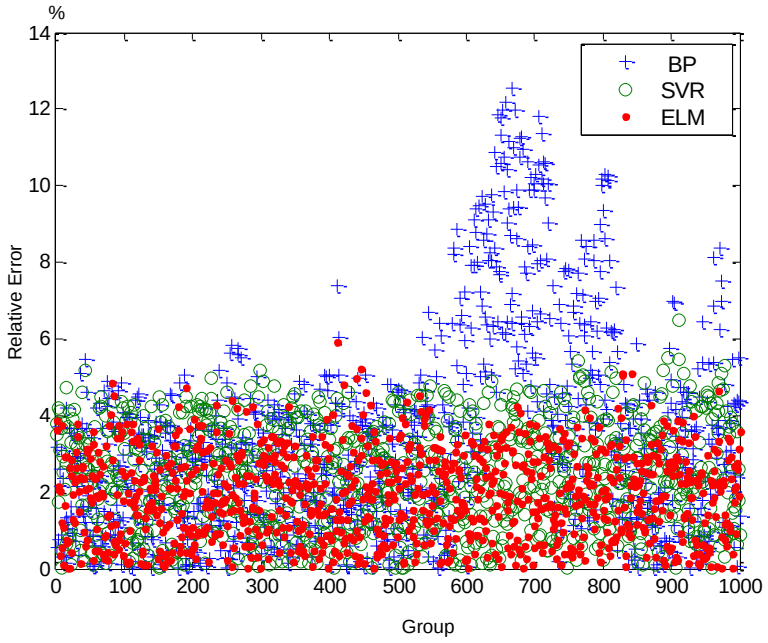

Figure 31 RME of P_c Testing

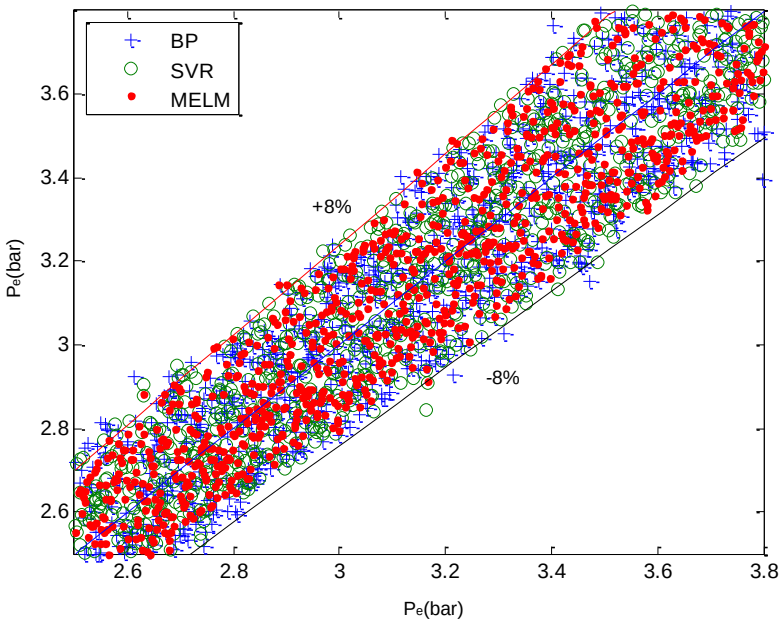

Figure 32 P_e Training Accuracy

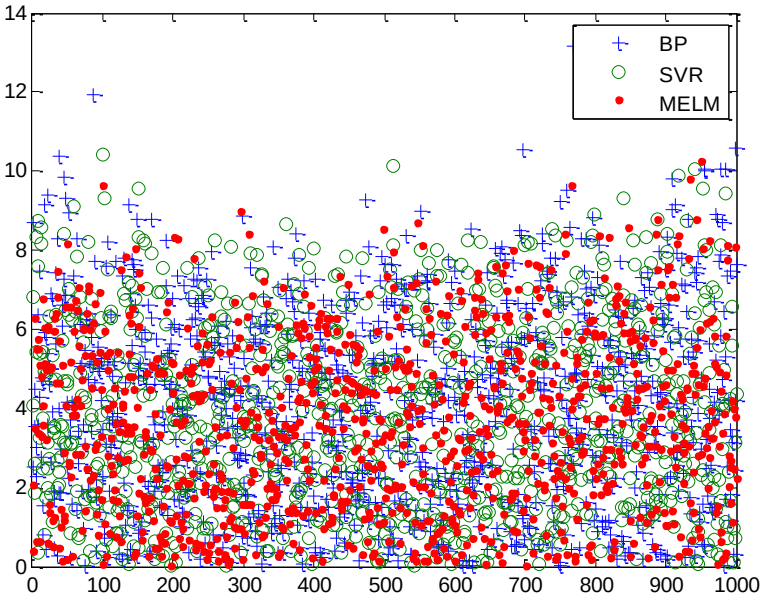

Figure 33 RME of P_e Training

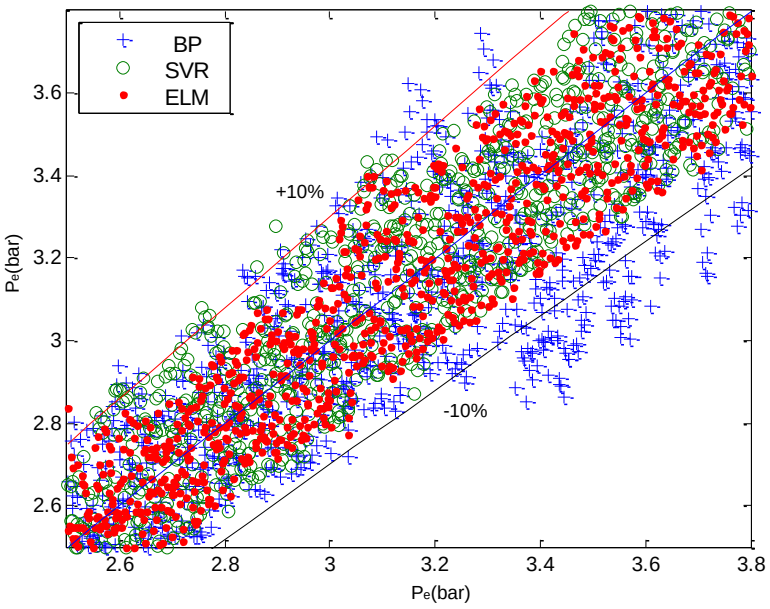

Figure 34 P_e Testing Accuracy

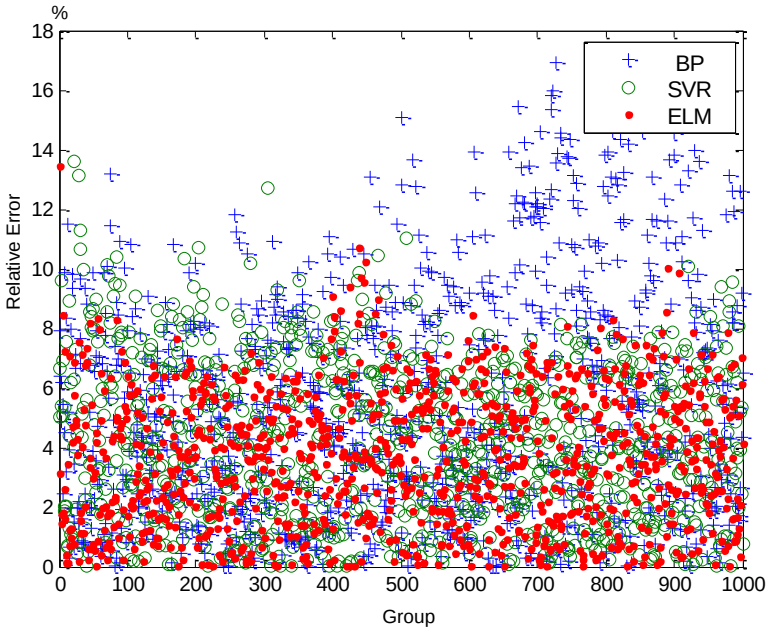

Figure 35 RME of P_e Testing

Recall that it is preferable for the vapor to be slightly super-heated for the purpose of compressor protection. According to the minimum stable signal (MSS) line proposed by Huelle [76], the temperature of the evaporator tube wall will fluctuate if the degree of superheat is below a certain value. Because of the 5C minimum superheat of the experiment system, both the SLFN training and testing set the range from 5 to 25C. Figure 36 to Figure 43 show the training and testing performances of the SH and the SC with the SLFNs trained with the ELM, the SVR and the BP, respectively. It has been seen that the prediction deviations of both SH and SC obtained from the SLFN with the BP are larger than 11% and 20% respectively. Furthermore, these prediction errors tend to increase as SH grows. However, the prediction errors of both the ELM and the SVR are within $\pm 7\%$. Furthermore, the prediction errors of SVR also shows the trend of growth for large SH, which is not found in SC prediction. In contrast, performances of ELM are stable in spite of a large testing range. It is also noticeable that the tested ELM consists of only 50 hidden nodes, considering that the advantage of ELM is its high speed for training large scale SLFN, if more hidden nodes are added, the prediction errors of ELM can be significantly reduced with a little more additional time.

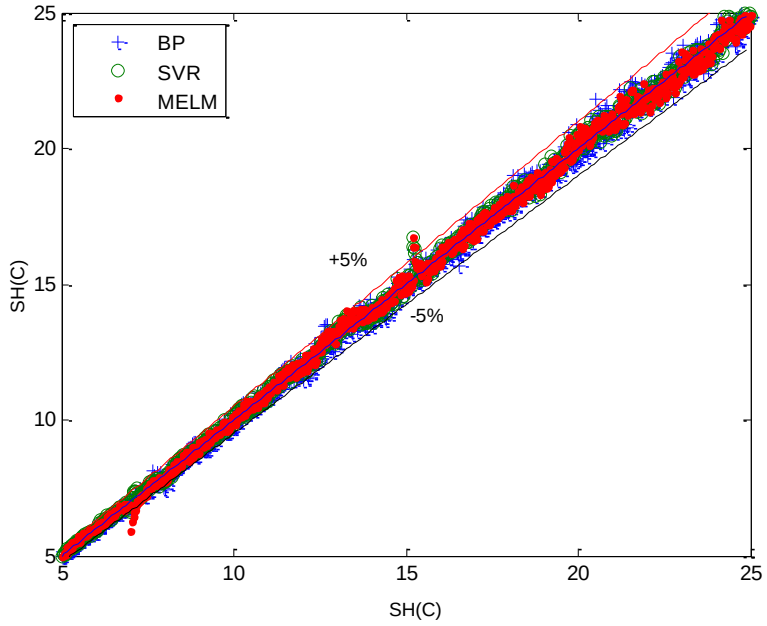

Figure 36 *SH* Training Accuracy

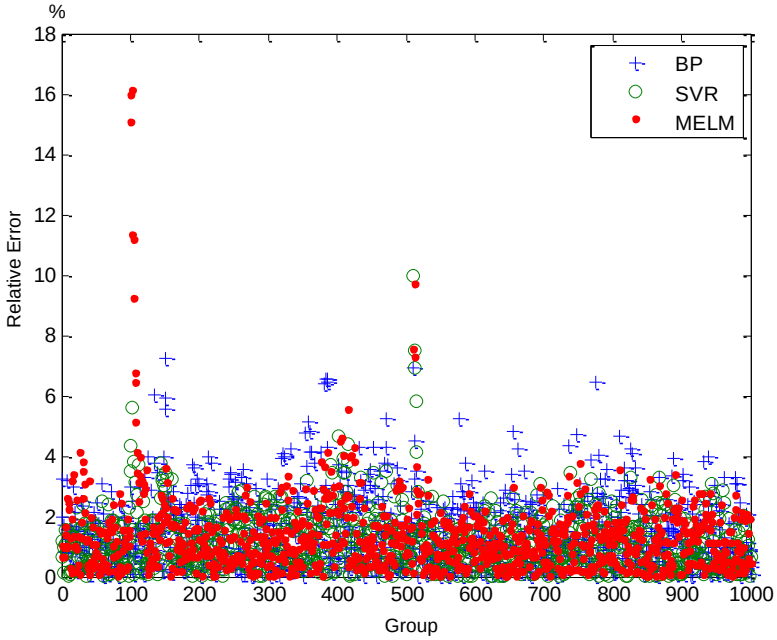

Figure 37 RME of *SH* Training

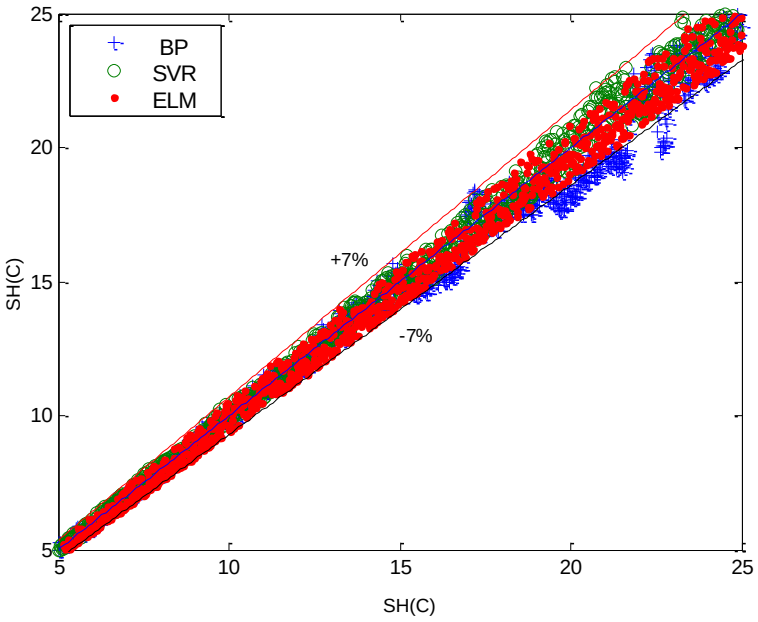

Figure 38 *SH* Testing Accuracy

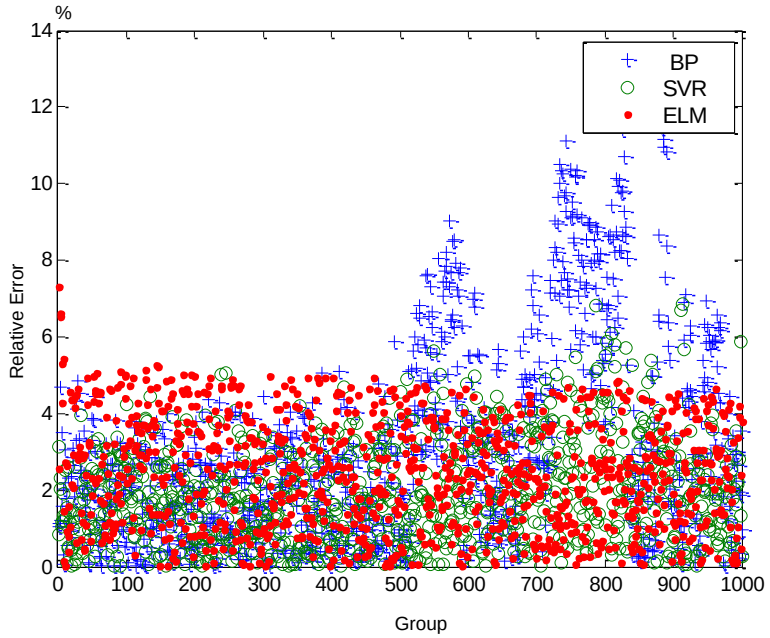

Figure 39 RME of *SH* Testing

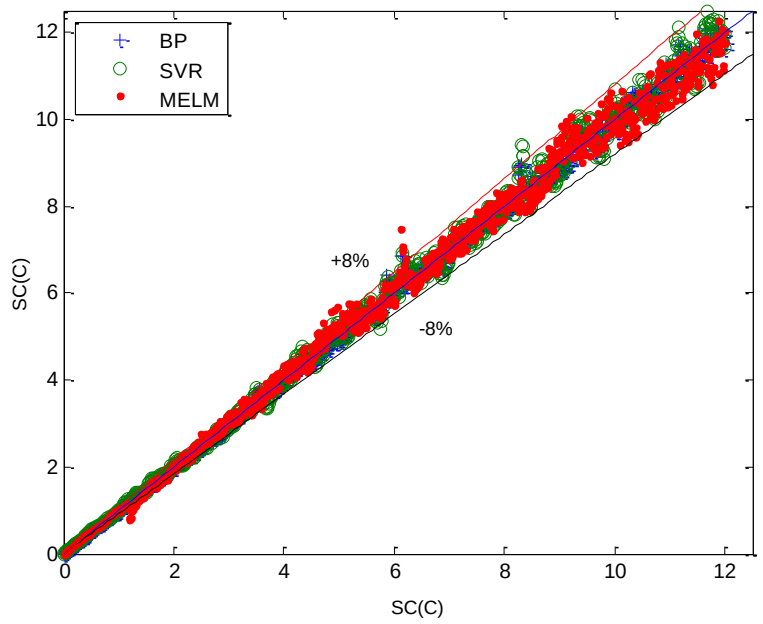

Figure 40 *SC* Training Accuracy

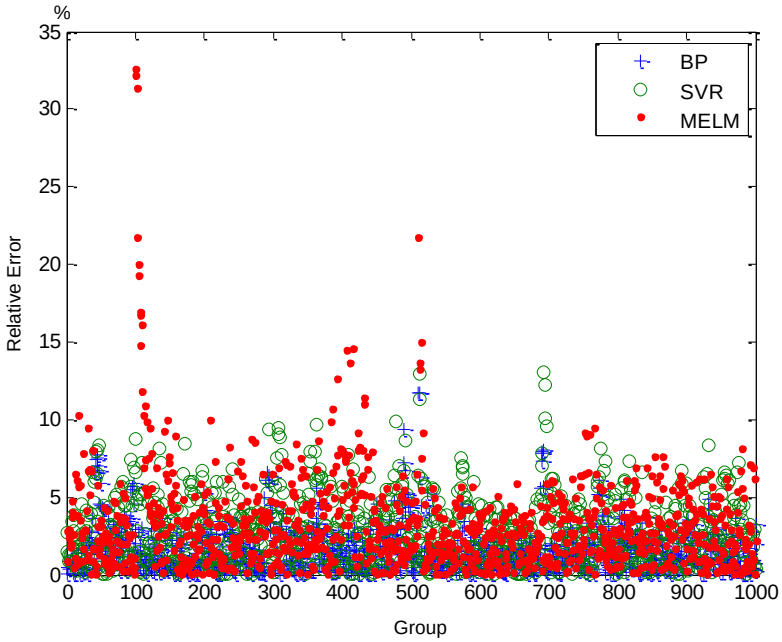

Figure 41 RME of *SC* Training

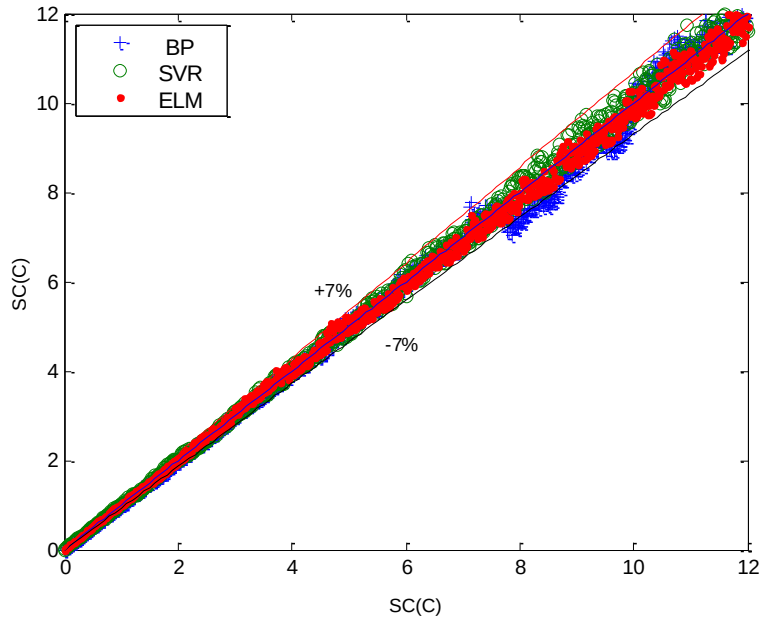

Figure 42 *SC* Testing Accuracy

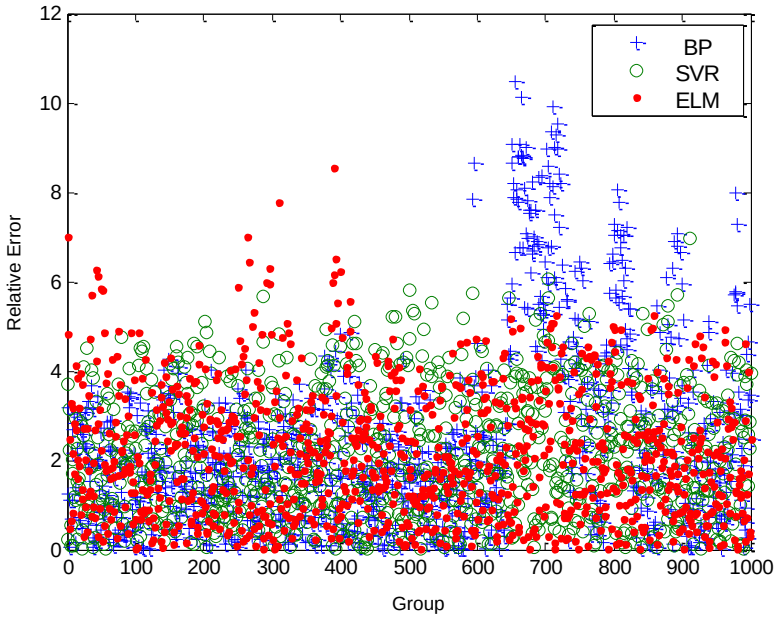

Figure 43 RME of *SC* Testing

The energy consumption, as an output of the SLFN model, aims at identifying the sum of the energy consumptions of compressor, condenser and evaporator fans. Because the power meter cannot directly measure the transient energy consumption, and all the energy

consumption devices have complex transient responses, the training and testing energy consumptions are all generated by using the hybrid model whose coefficients are determined with fitting the measured energy consumption data under the steady states.

It can be seen from Figure 44 to Figure 47 that the testing performance of the SLFN with BP is the worst compared with the ones with the SVR and the ELM. This is because the BP is based on the gradient decent method to search the global minimum in the weight space. How to improve the robustness of the trained weights is not considered in the BP algorithm. In addition, for the SLFN with a large number of hidden nodes, the BP training can be easily trapped at some local minima. It can be further seen from the figures that, although the performance of the SLFN with the SVR is better than the one with the BP, the characteristic of global optimization with the consideration of improving the robustness with respect to the disturbances in the cost function as well as the Lagrange function in (24) and (31) has made the SLFN trained with the ELM have the smallest the average RME, compared the ones with the BP and the SVR.

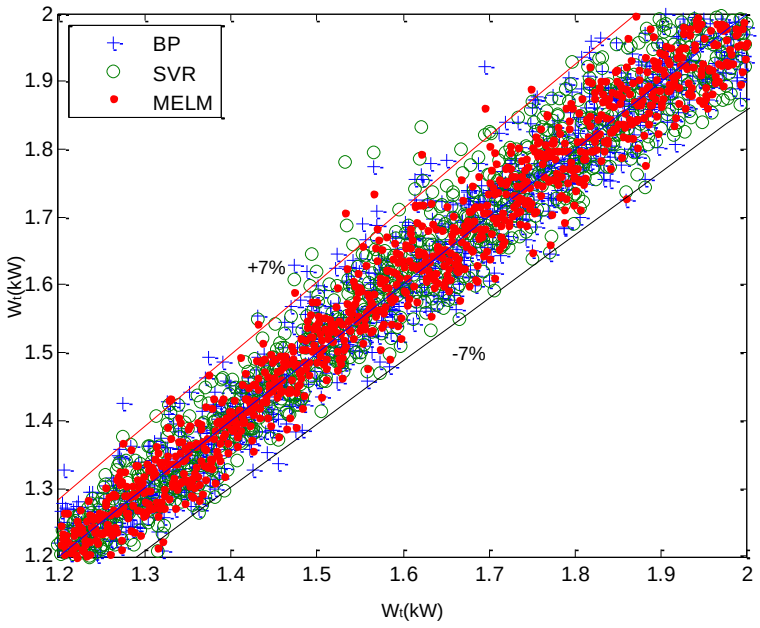

Figure 44 W_t Training Accuracy

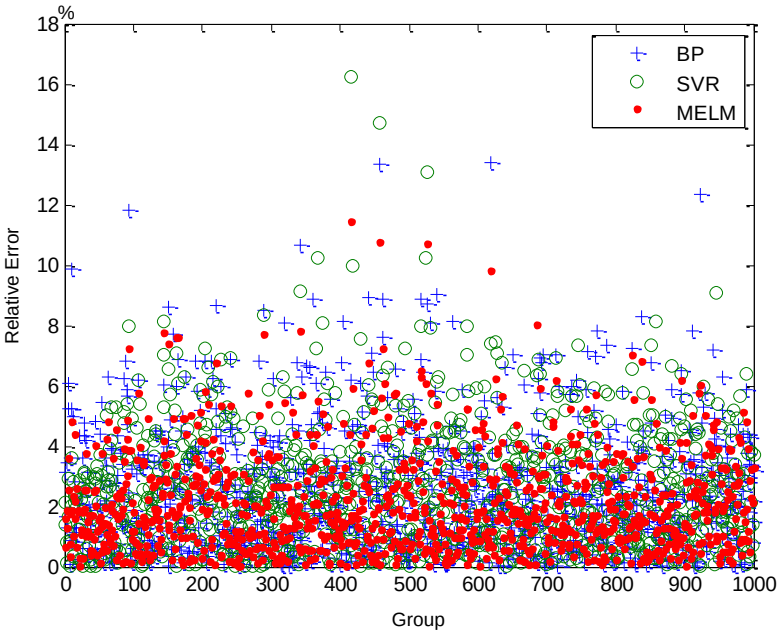

Figure 45 RME of W_t Training

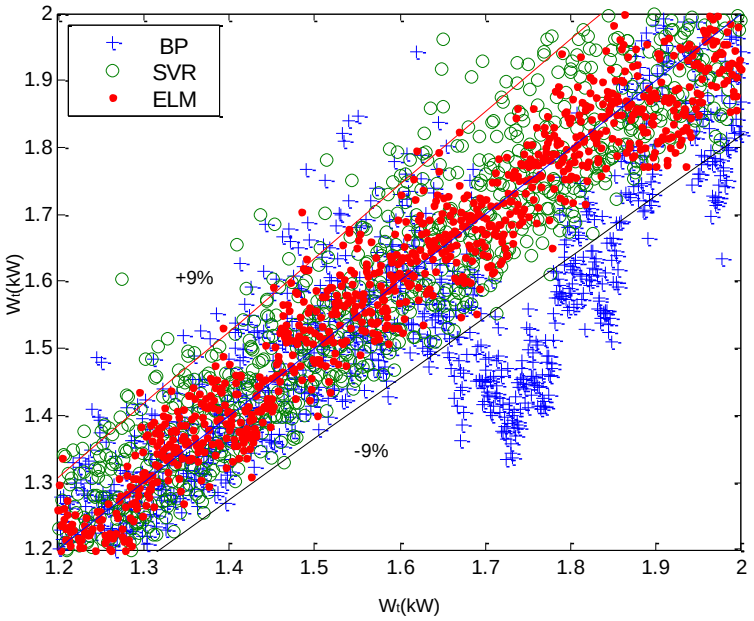

Figure 46 W_t Testing Accuracy

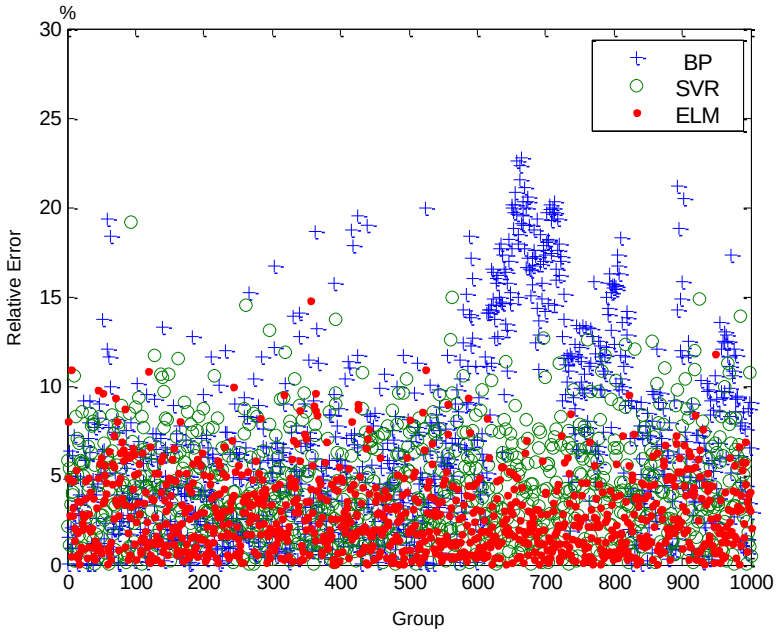

Figure 47 RME of W_t Testing

To specifically prove the accuracy of large scale SLFN trained with the proposed ELM, Table 3 shows the comparisons of both the MSEs and RMEs of the SLFN trained with the BP (with 30 hidden nodes), the SVR, and the ELM (with 500 hidden nodes), respectively. It has been seen that the training time for the SLFN with the BP is the longest because of its recursive feature for the training both the input weights and the output weights. However, the training time of the SLFN with the ELM is the shortest. This point can be easily understood in the sense that no updating is needed for the randomly selected input weights of the SLFN during the training.

Table 3 The comparison of training and testing accuracies

	BP				SVR				ELM			
	MSE		RME		MSE		RME		MSE		RME	
	train	test	train	test	train	test	train	test	train	test	train	test
P_c	0.2951	0.3828	2.28%	2.77%	0.2460	0.2767	1.90%	1.95%	0.2010	0.2261	1.53%	1.57%
P_e	0.1636	0.2387	4.00%	5.65%	0.1629	0.1732	3.99%	4.16%	0.1134	0.1261	2.76%	2.85%
SH	0.3112	0.6962	1.53%	3.34%	0.3087	0.4237	1.43%	2.71%	0.2460	0.3193	1.07%	1.91%

SC	0.2358	0.3363	2.03%	2.53%	0.2315	0.2668	2.02%	2.18%	0.1890	0.2010	1.60%	1.64%
Wt	0.0313	0.0929	2.52%	7.56%	0.0311	0.0510	2.55%	4.37%	0.0213	0.0270	1.71%	2.18%

Table 4 shows the comparisons of the training times as well as the testing times that are used for the SLFNs trained with the BP (30 hidden nodes), the SVR and the ELM (with 50, 200 and 500 hidden nodes), respectively. Obviously, the SLFN trained with the ELM performs the best.

Table 4 Computation of training times

Algorithm	Training Time(s)	Testing Time(s)
BP(30 hidden nodes)	12.2704	0.0622
SVR	15.7823	4.3642
ELM(50 hidden nodes)	0.0936	0.0570
ELM(200 hidden nodes)	0.1312	0.0624
ELM(500 hidden nodes)	0.5148	0.0980

4.7 Summary

In this chapter, the SLFN trained with the ELM has been used for modeling the dynamics of vapor compression cycle. It has been seen that the designed SLFN model trained with the ELM can achieve the smallest modeling error as well as improve the robustness with respect to disturbances and system uncertainties compared with other intelligent method such as BP and SVR. The testing results in the simulation section have further shown the excellent prediction accuracy and robustness of the SLFNs trained with the ELM with respect to the high frequency disturbances.

Chapter 5 Optimization of VCC Based on ELM

5.1 VCC optimization problem formulation

The objective of global optimization for vapor compression refrigeration cycle is to meet cooling load requirement of cold reservoir with minimal energy consumption. Mathematically, it can be formulated as

$$\begin{aligned} &\textbf{Min } \dot{W}_{sy} = f(F_{com}, F_{c,a}, F_{e,a}, A_v, T_{out}, T_{in}) \\ &\text{Subject to } \dot{Q}_e = \dot{Q}_{req} \end{aligned} \tag{103}$$

where $\dot{W}_{sy}$ and $\dot{Q}_{req}$ are total electricity power consumption and cooling load requirement, respectively.

To ensure system operates properly, system states must be within the permissible working range, the corresponding constraints are listed as following:

1. Air mass flow rates of condenser and evaporator fans

$$\begin{aligned} \dot{m}_{c,air,min} \le \dot{m}_{c,air} \le \dot{m}_{c,air,max} \\ \dot{m}_{e,air,min} \le \dot{m}_{e,air} \le \dot{m}_{e,air,max} \end{aligned} \tag{104}$$

   where $\dot{m}_{c,air,min}$, $\dot{m}_{c,air,max}$, $\dot{m}_{e,air,min}$ and $\dot{m}_{e,air,max}$ are minimal and maximal condenser air mass flow rates, minimal and maximal evaporator air mass flow rates, respectively.

2. Condensing and evaporating temperatures

$$\begin{aligned} T_{c,air,i} \le T_{c,r,o} \le T_{c,min} \le T_{c,r,sat} \le T_{c,max} \le T_{c,r,i} \\ T_{e,r,i} \le T_{e,min} \le T_{e,r,sat} \le T_{e,max} \le T_{e,air,i} \end{aligned} \tag{105}$$

   where $T_{c,min}$, $T_{c,max}$, $T_{e,min}$, and $T_{e,max}$ are minimal and maximal condensing temperatures, minimal and maximal evaporating temperatures, respectively.

3. Condensing and evaporating pressure

$$\begin{aligned} P_{c,min} \le P_c \le P_{c,max} \\ P_{e,min} \le P_e \le P_{e,max} \end{aligned} \tag{106}$$

   where $P_{c,min}$, $P_{c,max}$, $P_{e,min}$, and $P_{e,max}$ are minimal and maximal condensing pressure, minimal and maximal evaporating pressure, respectively.

4. Superheat

$$5^{\circ}C \le T_{e,sh} \le 25^{\circ}C \tag{107}$$

where $T_{e,sh}$ is the evaporator superheat, superheat temperature too low will cause oscillation in the cycle [76-78], while the COP of system will decrease steeply if the superheat temperature is too high [4]. The upper and lower limits depend on the system configurations.

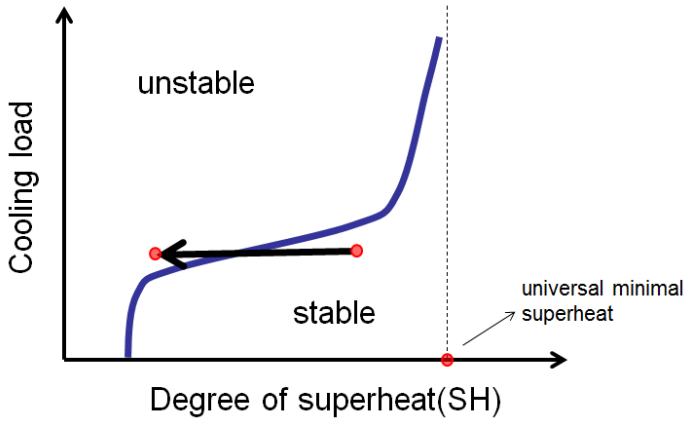

Figure 48 Superheat effects on system stability

5. Subcool

$$T_{c,sc} \ge 0 \tag{108}$$

where $T_{c,sc}$ is the subcool temperature. Subcool only has lower bound to ensure the refrigerant at expansion valve inlet is at liquid phase for flashing.

6. Compressor Frequency (for the testing system)

$$30Hz \le F_{com} \le 50Hz \tag{109}$$

This physical constraint is directly determined by compressor working range.

7. Mass flow rate of refrigerant

$$\dot{m}_{r,min} \le \dot{m}_r \le \dot{m}_{r,max} \tag{110}$$

where $\dot{m}_{r,min}$ and $\dot{m}_{r,max}$ are minimal and maximal refrigerant mass flow rate, respectively. The upper bound of mass flow rate of refrigerant is determined by expansion valve and compressor capacities, the lower bound is determined by flow meter working range.

8. EEV opening percentage

$$0 < A_v \leq 1 \tag{111}$$

Based on air conditioning optimization problem and ELM properties, the system optimization based on ELM can be separated into the following steps:

Normalization:

The training and testing data are usually normalized so that they fall in a specifically given interval. It can considerably accelerate weight learning and avoid saturation or overflow of the hidden and output neurons, since its activation values generally fall in the [0,1]. At last, an unnormalization step is necessary to convert ELM outputs back into unnormalized units.

The normalization method for the input variables and output variables can be described as follows:

$$\begin{aligned} x_{norm} &= \left(x - \min(x)\right) / \left(\max(x) - \min(x)\right) \\ y_{norm} &= (y - \min(y)) / (\max(y) - \min(y)) \end{aligned} \tag{112}$$

The operators min(⋅) and max(⋅) in Eq. (112) are used to select the minimum and maximum values from the given data series, respectively.

Classification:

It is necessary to analyze system stability under certain set point before determining the energy consumption, which can be regarded as a classification problem. The classification algorithm is provided with a set of training state sets where positive label indicates that system is in stable state while negative label represents system fluctuation. The success of the classification depends mainly on the manner in which the patterns are represented by discernible features. The features that are selected for this should allow a separation of the patterns in as unambiguous a manner as possible. To avoid the curse of dimensionality, PCA based on multiplication between two covariance matrices is employed for input features selection. The set of characters to be recognized were chosen to be the states of VCC cycle. The 6 * 1 vector as follows is used for their representation.

$$x = [\omega \quad F_c \quad F_e \quad Q_e \quad T_{out} \quad T_{in}] \tag{113}$$

This set of features allows a sufficient characterization of system stability. Since all these features are physically constrainted, the permissible input vectors form a high dimensional rectangle that is regarded as the working rectangle. All classifications and optimizations are performed only inside this rectangle. Therefore, the classifier can be constructed as illustrated in Figure 49.

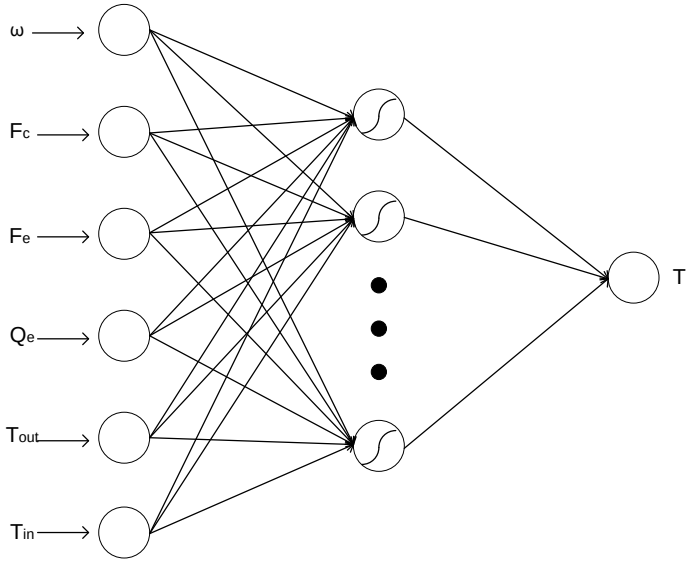

Figure 49 Stability Classifier

ELM is employed to train the classifier. The number of hidden layer nodes is determined to balance training performance and speed. The activation function in the hidden layer, an important feature influencing the network performance, was chosen as sigmoid function, as follows:

$$f(x) = \frac{1}{1+e^{-x}} \tag{114}$$

Energy Consumption Model:

The key to any successful optimization scheme in VCC is an accurate model of system energy consumption. Similar to the classifier, SLFN is used for modeling energy consumption. A total of six variables were used as the input parameters for the input nodes of the input layer. Three variables were related to the energy consumption of the whole system (energy consumption of compressor, condenser and evaporator fans). In general, frequencies of compressor, evaporator and condenser fans are critical to energy consumption modeling. Therefore, these three variables together with cooling load,

indoor and outdoor temperatures are used to account for system performance. The architecture of SLFN for modeling is shown in Figure 50. The transfer function adopted for the hidden layer neurons is sigmoid function. It is noticeable that the proposed energy consumption model consists of one additional summation layer, which aims at analyzing the prediction accuracy of the three components separately. Weights of this layer are fixed at 1. The weights of first layer and second layer are randomly assigned and calculated through least square method respectively, according to ELM.

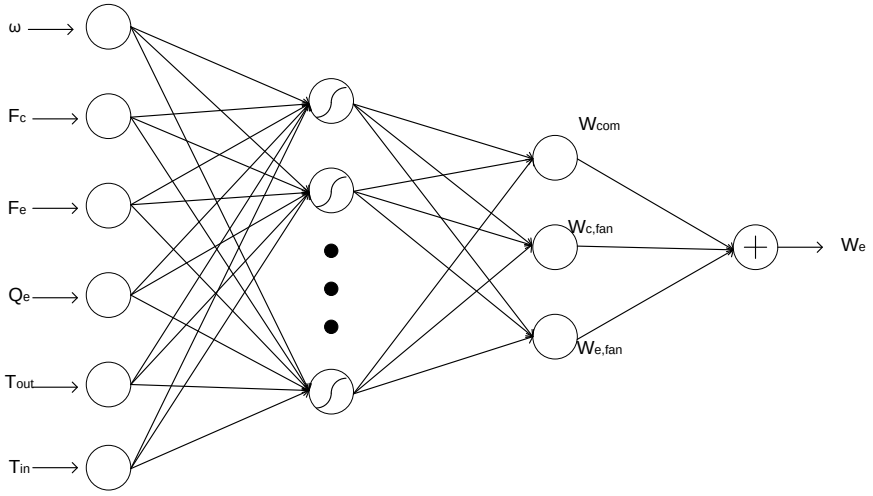

Figure 50 Energy consumption model

Grid Search:

VCC optimization can be regarded as a large-scale and highly nonlinear optimization problem. Some difficulties may rise when trying to solve this problem using gradient based methods. This difficulty together with the high speed of ELM training necessitates the employment of direct grid search method to find the optimal set points.

Specifically, to obtain required cooling capacity under certain outdoor and indoor air temperatures, combinations of different value of independent variables within the working rectangle are classified and input to the energy prediction model for evaluation. Its pseudo code is as following:

initialize Sol, $Q_e, T_{out}, T_{in}, W_{e,\min}$

for $\omega=\omega_{\min}$ to $\omega_{\max}$ step $\omega_{interval}$

for $F_{ca} = F_{ca,\min}$ to $F_{ca,\max}$ step $F_{c,interval}$

for $F_{ea} = F_{ea,\min}$ to $F_{ea,\max}$ step $F_{e,interval}$

$T = f_{classifier}(\omega, F_{ca}, F_{ea}, Q_e, T_{out}, T_{in})$

if $T > 0$

$W_t = f_{ELM}(\omega, F_{ca}, F_{ea}, Q_e, T_{out}, T_{in})$

if $W_{t,\min} > W_t$

$W_{t,\min} = W_t$

$Sol = [\omega, F_{ca}, F_{ea}]$

end if

end if

end for

end for

end for

5.2 Solution procedure

The algorithm procedure:

The proposed optimization algorithm procedure is illustrated by Figure 51

Step 1: Data collection

Collect the indoor and outdoor environment data $\dot{Q}_{e,req}, T_{in}, T_{out}$. These uncontrollable variables are considered as constants during the whole sampling period..

Step 2: Normalize the experiment data

All the input and output values were normalized through Eq. (112). Initialize the optimal energy consumption marker, which is used to store the minimal energy consumption of searched range.

Step 3: Determine input variables

Choose independent variables within the operating range according to the grid search method.

Step 4: Check feasibility

Check whether the input variables are feasible with classifier, if not feasible, return to Step 3.

Step 5: Calculate energy consumption

Calculate the energy consumption of the input variables determined in step 3 with ELM.

Step 6: Comparison

Compare the energy consumption obtained in step 5 with the minimal energy consumption marker, if the former one is smaller, replace the optimal solution and minimal energy consumption with the curr5ent input.

Step 7: If all the independent variables reach their maximum, terminate the optimization process, else, return to step 3.

Step 8: Test the optimization results on the experiment system.

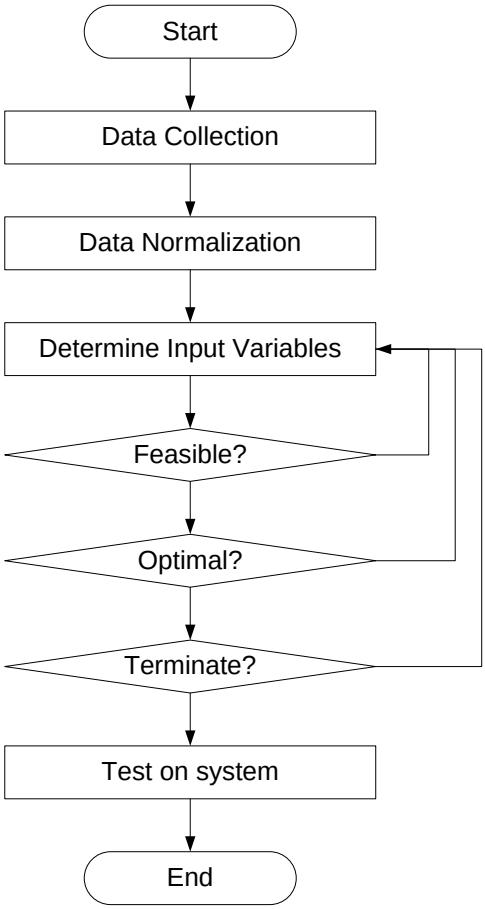

Figure 51 Flow chart of optimization algorithm based on ELM

5.3 Simulation and experiment

5.3.1 ELM classification results evaluation:

For comparison purpose, we have implemented the trainings of the classifiers with the BP, the SVR and ELM, respectively, with the training data pairs measured under different

conditions covering the working rectangle. To evaluate the generalization performance after training, the classifiers are tested with 100 groups of measured data with or without fluctuation.

The training and testing performance of SLFN with BP, SVM and ELM are shown in Figure 52 and Figure 53.

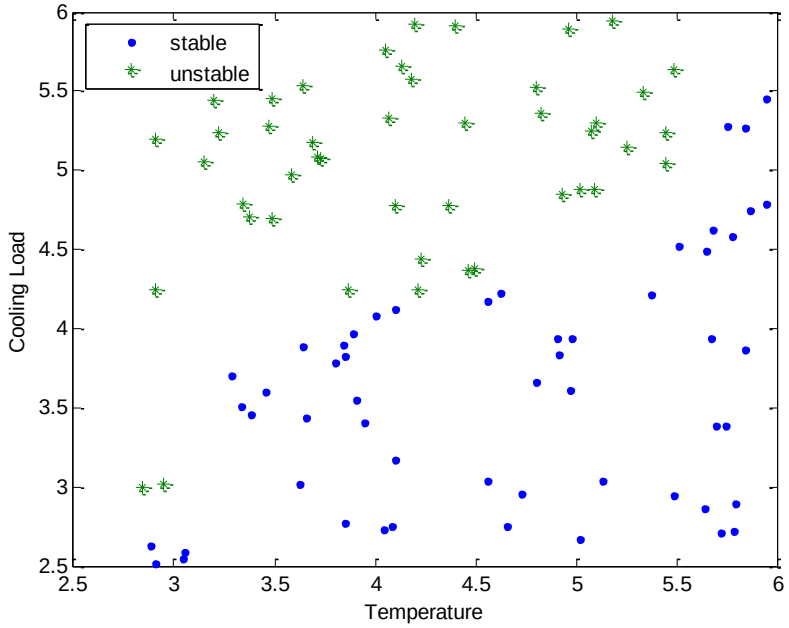

Figure 52 Training results of classification

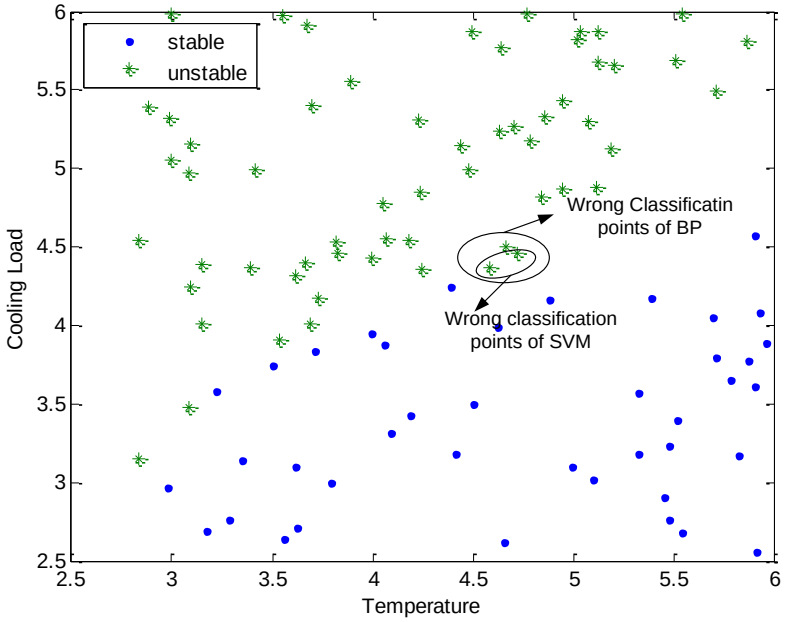

Figure 53 Testing results of classification

Recalling the minimum stable signal (MSS) line proposed by Huelle [76], since cooling load and superheat are two key factors to determine system stability, they will be regarded as abscissa and ordinate in the classification figures. Figure 52 and Figure 53 show the classification performances of stability with the SLFNs trained with the ELM, the SVR and the BP, respectively. It has been seen that all three algorithms can classify the training set with 100% accuracy. However, the SLFN trained with SVR and BP had wrong classification for testing. BP and SVR regarded three and two unstable points as stable, respectively. These wrong classifications can cause fluctuation and may destroy the compressor. In contrast, the classifier trained with ELM shows better generalization capability, classifies all testing points correctly. Furthermore, the training time of SLFN with ELM, SVR and BP are 0.0312s, 2.0546s and 1.8408s, respectively. If large scale training set is used for training, the speed advantage of ELM will be more obvious. This speed advantage also indicates that ELM has bright potential in on-line modeling and optimization.

5.3.2 ELM fitting energy consumption results evaluation:

To illustrate the SLFN modeling for energy consumption proposed in this paper, we consider an SLFN with 50 hidden nodes, one output node and six input nodes, to model

the measured system energy consumption under different cooling load. The input data vectors to the SLFN are operating states with different cooling loads. The desired output reference values of the SLFN, provided with the desired values of the model, for all input data vectors, are measured by power-meter.

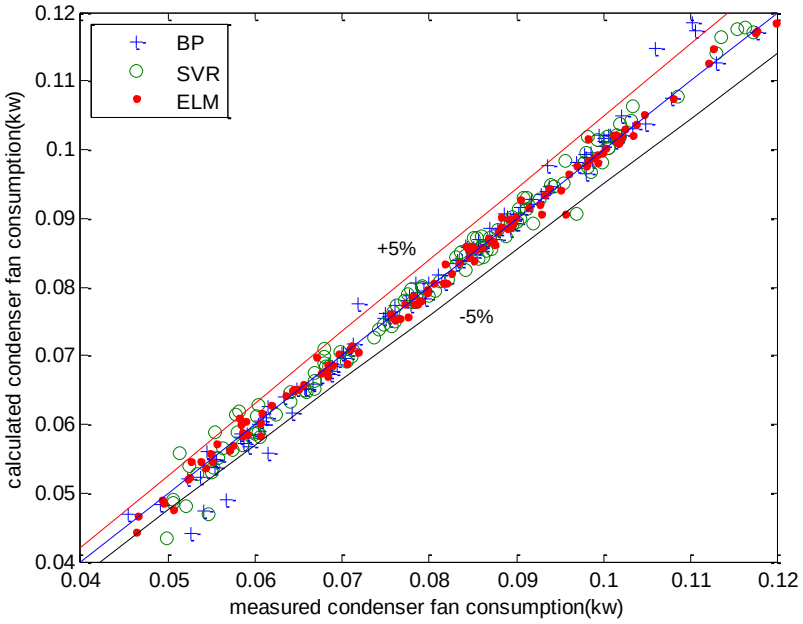

Figure 54 Condenser fan energy consumption of test group

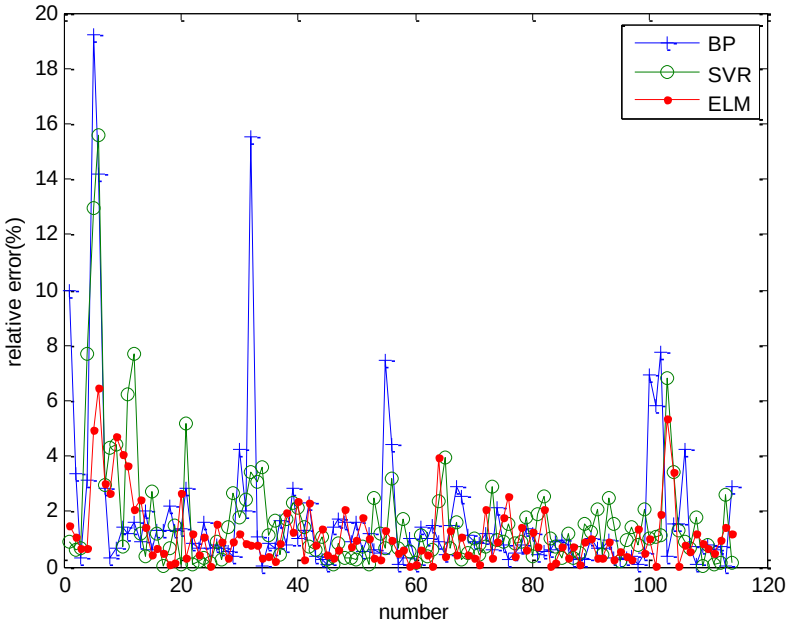

Figure 55 Relative errors of condenser fan model

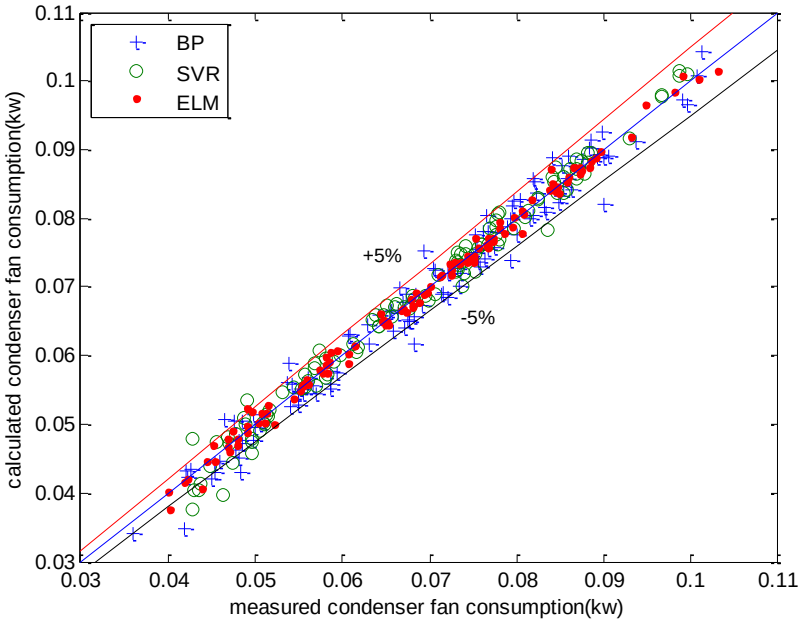

Figure 56 Evaporator fan energy consumption of test group

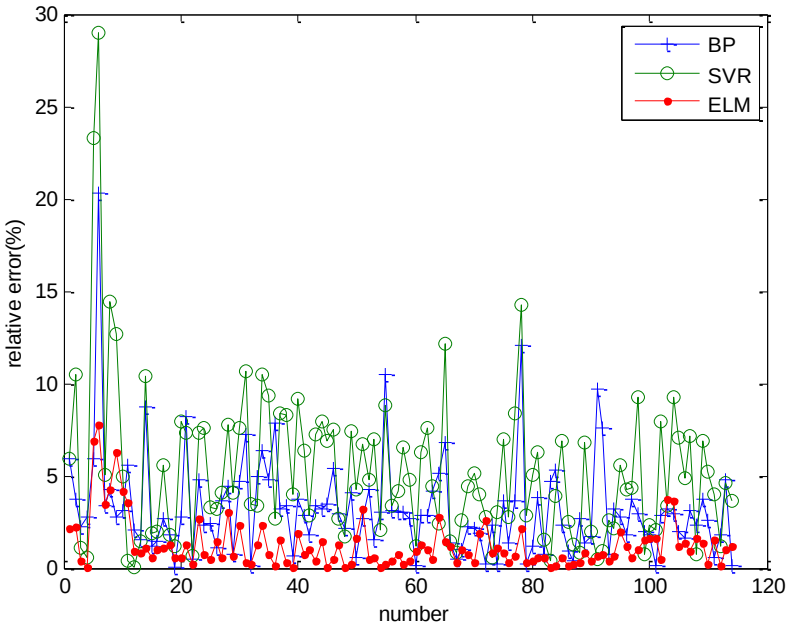

Figure 57 Relative errors of evaporator fan model

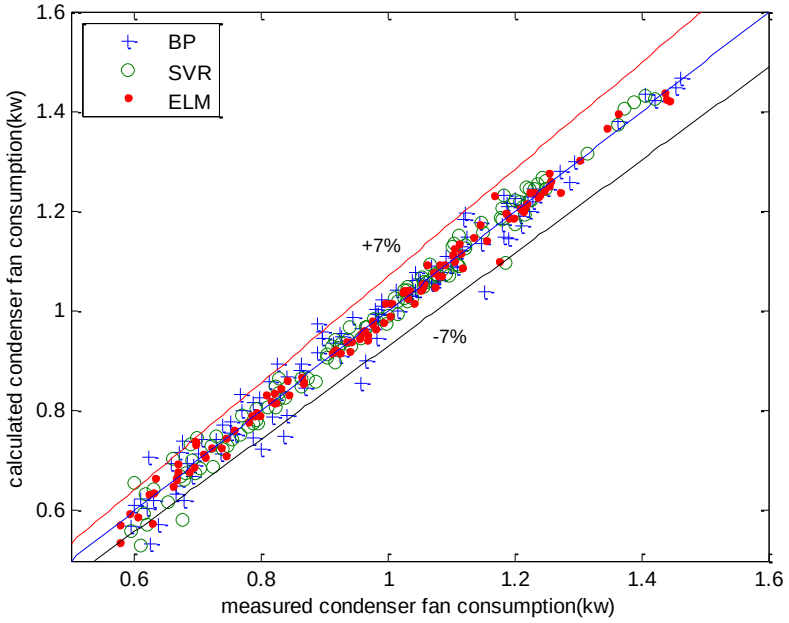

Figure 58 Compressor energy consumption of test group

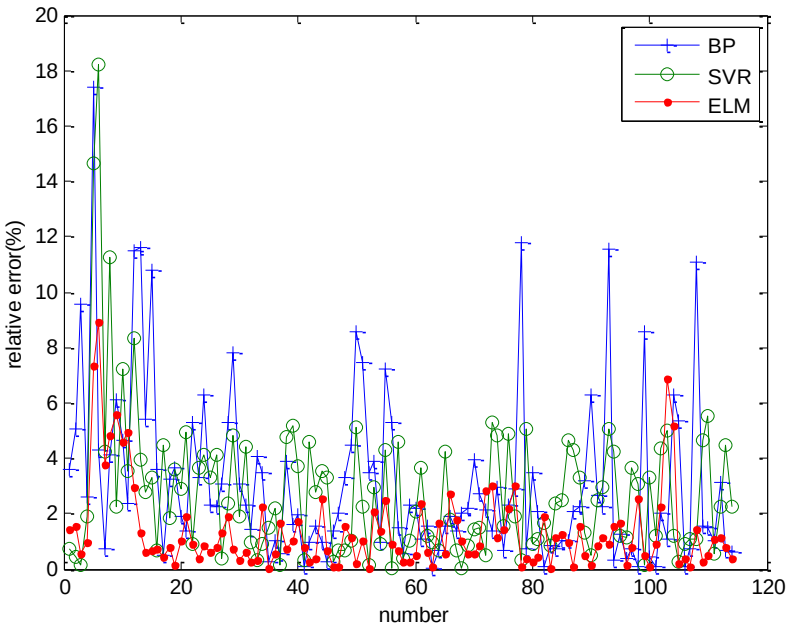

Figure 59 Relative errors of compressor model

Both the predicted and the measured experimental values for energy consumptions of test groups are depicted in Figure 54 to Figure 59, where the predicted values are provided by the SLFNs trained with the BP, the SVR and the ELM, respectively. The fitting results

validate the former claim that ELM has the best test performance for VCC modeling compared with BP and SVR. The testing deviations of ELM are within 4%, 3% and 5% for condenser fan, evaporator fan and compressor. The corresponding deviation for BP and SVR are 8%, 10% and 12%; 8%, 11% and 6%.

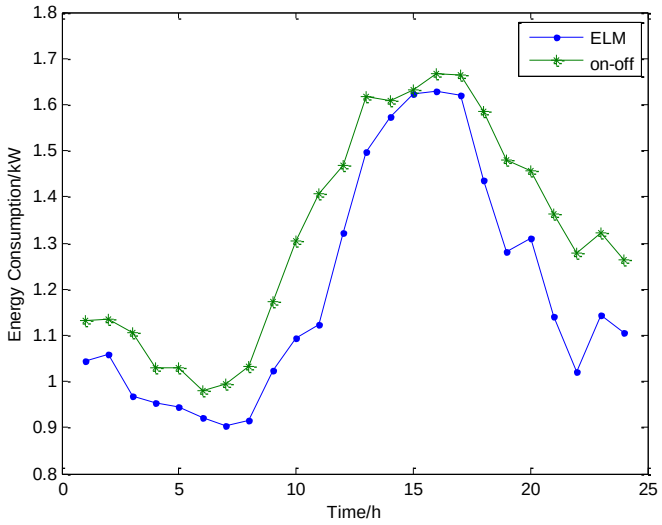

Figure 60 Experiment Results of ELM based optimization

With regard to the experiment results, the accuracy of system model and the effect of the optimization method can be justified. The energy consumptions of ELM based optimization are smaller than that of on-off control for all time intervals. When the cooling load is close to the maximum value, the energy saving effect decreases, giving the optimal effects when the cooling load is around 75% of the full load. The overall energy saving effect of ELM is 6.64% compared to on-off control.

5.4 Summary

The global optimization method for VCC system has been developed based on neural modeling and grid search method. SLFN trained with ELM is introduced to classify system stability and to predict its energy consumption, based on other controllable and environmental parameters, for calculating the optimal set point concerning a VCC system in which four controllable variables are to be optimized. The training and testing results of SLFN with BP, SVM and ELM are compared to show the advantages of proposed method in terms of speed and generalization capability. The SLFN with ELM classifies all points correctly and has the best generalization performance while the SLFN with BP and SVM

has 3% and 2% testing error, respectively. The relative mean training error of energy consumption prediction with ELM, BP and SVM are within 3%, 5% and 11%, respectively. Their counterparts in the testing sets are within 5%, 7% and 24%, respectively. These results show the excellent prediction accuracy of the proposed method as well as its remarkable speed. The results of energy conservation (system coefficient of performance) under optimal operation and non-optimal operation manifest that the energy conservation brought by the ELM based optimization scheme will become more significant under lower load operation of the air-conditioning system, and the overall energy conserved for one typical day is 6.64%. The simulation and experiment results show that the optimization algorithm based on ELM can effectively optimize system operation.

Chapter 6 Centralized Optimization of VCC

6.1 Introduction

Aiming at saving vapor compression refrigeration cycles energy consumption, many research works has been done on improving the system coefficient of performance (COP) through control or optimization. Stoecker [4]claimed that the slightly sub-cooled refrigerant leaving industrial refrigeration condensers is not normally desired as some of the condenser surface which supposes to be used for condensation is used for cooling liquid state refrigerant, resulting in efficiency degrade. Similarly, although the superheat at the outlet of the evaporator protects the compressor from damage, it reduces the efficiency of evaporator. Jensen and Skogestad [79] further investigated the effect of subcooling for a given cold source temperature and a given condenser area and found that with given equipment, sub-cooling in the condenser may give savings in energy usage (compressor power) in the order of 2%. This result was proved by an ammonia case study. Larsen et.al proposed a gradient method to find the suboptimal solution for condensing pressure, while keep the superheat and evaporating pressure constant [20]. Selbas et.al[80] applied thermoeconomic optimization techniques to subcooled and superheated vapor compression refrigeration system to find the optimum heat exchanger areas and optimum subcooling and superheating temperatures under various operating conditions of system from exergy point of view. The relation between cost function variation, irreversibility of condenser and evaporator, subcooling as well as superheating temperatures was investigated. Vidal and Colle [81]applied thermo-economical optimization technique to a solar assisted combined ejector vapor compression cycle, in order to find the optimal the intercooler temperature and the flat plate solar collector area, when other parameters including the capital cost of the collectors, ejector cooler, the capital cost of equivalent mechanical compression cooler, specific costs of the auxiliary energy and electric energy are given. Zhou et.al [82]employed Pareto optimization approach to find the optimal steady-state operating conditions for high heat flux removal electronics cooling system to remove the given heat fluxes, such that the system COP is optimized while satisfying the critical heat flux and other system operation constraints. Ratts and Brown [83] investigated the fundamental thermodynamic aspects for vapor compression refrigeration

cycle efficiency improvement. They separately considered the superheat loss and throttling loss encountered in the vapor compression refrigeration cycle. The entropy generation minimization method is used to analyze the system states to study optimal cascade system design based on the thermodynamic property: entropy.

Since system states of vapor compression refrigeration cycle are severely interacted, it is highly possible that solutions of classical methods are trapped in local minimum instead of global minimum. On the other hand, the newly developed artificial intelligence computation techniques; have been successfully used in optimization of air conditioning and HVAC systems. Fong et.al [84]proposed a robust evolutionary algorithm (REA) to tackle this nature of the HVAC simulation models. It is based on the evolutionary algorithm paradigms; evolution strategy, which is a stochastic population based searching technique. The combination of REA with Cauchy deterministic mutation, tournament selection and arithmetic recombination has the synergetic effect in the searching process. This algorithm is proved to be effective when copes with other complex simulation models, as well as those HVAC engineering optimization problems with explicit mathematical expressions. Kusiak et al. [85-87] derived predictive model based on neural network, which is further optimized with a strength multi-objective particle-swarm optimization algorithm. Experiment results show that the control settings based on optimal model can efficiently minimize energy consumption while still provide comfort to occupants. Furthermore, to provide additional economic benefit, Hovgaard et.al [88] constructed a new cost function that contributes with ancillary services to the balancing power market. The largest difference between this optimization problem and the former ones is that they took probabilistic constraints into account and used a novel economic model predictive control scheme to reduce the operating cost of supermarket refrigeration system based on second Order Cone Programming techniques. They further developed a model predictive control scheme that reduces operating costs with the aid of thermal storage capabilities and a nonlinear optimization tool, which is especially effective for flexible outdoor temperature and electricity prices. Lu et.al [89, 90] proposed novel formulation of objective function of global optimization based on the constraints and hybrid models of the major components and developed a systematic approach; optimal set point control for overall HVAC systems is proposed for solving the mixed integer

nonlinear constraint optimization problem based on a modified genetic algorithm that is particularly devised for higher calculation speed and simulation accuracy.

In this chapter, we formulate the centralized optimization problem of VCC and propose a modified genetic optimization technique to tackle the optimization problem of vapor compression refrigeration cycle. The objective function is formulated based on mathematical models of the major components. The thermodynamic characteristics of the heat exchangers are predicted with the hybrid models, which are simple yet accurate with some physical significance. The power consumptions of the power consuming equipment are predicted also using the hybrid models. The developed modified genetic algorithm is used to search the optimal settings. Simulation and experimental results on a lab scale pilot plant demonstrate that a significant operating cost can be saved by the proposed centralized optimization method.

6.2 Problem formulation

6.2.1 Power consumptions

The objective of global optimization for vapor compression refrigeration cycle is to satisfy cooling load requirement of cold reservoir with minimal energy consumption. Mathematically, it can be formulated as

$$\begin{aligned} &\textbf{Min } \dot{W}_{total} = \dot{W}_{com} + \dot{W}_{c,fan} + \dot{W}_{e,fan} \\ &\text{Subject to } \dot{Q}_e = \dot{Q}_{req} \end{aligned} \tag{115}$$

where $\dot{W}_{total}, \dot{W}_{com}, \dot{W}_{c,fan}, \dot{W}_{e,fan}$ and $\dot{Q}_{req}$ are total power consumption, power consumption of compressor, condenser fan power consumption, evaporator fan power consumption and required cooling load, respectively. The power consumption models of the compressor, condenser fan and evaporator fan are formulated according to their working principles.

Power consumption of compressor:

Using a hybrid model to describe the delivery coefficient of compressor, η_{com} [41]

$$\eta_{com} = c_{com,\eta,1} + c_{com,\eta,2}(P_c / P_e)^{c_{com,\eta,3}} \tag{116}$$

the power consumption of compressor is given as

$$\dot{W}_{com} = \frac{\dot{Q}_{com}}{\eta_{com}} \tag{117}$$

where $c_{com,\eta,1}$, $c_{com,\eta,2}$ and $c_{com,\eta,3}$ are constants calculated by fitting experiment data.

Power consumptions of condenser fan and evaporator fan:

The power consumptions of fans are influenced by two parameters: mass flow rates of fluids and the pressure difference between the inlets and outlets and can be described by [91]:

$$\dot{W}_{c,fan} = \dot{W}_{c,fan,nom}\left(c_{c,fan,0} + c_{c,fan,1}\left(\frac{\dot{m}_{c,air}}{\dot{m}_{c,air,nom}}\right) + c_{c,fan,2}\left(\frac{\dot{m}_{c,air}}{\dot{m}_{c,air,nom}}\right)^2 + c_{c,fan,3}\left(\frac{\dot{m}_{c,air}}{\dot{m}_{c,air,nom}}\right)^3\right)$$
$$\dot{W}_{e,fan} = \dot{W}_{e,fan,nom}\left(c_{e,fan,0} + c_{e,fan,1}\left(\frac{\dot{m}_{e,air}}{\dot{m}_{e,air,nom}}\right) + c_{e,fan,2}\left(\frac{\dot{m}_{e,air}}{\dot{m}_{e,air,nom}}\right)^2 + c_{e,fan,3}\left(\frac{\dot{m}_{e,air}}{\dot{m}_{e,air,nom}}\right)^3\right) \tag{118}$$

respectively, where $c_{c,fan,0}$ to $c_{c,fan,3}$ and $c_{e,fan,0}$ to $c_{e,fan,3}$ are coefficients determined by catalog or experiment data, $\dot{W}_{c,fan}$, $\dot{W}_{e,fan}$, $\dot{W}_{c,fan,nom}$, $\dot{W}_{e,fan,nom}$, $\dot{m}_{c,air,nom}$ and $\dot{m}_{e,air,nom}$ are measured power consumptions of condenser fan, measured power consumption of evaporator fan, nominal power consumption of condenser fan, nominal power consumption of evaporator fan, nominal mass flow rate of condenser fan and mass flow rate of evaporator fan, respectively.

The fitting results for the fans in experiment system are shown in Figure 61 to Figure 64:

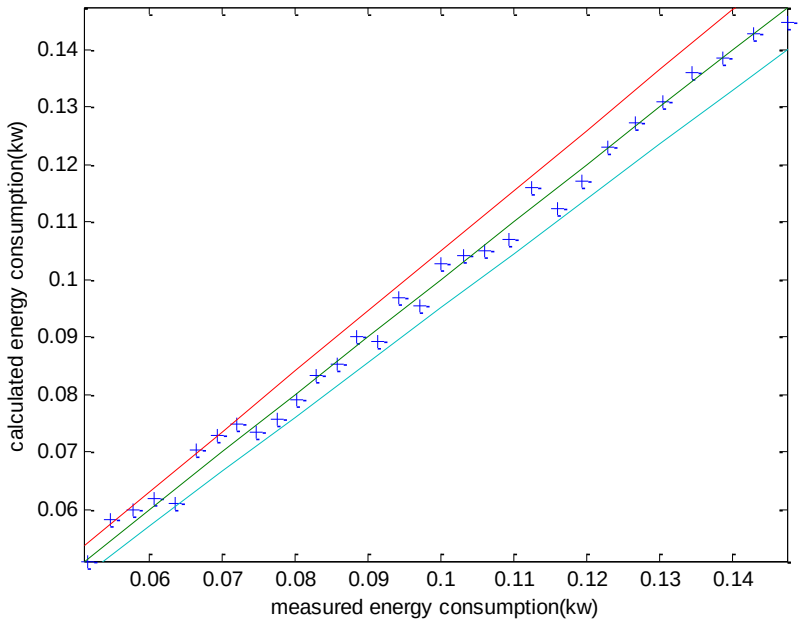

Figure 61 Fitting results of condenser fan model

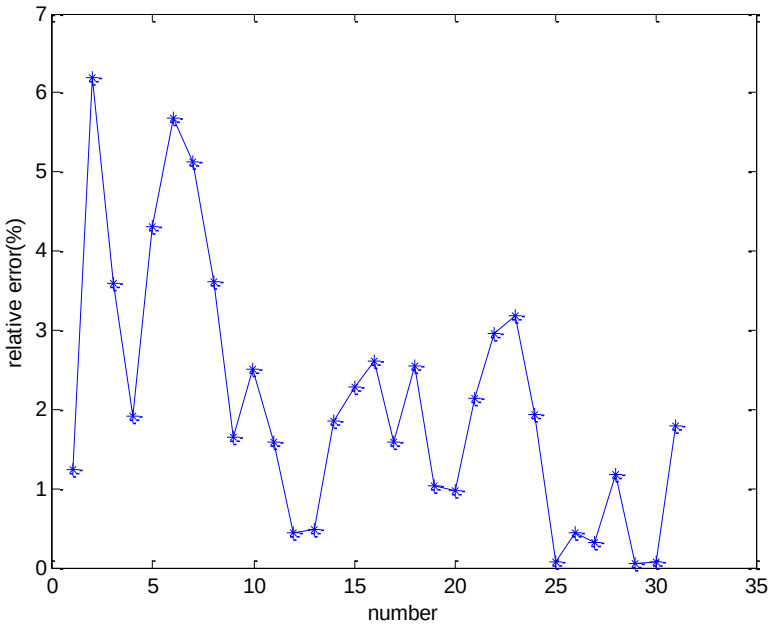

Figure 62 Relative error of condenser fan model

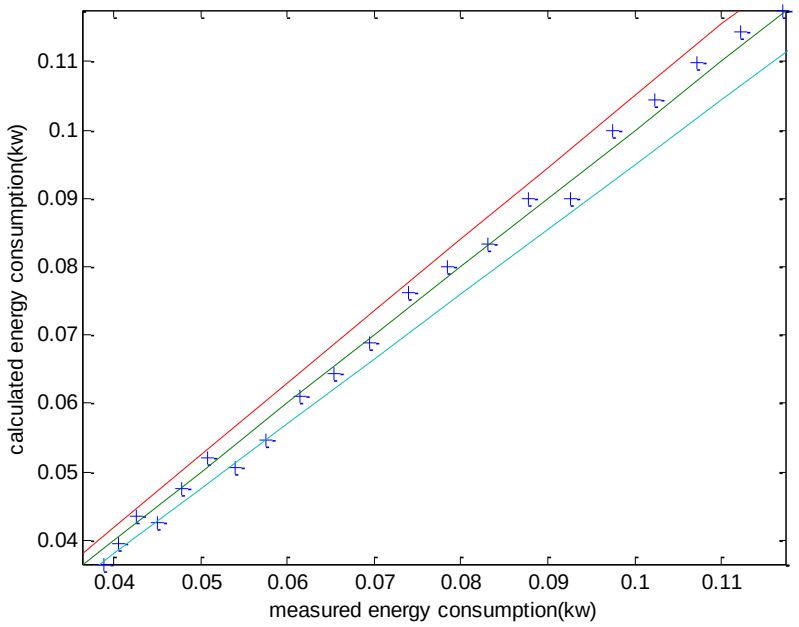

Figure 63 Fitting results of evaporator fan model

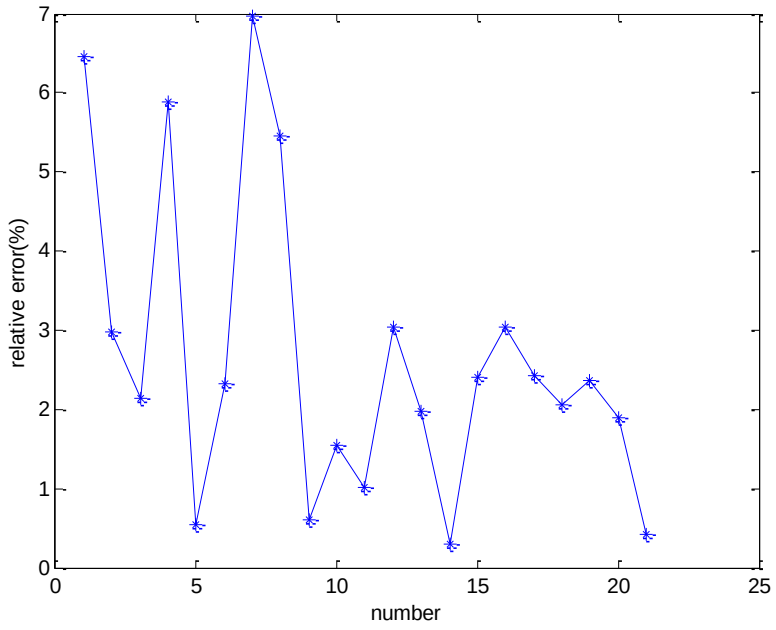

Figure 64 Relative error of evaporator fan model

6.2.2 Constraints

In the optimization problem, there are two types of constraints, i.e., interactions between the components and physical limitations:

Component interactions:

The hybrid model Eq. (29) introduced in Chapter 3 indicates evaporator heat transfer. In addition, an energy balance equation, i.e., energy absorbed by the refrigerant is equal to energy reduced in the cold reservoir, *i.e.*

$$\dot{Q}_e = \dot{m}_r (H_{e,r,o} - H_{e,r,i}) \tag{119}$$

will also be used in later development, where $H_{e,r,o}$ is refrigerant enthalpy at evaporator outlet (see Appendix A for the calculation of $H_{e,r,o}$).

The condenser hybrid model (33) describes the heat transfer at condenser. The corresponding energy balance equation is

$$\dot{Q}_c = \dot{m}_r (H_{c,r,i} - H_{c,r,o}) \tag{120}$$

where $H_{c,r,i}$ and $H_{c,r,o}$ are enthalpy of inlet and outlet refrigerant, respectively (see Appendix A for the calculations of $H_{c,r,i}$, and $H_{c,r,o}$).

The interactions of compressor and system are represented by (34), (36), (37) and the following cycle energy balance equation [92]:

$$\dot{Q}_c = \dot{Q}_{com} + \dot{Q}_e \tag{121}$$

Physical limitation:

Physical limitations of the components and fluids, including Eq. (104) to (111) as described in Chapter 4.

6.3 Optimization algorithm

6.3.1 Implementation of genetic algorithm

To solve the constrained nonlinear optimization problem, a modified genetic algorithm (MGA) combined with a solution strategy for a group of nonlinear equations is devised for higher efficiency and less computation complexity. This algorithm is divided into four parts: encoding, construction of fitness function, evolution and termination [17], which are briefly discussed below.

Encoding: Each independent variable in constraint Equations is converted into a binary string. All of these strings are combined together to form a chromosome. Gray coding is preferred for overcoming the hidden representative bias in binary representation. The

lengths of the binary strings are determined by the control precision of the corresponding variables: the more precise set point control requires the longer binary string. For instance, if the compressor controller's accuracy is 10^{-2}, then 10 bits is enough for ω to describe the compressor setting. After encoding, a random of population of chromosomes, is generated such that, when decoded to real values, the variable values lie within their limitations. The whole generation should possibly try to include the entire range of values.

Constructing fitness function: After setting the random variables, eight dependent variables are solved according to interaction constraint equations based on the coded independent variables (see Appendix A). Since the objective of this optimization problem is to minimize $\dot{W}_{total}$, the fitness function should be constructed to give the maximum value to the smallest $\dot{W}_{total}$. In addition, the fitness function should reflect whether the chromosome violates the constraints. Based on these considerations, the fitness function is constructed as follows:

$$fitness = \frac{1}{(\dot{W}_{com} + \dot{W}_{e,\,fan} + \dot{W}_{c,\,fan} + K_{total})} \tag{122}$$

where the definition of total system penalty function K_{total} is as following:

$$K_{total} = \begin{cases} 0 & if \quad \sum_{i=1}^{8} K_i = 0 \\ c_p + \sum_{i=1}^{8} K_i & if \quad \sum_{i=1}^{8} K_i \neq 0 \end{cases} \tag{123}$$

where K_i, i=1,…,8 are the individual state penalty functions (see Appendix A and C for the detailed definition and calculation), c_p is a constant which can be specified by user, the rule of thumb of the selection is 3 times of the rated compressor power. By calculating Eq. (123), the fitness value of each individual chromosome is converted into predetermined interval to control the evolution speed in an acceptable range.

Evolution: In evolution, four major evolutionary operations: selection, crossover, mutation and reinsertion are performed. The elitist roulette wheel selection [17], single point crossover and single bit mutation operators are employed. The crossover and mutation points are selected randomly in each generation.

Termination: The genetic algorithm terminates if one of the following criterion is satisfied:

1. Predetermined maximal generation number is reached.
2. The optimal fitness of group does not change much over several steps, the bound for determining whether its value changes too much is predetermined according to experience.
3. All chromosomes converge to nearly the same fitness groups.

Compared with the traditional genetic algorithm, there is a difference of the proposed algorithm, particularly modified for such kind of problems, which is discussed in the following remark.

Remark: A main drawback of traditional genetic algorithm when applied to vapor compression refrigeration cycle is that when $\dot{Q}_e$ is approaching to system cooling capacity, it is highly possible that all individuals in last generation do not satisfy the physical constraints, even though several individuals in previous generation do, the good chromosome might lost after evolution. The proposed algorithm is to store the individuals that satisfy the physical constraints with maximum fitness value in each generation step when $\dot{Q}_e$ is large. As a result, only chromosome with maximal fitness is stored for each generation and to compare with the final generation, this modification increases the possibility of finding a feasible solution.

6.3.2 Discussion of state variables

To reduce the variables and simplify the solution procedures, we notice that

- P_c , $H_{c,fg}$ and $T_{c,r,sat}$,
- P_e ,$H_{e,g}$, and $T_{e,r,sat}$
- $H_{c,r,o}$ and $H_{e,r,i}$

have same physical properties, therefore, we can use P_c ; P_e; and $H_{c,r,o}$ to replace $T_{c,r,sat}$ and $H_{c,fg}$; $T_{e,r,sat}$ and $H_{e,g}$; $H_{e,r,i}$, respectively, in the system objective, constraints and power consumption equations. All variables used in the optimization problem, according to their rules, can be further classified into three groups:

- ***Uncontrollable variables ($\dot{Q}_e$, $T_{c,air,i}$, $T_{e,air,i}$):*** They are determined by user demand or environmental conditions, these variables are fixed during each calculation step. Among these three variables, the outdoor air temperature, $T_{c,air,i}$, is the most critical data, the other two uncontrollable variables, $T_{e,air,i}$ and $\dot{Q}_e$, are also affected by $T_{c,air,i}$.
- ***Independent variables (P_c, P_e, ω, $T_{c,r,o}$):*** Independent variables can be selected randomly within the constraint limits to meet the optimization objective. The obvious choices for independent variables are ω, A_v, $\dot{m}_{c,air}$, $\dot{m}_{e,air}$ as they are directly controlled by compressor, EEV and fan frequencies, respectively. However, P_e, P_c, ω and $T_{c,r,o}$ are assigned to be independent variables in this work in order to reduce the complexity of solving process as well as to increase solution accuracy.
- ***Dependent variables:*** ($\dot{m}_r$, $T_{c,r,i}$, $\dot{m}_{c,air}$, $T_{e,r,o}$, $\dot{m}_{e,air}$, $\dot{Q}_c$, $\dot{Q}_{com}$ and A_v) These values can be resolved through the interaction and physical constraint equations for the given independent variables. These variables can then be used to calculate the power consumption equations.

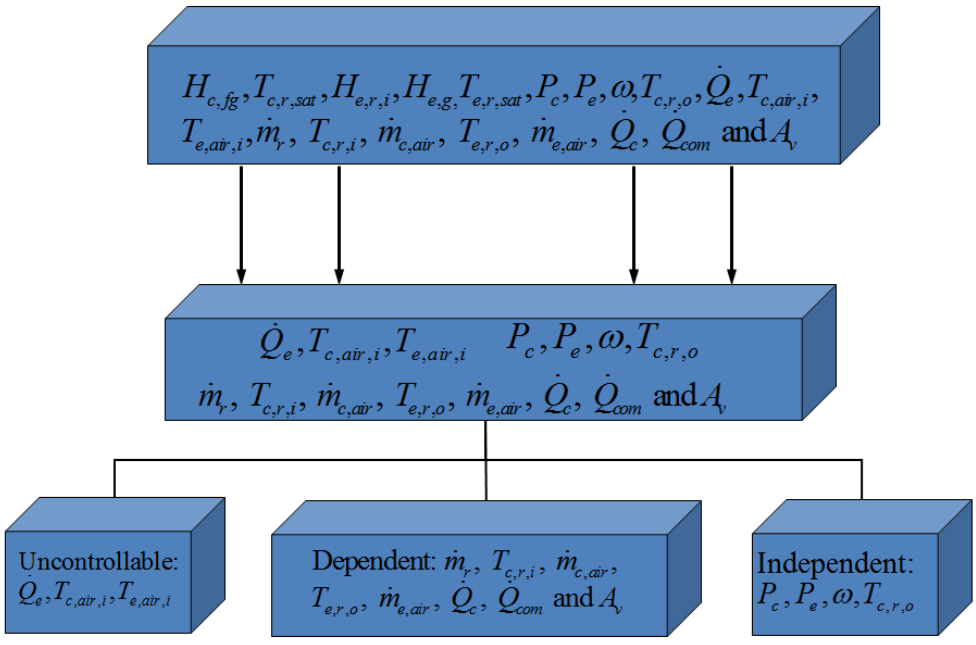

Figure 65 State variables classification

6.3.3 Solution procedure

The flow chart of MGA for optimization of vapor compressor cycle is illustrated in Figure 66 which can be summarized as follows:

Step 1: Determine the parameters of the component models by catalog or experimental data;

Step 2: Measure $T_{e,air,i}$ and $T_{c,air,i}$, and calculate $\dot{Q}_e$;

Step 3: Initialize the parameters of MGA: population size, maximum number of generations, precisions of variables, generation gap and probabilities of crossover and mutation.

Step 4: Perform the evolutionary operations.

Step 5: Repeat Step 5 and store chromosome according to Remark until termination criterion is satisfied.

Step 6: Find the chromosome with largest fitness value among all generations and calculate corresponding power consumption.

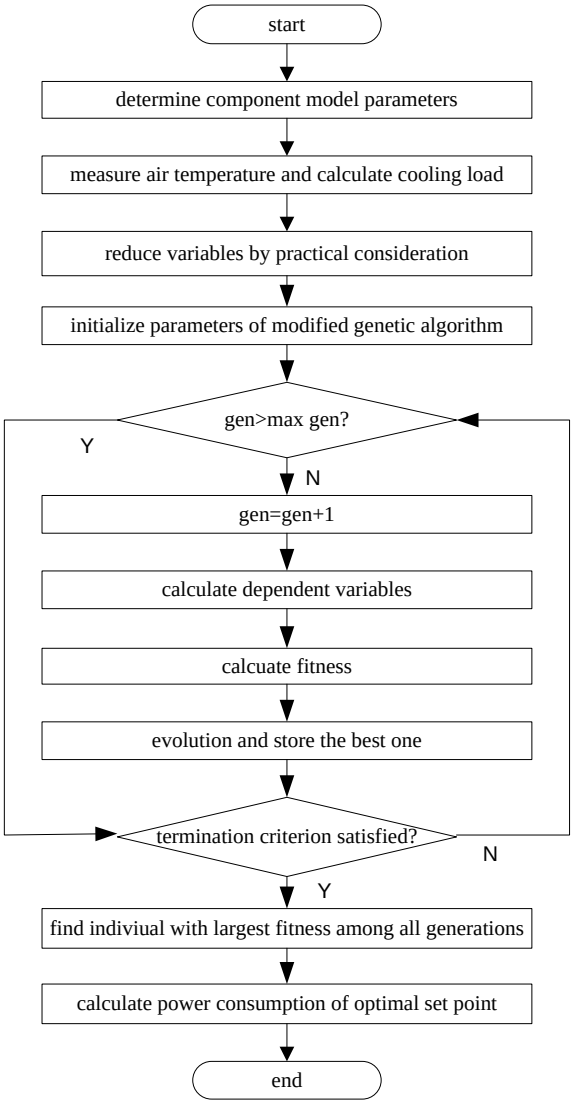

Figure 66 Flow chart of centralized optimization procedure

6.4 Simulation results

The simulation studies are based on the models of a Lab scale pilot plant. The coefficients of models are determined through catalog fitting 200 groups of experiment data which are obtained by different compressor, condenser fan and evaporator fan frequencies. All constraints also follow the system physical limits listed as in Table 5.

Table 5 Physical limits of variables

Variables	Lower bound	Upper bound
$F_{c,fan}$	15Hz	35Hz
$F_{e,fan}$	15Hz	30Hz
$T_{c,r,sat}$	$T_{c,air,i}$	$T_{c,r,i}$

$T_{e,r,sat}$	-12 ℃	$T_{e,air,i}$
P_c	8 bar	15 bar
P_e	2 bar	5 bar
$T_{e,sh}$	5 ℃	25 ℃
$T_{c,sc}$	0 ℃	NA
F_{com}	30Hz	50Hz
$\dot{m}_r$	0.008kg/s	0.03kg/s

To simulate the energy saving effect in practical situations, environmental temperatures of two consecutive days are measured as shown in Figure 67.

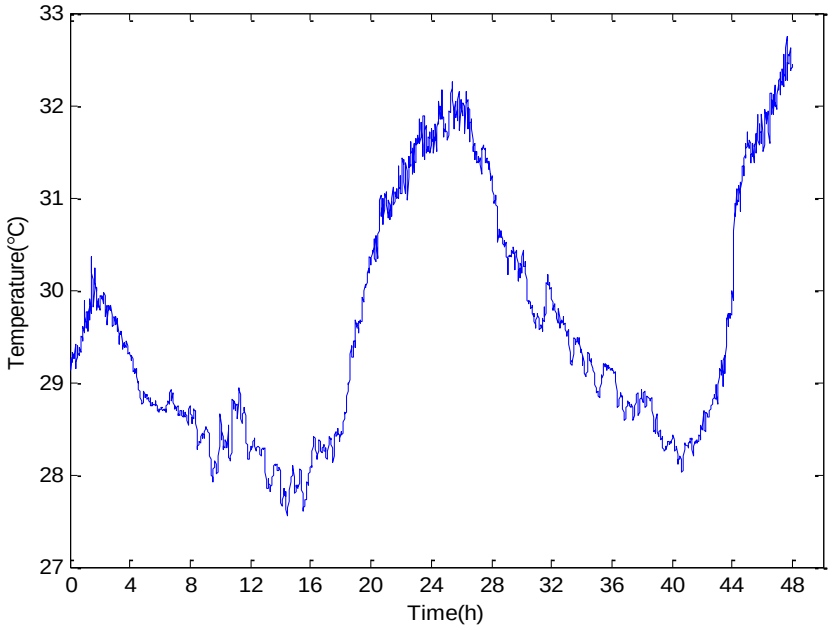

Figure 67 Measured temperatures for two consecutive days

Assuming the set point of indoor temperature is 23 ℃ and the highest cooling load is equal to the maximum cooling capacity of the pilot plant, the measured temperature data can then be proportionally converted to the cooling load shown as in Figure 68.

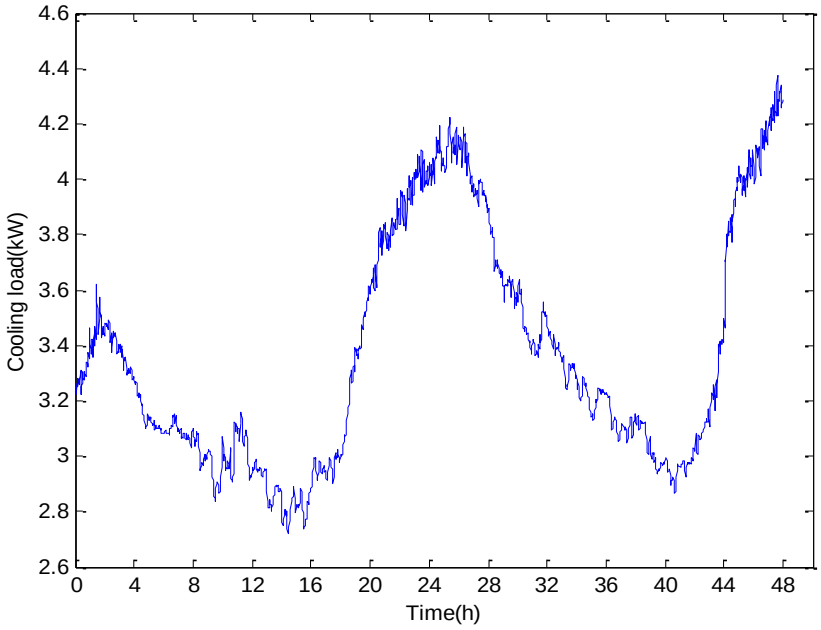

Figure 68 Assumed cooling load profiles in simulation

The simulation results for energy consumption of the proposed MGA and traditional on-off control scheme from 8am to 19pm are illustrated in Figure 69. It can be seen that energy consumptions of MGA are lower than that of on-off control scheme for all cooling loads, but the difference is smaller when the cooling load is near its maximum cooling capacity. The energy consumptions of the two schemes have the same trends, but MGA is more sensitive to the change of cooling load. The largest and smallest energy saving of MGA compared with on-off control scheme are 14.78% and 1.44%, respectively.

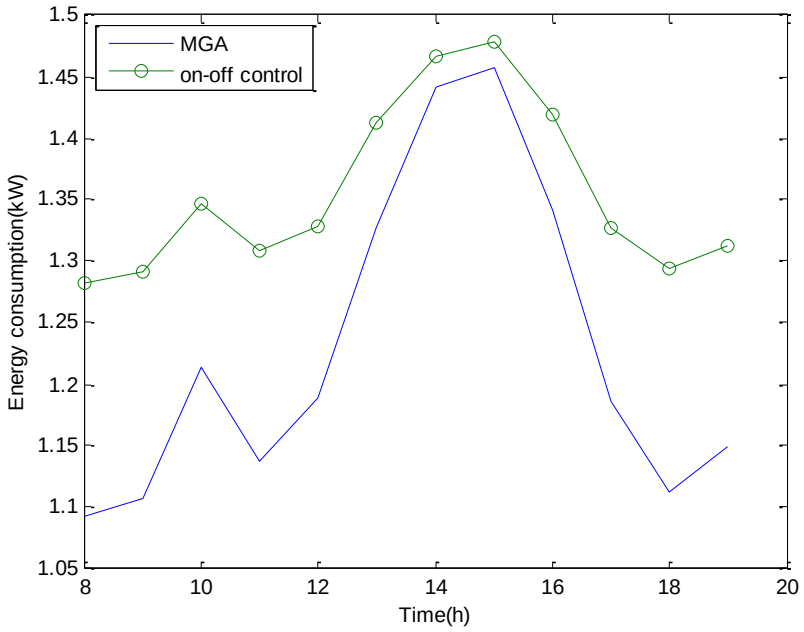

Figure 69 Energy consumptions for working hours

To analyze the energy consumptions at different temperature conditions, the measured temperatures are regrouped according to the temperature range. The percentage of temperature in the measured day from 8am to 19pm is shown as in Figure 70.

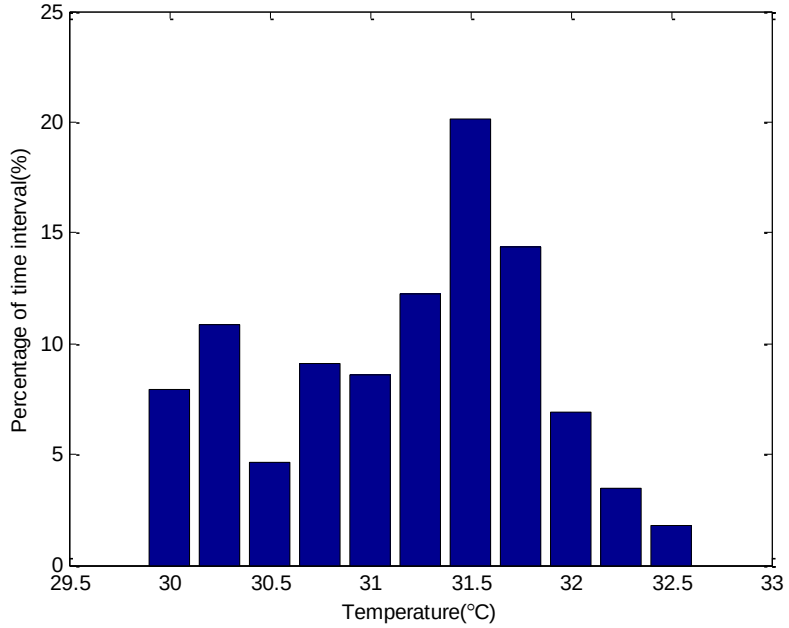

Figure 70 Bar chart of one day temperature profile

To estimate the energy saving effect of MGA, the total energy consumptions for both MGA and on-off control schemes of the temperature profile in Figure 68 are calculated and presented in Figure 71, which shows that the average energy saving of 8.52% is achieved.

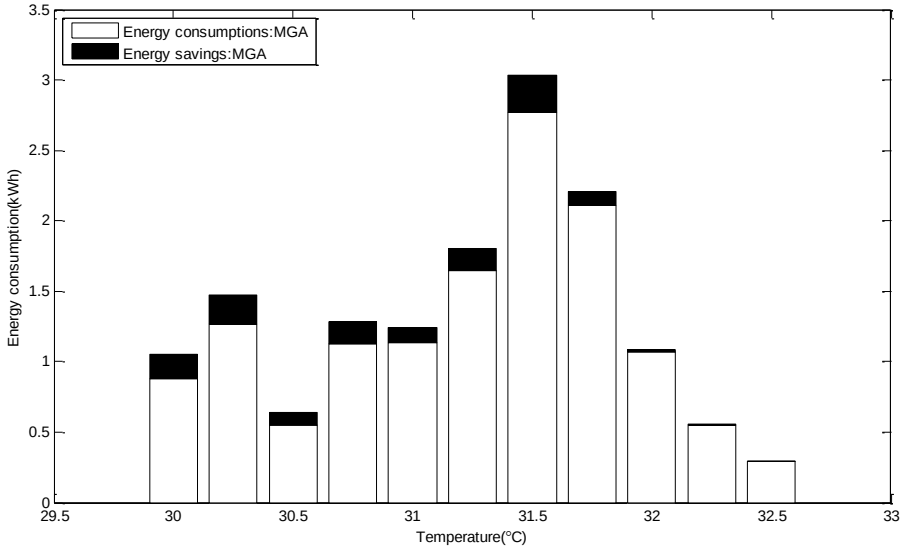

Figure 71 System energy consumptions and savings

6.5 Experimental results

To verify the effect of the proposed MGA, experimental tests are conducted on a lab scale multi-evaporator vapor compression cycle.

The schematic and photo of the experimental system are illustrated in Figure 72 and Figure 73, respectively.

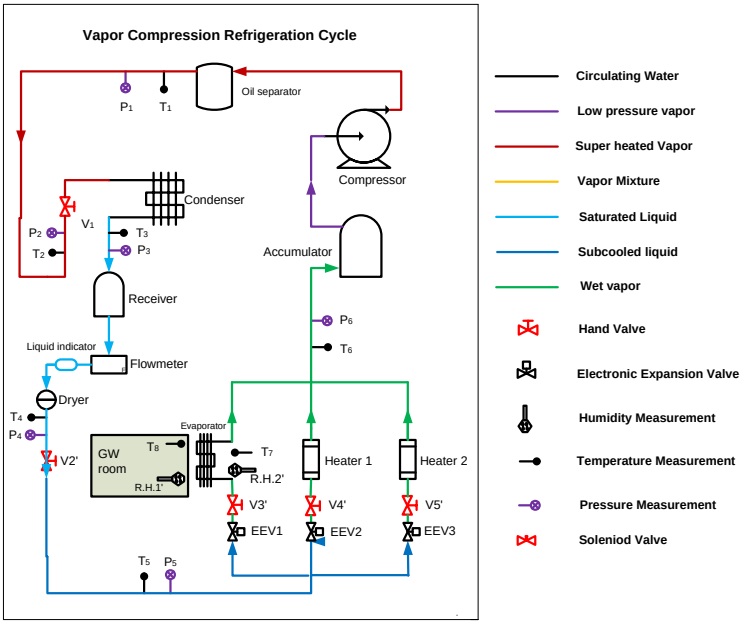

Figure 72 Schematic of the vapor compression refrigeration system

Figure 73 Picture of the lab scale vapor compression refrigeration system

The test bench consists of a single-stage vapor compression formed by basic components: variable speed compressor, fin-tube condenser, thermostatic expansion valve and isolated fin-tube evaporator. The heat exchangers work with secondary fluids loops, which represents and simulates environmental and thermal load.

The experiment system includes a semi-hermetic reciprocating compressor, an air-cooled finned-tube condenser, three electronic expansion valves and three evaporators (one air-cooled finned-tube evaporator and two electronic evaporators). One air duct heater controls the inlet air temperature of condenser for simulating outdoor condition, and the inlet air temperature of evaporator is constantly kept as 25 ℃ by HVAC system. The working fluid used for the system is R134a. The compressor, the condenser fan and the evaporator fan are equipped with inverters to adjust their corresponding frequencies. An air duct heater is installed in front of the condenser to control the temperature of condenser inlet air. In addition, several temperature and pressure sensors are installed for detecting state variables. To measure the mass flow rate, a flow meter with maximum 4% full scale error is used. The measurement range of the pressure transducers and the temperature transmitters are 0~16 bar and -40 ℃ to 200 ℃, with their maximum full scale error are within ±0.3% and ±0.3 ℃, respectively. The positions of these sensors are as following (refer to Figure 72):

- refrigerant temperature and pressure at compressor outlet (T_1 and P_1);
- temperature and pressure at condenser inlet (T_2 and P_2);
- temperature and pressure at condenser outlet (T_3 and P_3);
- temperature and pressure at EEV inlet (T_5 and P_5);
- temperature and pressure at evaporator outlet (T_6 and P_6);
- mass flow rate after receiver ($\dot{m}_r$);.
- humidities at evaporator inlet and outlet (*R.H.1, R.H.2*).

To simplify the test and calculation, the average temperatures and cooling load demands of each hour from 8am to 19pm are used during testing. The energy consumptions of both MGA and on-off control schemes for results of both simulation and testing are compared in Figure 74. It shows that energy consumptions (EC) are higher in the experiment results than that of simulation for nearly all testing groups, the average and largest difference between experiment and simulation results are 3.43% and 10.47%, which might be caused by the modeling errors. However, the results are accurate enough for the MGA to be implemented in practical applications. Moreover, the difference between experimental results of MGA and on-off control scheme verifies the energy saving effect of proposed

method. The smallest and largest differences between these two groups of data are 0.03% and 13.14% with the average overall energy saving (ES) of 8.45% as shown in Figure 75.

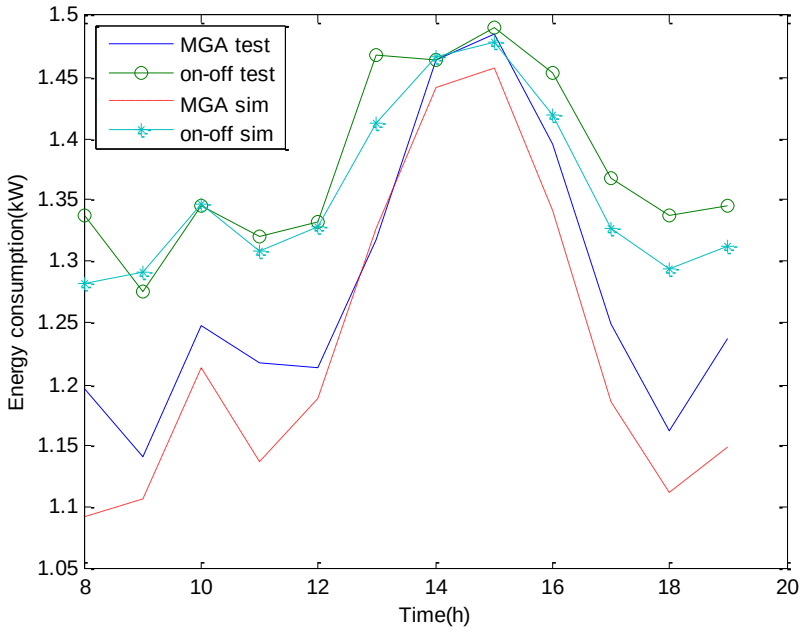

Figure 74 Energy consumptions of different methods

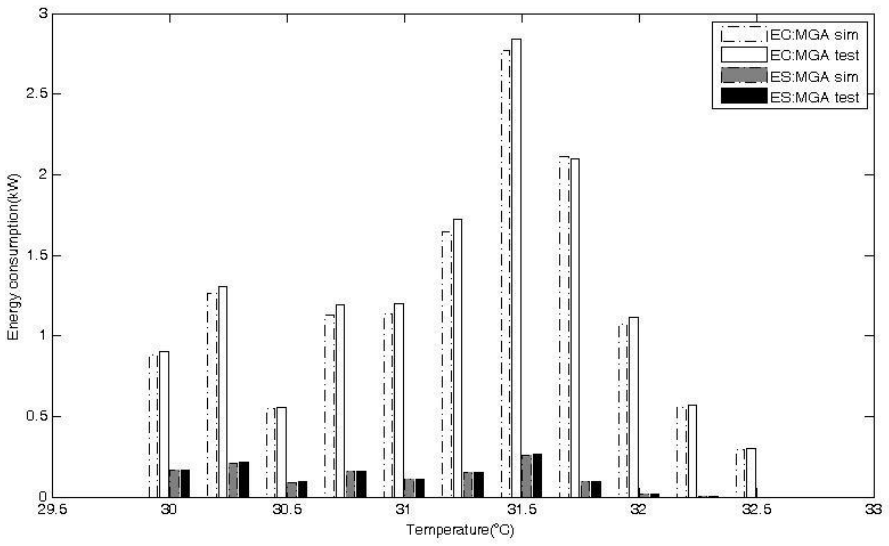

Figure 75 System energy consumptions and savings

6.6 Summary

In this chapter, a model-based optimization strategy for the vapor compression refrigeration cycle has been developed. It has been seen that the minimization of the total operating cost of the energy consuming devices is performed subject to the constraints of mechanical limitations, component interactions, environment conditions and cooling load demands. A modified genetic algorithm together with a solution strategy for a group of nonlinear equations has been proposed for effectively achieving the optimal set point under different operating conditions. The experimental results have confirmed that the set points calculated by MGA can help to reduce energy consumption compared with the traditional on-off control strategy, the overall energy saving for a typical day from 8am to 19pm is 8.45%. Furthermore, the average difference between the simulated and the experimental results for energy consumptions is 3.43%, which has sufficiently demonstrated the effectiveness of the proposed method.

Chapter 7 Decentralized Optimization of VCC

7.1 Basics of decentralized optimization and Pareto Optimality

Although the centralized optimization methods have been proved to be effective, the computation burden of the existing centralized optimization algorithms is very heavy for online optimization. The convergence time, though can be neglected in academic research, is an important factor in practice. Considering the interaction between different components complicates the optimization problem as well as the solving procedures, one alternative method is to optimize the component operation individually, including the optimization of heat exchanger and compressor.

The heat exchanger optimization has attracted a large amount of research interests. Hermes [93-95] derived an algebraic model that expresses the dimensionless rate of entropy generation. It is represented by a function of the fluid properties, the number of transfer units, the thermal hydraulic characteristics, the operating conditions and the operating conditions for heat exchangers with uniform wall temperature. Based on this model, he further developed an expression for the optimal heat exchanger effectiveness as a function of the working conditions, heat exchanger geometry and fluid properties. When the design data are known, Granryd [96] deduced the optimum flow rates that will result in highest overall COP of system including the compressor and fans energy consumptions, which equals to the optimal solution with fixed cooling load requirement. The deduced relation brought benefits to design purposes as well as for determining optimal flow rate in a given plants. Accadia and Vanoli [97] formulated a cost function summing up the following two contributions: (i) the amortisation cost of the condenser, related to the heat exchange area;(ii) the operating cost of the electric-driven heat pump in which the heat exchanger will work, depending on the overall exergy destruction rate in the system, which is related to the local irreversibility rate in the condenser, using the so-called structural approach. Through optimizing this cost function, they also investigated the optimal trade-off between amortisation and operating cost. On the other hand, there are also lots of researchers focused on the compressor optimization.

On the other hand, Roytta et. al [98] proposed to evaluate the the performance of the centrifugal compressor based on semi-empirical specific-speed curves and the effect of

the Reynolds number, surface roughness and tip clearance. Iterative optimization method containing several nesting iteration loops was then employed to calculate the optimal solution. In the optimization process, the condensing and evaporating pressures and temperature after intercooler are fixed. Schiffmann and Favrat [20] claimed that an appropriate turbo compressor in heat pump system usually requires the ability to operate on a wide range of pressure ratios and mass flows. It is necessary to make a compromise between range and compressor efficiency, thus they applied a multi-objective optimizer based on evolutionary algorithm to fit the compressor design into the possible specifications field while keeping the high efficiency on a wide operational range. However, from systematic point of view, it is necessary to integrate the individual optimization results without bring too much computation burden. An effective and direct way is decentralized optimization. The thought of decentralized algorithm can trace back to Braun [99, 100], he developed the fundamental concepts that form the basis of the collaborative optimization architecture, demonstration method was then proposed that can pose any general set to suit the collaborative architecture, regardless of the interdisciplinary coupling structure, finally the basic architecture was redefined to improve system level performance. Miguel et.al [101] proposed two novel decomposition optimization algorithms for smooth problems and showed that both algorithms overcome the difficulties associate with collaborative optimization even when only the linear independence constraint qualification holds instead of the more restrictive strong linear independence constraint qualification. As a consequence, fast local convergence can be expected from optimization algorithms for smooth problems when applied to the proposed master problems and subproblems. Based on their work, Inalhan et.al developed a relatively novel optimization method called decentralized optimization [102-104]. In the decentralized optimization algorithm, the original problem can be separated into several subsystem optimizations with constraints updating. It has been proved that decentralized optimization can converge to Nash Equilibrium of the original problem with much higher speed and lower computation burden. Therefore, decentralized optimization is a promising alternative optimization method to balance minimizing energy consumption and converging speed.

In this chapter, we apply the decentralized optimization algorithm to the VCC by 1) decompose the complex global optimization problem of VCC into evaporator, condenser and compressor optimization subproblems based on component hybrid models and interactive constraints; 2) propose a modified decentralized optimization method to simplify the original problem by transforming it into unconstrained subsystem optimization problems so that gradient based search methods can then be easily applied to each subsystem. Simulation and experimental results on a lab scale pilot plant demonstrate that the performance of the proposed decentralized optimization method is comparable to that of centralized optimization method. However, the reduction in computation time is on the scale of 100 times [105].

7.2 Introduction to decentralized optimization

In practical optimization, when the dimension of optimization problem is high, computation burden and risk of local minimum will be significantly increased. To realize real-time control, it is inclined for modeling process to shrink variable dimension, this could also lower the risk of solution trapped in local minimum. Among several decomposition and decentralized optimization methods proposed[100, 101, 106-109], to the best of our knowledge the simplest method for reducing variable dimension as well as maintain suboptimal characteristic is the decentralized optimization method [102]:

The centralized optimization problem is as following:

$$\begin{aligned} &\min_{x\in R^n} \quad \left[f_1(x_1),\dots f_i(x_i),\dots f_m(x_m) \right] \\ &\text{subject to } \begin{cases} g(x) \le 0 \\ h(x) = 0 \end{cases} \end{aligned} \tag{124}$$

where m is the number of subsystem, n is the number of variables, x_i are the variables of the ith decision maker. f is the penalty function of ith subsystem. $x = \left[x_1^T, x_2^T \dots x_m^T \right]^T \in R^n$ corresponds to the collection of optimization variables from each decision maker. After decentralizing, the system are transformed into separate subsystems, the corresponding optimization problem for each subsystem is as following:

$$\begin{aligned} &\min_{x_i \in R_i} \quad f_i(x_i) \\ &\text{subject to} \begin{cases} g(x_i \mid \{x_j\}_i) \begin{cases} g_{li}(x_i) \le 0 \\ g_{gi}(x_i \mid \{x_j\}) \le 0 \end{cases} \\ h(x_i \mid \{x_j\}_i) \begin{cases} h_{li}(x_i) = 0 \\ h_{gi}(x_i \mid \{x_j\}) = 0 \end{cases} \end{cases} \end{aligned} \tag{125}$$

where $\{x_j\}_i$ is the neighborhood of *i*th subsystem, $g_{li}\{\bullet\}$ and $h_{li}\{\bullet\}$ refer to local constraints of *i*th subsystem, $g_{gi}\left\{\bullet \mid \{x_j\}_i\right\}$ and $h_{gi}\left\{\bullet \mid \{x_j\}_i\right\}$ are global constraints related to *i*th subsystem.

Inalhan et.al proved that the optimum of decentralized optimization problem is Nash Equilibrium of original centralized problem, the relation between Nash Equilibrium and Pareto optimality is as follows:

Penalty methods provide a direct tool for solving the decentralized optimization problem, the penalty functions have following form:

$$F_i = \beta_i f_i(x_i) + P_{li}(x_i) + P_{gi}(x_i \mid \{x_j\}_i) \tag{126}$$

where β_i is coefficient of penalty function and decrease to 0 in iteration, in each step, $P_{li}(\bullet)$ and $P_{gi}(\bullet)$ are the local and global penalty function of *i*th subsystem, the task is to find

$$\left\{x_i^* \mid \beta_i, \{x_j\}_i\right\} = \arg\min\left\{F\left(x_i \mid \beta_i, \{x_j\}_i\right)\right\} \tag{127}$$

As β_i gradually converges to 0, x_i^* converges to optimum of *i*th subsystem.

7.3 Decentralized optimization problem formulation

In decentralized optimization, the whole refrigeration cycle is first separated into several loosely related subsystems, i.e.: evaporator, condenser and compressor due to their physical and geometrical independence. Moreover, EEV is integrated into compressor subsystem due to the similarity of their function upon controlling pressure and refrigerant mass flow rate. The interactions between the subsystems are defined as interactive constraints in the process of formulation.

7.3.1 Problem formulation of evaporator decentralized optimization

The objective for isolated evaporator subsystem optimization would be minimizing evaporator fan energy consumption subject to cooling load requirement of cold reservoir, where the power consumption of evaporator fan is influenced by two parameters: mass flow rates of fluids and the pressure difference between the inlets and outlets can be described by [110]

$$\dot{W}_{e,fan} = \dot{W}_{e,fan,nom}\left(c_{e,fan,0} + c_{e,fan,1}\left(\dot{m}_{e,air}\right) + c_{e,fan,2}\left(\dot{m}_{e,air}\right)^2 + c_{e,fan,3}\left(\dot{m}_{e,air}\right)^3\right) \tag{128}$$

Since the three subsystems are closely coupled, other two subsystems will impose interactive constraints to the evaporator subsystem. These interactive constraints include:

1. Evaporator inlet refrigerant enthalpy: the analysis of EEV shows that the refrigerant enthalpy of evaporator inlet equals to that of condenser outlet

$$H_{e,r,i} = H_{c,r,o} \tag{129}$$

2. Evaporator outlet refrigerant temperature: since heat transfer in pipe is neglected, the refrigerant temperature at evaporator outlet should be equal to at compressor inlet

$$T_{e,r,o} = T_{com,r,i} \tag{130}$$

   where $T_{com,r,i}$ is refrigerant temperatures at compressor inlet.

3. Evaporating pressure: evaporating pressure in evaporator is the same as that in compressor

$$P_{e,e} = P_{com,e} \tag{131}$$

   where $P_{e,e}$ and $P_{com,e}$ are evaporating and compressor inlet pressures, respectively.

4. Energy balance equation (119)
5. Evaporator hybrid model (29)

Several physical constraints are imposed to restrict the state variables for proper operation of evaporator, including:

1. Evaporator air mass flow rate: determined by characteristic of evaporator fan

$$\dot{m}_{e,air,min} \le \dot{m}_{e,air} \le \dot{m}_{e,air,max} \tag{132}$$

where $\dot{m}_{e,air,min}$ and $\dot{m}_{e,air,max}$ are the lower and upper bounds of evaporator air mass flow rate, respectively.

2. Evaporating temperature: the heat absorption in evaporator results the increase of refrigerant temperature [2]

$$T_{e,r,i} \le T_{e,r,sat} \le T_{e,r,o} \tag{133}$$

where $T_{e,r,i}$ and $T_{e,r,o}$ are refrigerant temperature at evaporator inlet and outlet.

3. Superheat: superheat temperature which is defined as outlet refrigerant temperature minus saturated temperature, if too low, will cause hunting in the cycle [78]. On the other hand, the COP of system will decrease steeply if the superheat temperature is too high [4, 44].

$$T_{e,sh,min} \le T_{e,sh} \le T_{e,sh,max} \tag{134}$$

where $T_{e,sh,min}$ and $T_{e,sh,max}$ are lower and upper bounds of superheat which depend on the system configurations.

By taking consideration of cooling load requirement, energy consumption, physical and interactive constraints, the decentralized optimization problem for the evaporator subsystem can be formulated into a penalty function with its objective function expressed as:

$$\textbf{Min} \quad C_e = \beta_e \dot{W}_{e,fan} + d_{e,1} K_{e,i} + d_{e,2} K_{e,o} + d_{e,3} \left(\dot{Q}_e - \dot{Q}_{req} \right)^2 \tag{135}$$

where $d_{e,1}$,$d_{e,2}$ and $d_{e,3}$ are constant coefficients of penalty terms derived from constraints, β_e, is the coefficient of evaporator fan energy consumption; $K_{e,i}$ and $K_{e,o}$ are the terms of interactive and physical constraints on the penalty function, expressed by

$$K_{e,i} = \left(T_{e,r,o} - T_{com,r,i} \right)^2 + \left(H_{e,r,i} - H_{c,r,o} \right)^2 + \left(P_{e,e} - P_{com,e} \right)^2 \tag{136}$$

and

$$K_{e,o} = \frac{1}{\dot{m}_{e,air,max}} \left\{ \max\left[\max\left(\dot{m}_{e,air,min} - \dot{m}_{e,air}, 0 \right), \max\left(\dot{m}_{e,air} - \dot{m}_{e,air,max}, 0 \right) \right] \right\}^2 + \\ + \frac{1}{T_{e,max}} \left\{ \max\left[\max\left(T_{e,min} - T_{e,r,sat}, 0 \right), \max\left(T_{e,r,sat} - T_{e,max}, 0 \right) \right] \right\}^2 + \\ + \frac{1}{T_{e,sh,max}} \left\{ \max\left[\max\left(T_{e,sh,min} - T_{e,sh}, 0 \right), \max\left(T_{e,sh} - T_{e,sh,max}, 0 \right) \right] \right\}^2 \quad (137)$$

respectively.

The structure of evaporator decentralized problem is shown in Figure 76

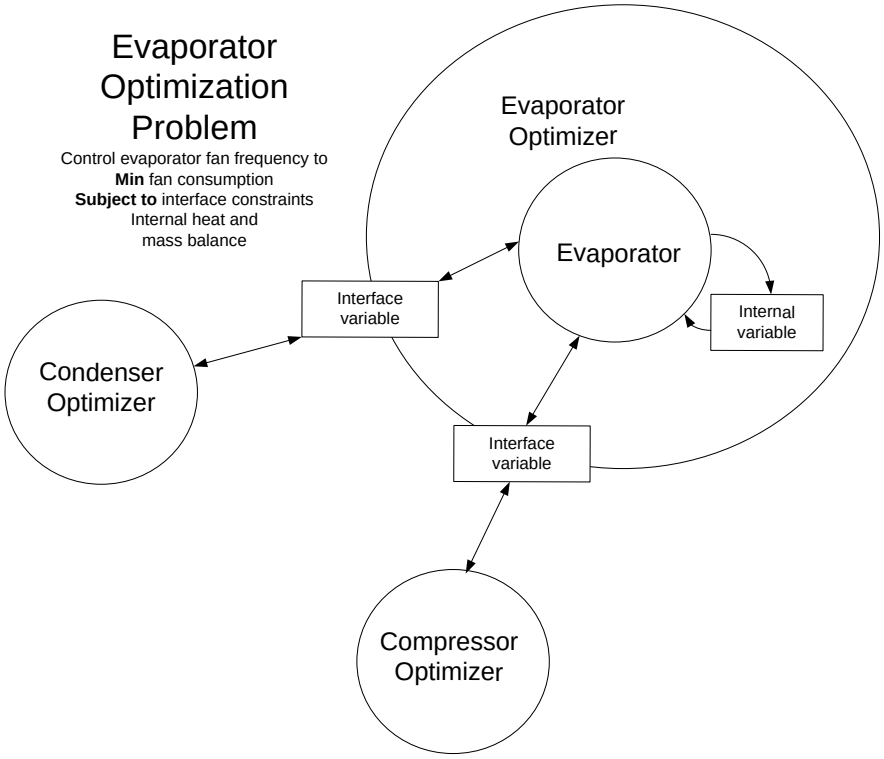

Figure 76 Decentralized optimization problem of evaporator

7.3.2 Problem formulation of condenser decentralized optimization

Similar to evaporator subsystem, the objective of decentralized optimization for condenser subsystem can be formulated minimizing the power consumption of condenser fan, which can be calculated through [110]

$$\dot{W}_{c,fan} = \dot{W}_{c,fan,nom} \left(c_{c,fan,0} + c_{c,fan,1} \left(\dot{m}_{c,air} \right) + c_{c,fan,2} \left(\dot{m}_{c,air} \right)^2 + c_{c,fan,3} \left(\dot{m}_{c,air} \right)^3 \right) \quad (138)$$

The interactive constraints from the other two subsystems to the condenser subsystem include:

1. Condenser inlet refrigerant temperature: the refrigerant temperatures at condenser inlet ($T_{c,r,i}$) and at compressor outlet ($T_{com,r,o}$), are equal as the energy loss is negligible

$$T_{c,r,i} = T_{com,r,o} \tag{139}$$

2. Condenser outlet refrigerant enthalpy: the refrigerant enthalpies at condenser inlet and at compressor outlet are equal

$$H_{c,r,o} = H_{e,r,i} \tag{140}$$

3. Condensing pressure: condensing pressures in condenser, $P_{c,c}$, and compressor, $P_{com,c}$, (discharge pressure) should be equal.

$$P_{c,c} = P_{com,c} \tag{141}$$

4. Energy balance equation (120)
5. Heat Exchanger Hybrid Model (33)

Similar to evaporator, the physical constraints of state variables of the condensers are listed as follows:

1. Condenser air mass flow rate: similar to evaporator fan, condenser fan limits the maximal and minimal air mass flow rates

$$\dot{m}_{c,air,min} \le \dot{m}_{c,air} \le \dot{m}_{c,air,max} \tag{142}$$

where $\dot{m}_{c,air,min}$ and $\dot{m}_{c,air,max}$ are the lower and upper bounds of condenser air mass flow rate

2. Condensing temperature: as refrigerant rejects heat in condenser, the condensing temperature is lower than inlet refrigerant temperature while higher than outlet refrigerant temperature [2].

$$T_{c,r,o} \le T_{c,r,sat} \le T_{c,r,i} \tag{143}$$

3. Subcool: subcool ($T_{c,sc}$) is defined as refrigerant condensing temperature minus refrigerant temperature at condenser outlet, the working principle of air conditioner requires that subcool should not be negative [1], thus

$$T_{c,sc} \ge 0 \tag{144}$$

Consequently, the simplified unconstraint optimization problem for condenser is formulated as

$$\textbf{Min} \quad C_c = \beta_c \dot{W}_{c,fan} + d_{c,1} K_{c,i} + d_{c,2} K_{c,o} \tag{145}$$

where $d_{c,1}$ and $d_{c,2}$ are constant coefficients of penalty terms for violating interactive constraints and physical constraints of evaporator, respectively, β_c is the coefficient of energy consumption of condenser fan which gradually decrease during optimization.

$$K_{c,i} = \left(T_{c,r,i} - T_{com,r,o}\right)^2 + \left(H_{c,r,o} - H_{e,r,i}\right)^2 + \left(P_{c,c} - P_{com,c}\right)^2 \tag{146}$$

and

$$\begin{aligned} K_{c,o} = & \frac{1}{\dot{m}_{c,air,max}} \left\{ \max\left[\max\left(\dot{m}_{c,air,min} - \dot{m}_{c,air}, 0\right), \max\left(\dot{m}_{c,air} - \dot{m}_{c,air,max}, 0\right) \right] \right\}^2 + \\ & + \frac{1}{T_{c,max}} \left\{ \max\left[\max\left(T_{c,min} - T_{c,r,sat}, 0\right), \max\left(T_{c,r,sat} - T_{c,max}, 0\right) \right] \right\}^2 + \\ & + \left\{ \max\left(-T_{e,sh}, 0\right) \right\}^2 \end{aligned} \tag{147}$$

The structure of condenser decentralized optimization problem is as follows:

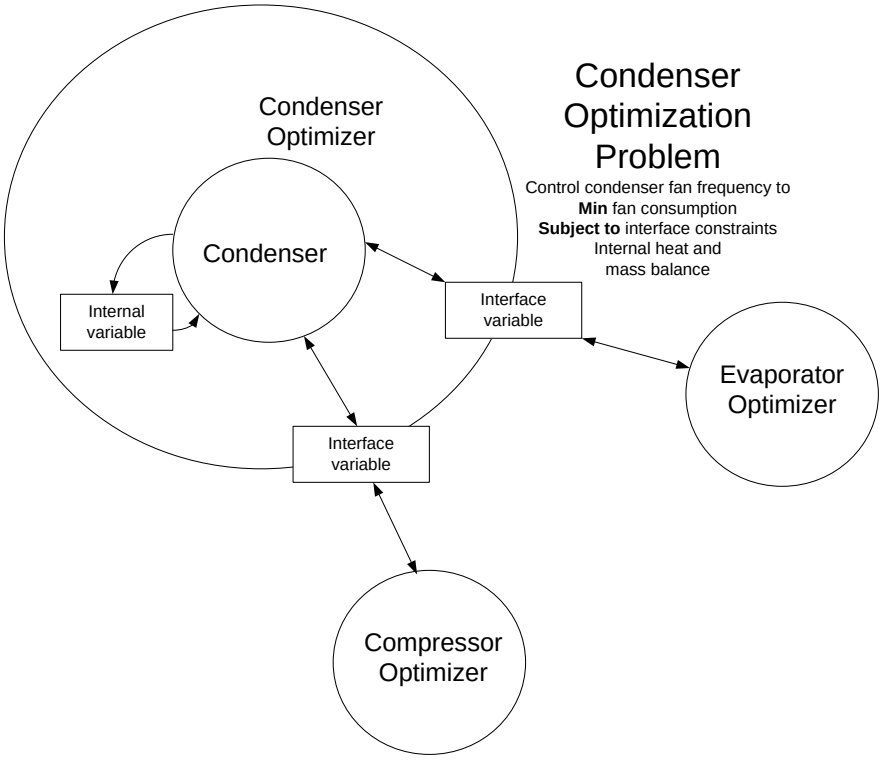

Figure 77 Decentralized optimization problem of condenser

7.3.3 Problem formulation of compressor decentralized optimization

The objective of decentralized optimization for compressor optimization is to minimize the power consumption of compressor, which is determined by Eqs. (116) and (117) [41][41][41][41][41][41][41][41][41][41][41][41][40][39][38].

The interactive constraints from the other two subsystems to the compressor subsystem include:

1. Interface constraints:

$$\begin{cases} T_{com,r,o} = T_{c,r,i} \\ T_{com,r,i} = T_{e,r,o} \\ P_{com,c} = P_{c,c} \\ P_{com,e} = P_{e,e} \\ \dot{Q}_e = \dot{Q}_{e,req} \end{cases} \tag{148}$$

2. Energy balance equation:

$$\dot{Q}_{com} = \dot{m}_r (H_{com,r,o} - H_{com,r,i}) \tag{149}$$

3. Compressor hybrid model (35)

In addition, physical constraints of compressor are as following:

1. Compressor Frequency: the following physical constraint is directly determined by compressor working range.

$$30Hz \le F \le 50Hz \tag{150}$$

2. Compressor refrigerant mass flow rate:

$$\dot{m}_{r,min} \le \dot{m}_r \le \dot{m}_{r,max} \tag{151}$$

where $\dot{m}_{r,min}$ and $\dot{m}_{r,max}$ are the minimal and maximal refrigerant mass flow rates of the system, both of which are determined by system characteristics.

3. Condensing and evaporating pressures in compressor: they are bounded for protecting compressor from being damaged

$$\begin{aligned} P_{c,min} \le P_c \le P_{c,max} \\ P_{e,min} \le P_e \le P_{e,max} \end{aligned} \tag{152}$$

where $P_{c,min}, P_{c,max}, P_{e,min}$ and $P_{e,max}$ are lower and upper bounds of condensing pressure (discharge pressure) and of evaporating pressure (suction pressure).

Expansion valve

The mass flow rate of expansion valve is determined by valve opening percentage, pressure difference and inlet refrigerant density. Its mass flow rate is given by [42]

$$\dot{m}_r = (c_{ev,1} + c_{ev,2} A_v)\sqrt{\rho(P_c - P_e)} \tag{153}$$

where $c_{ev,1}$ and $c_{ev,2}$ are constants, A_v and ρ are opening percentage of electronic expansion valve and density of inlet refrigerant, respectively (see Appendix A for the calculation of ρ). The inlet and outlet enthalpy should be equal, consequently refrigerant enthalpy is constant which implies $\dot{Q}_{ev} = 0$ [111].

Furthermore, the Opening Percentage of EEV is bounded as following:

$$0 < A_v \leq 1 \tag{154}$$

By combining of energy consumption, physical and interactive constraints, the decentralized optimization problem for the compressor subsystem can be formulated as:

$$\textbf{Min} \quad C_{com} = \beta_{com} \dot{W}_{com} + d_{com,1} K_{com,i} + d_{com,2} K_{com,o} \tag{155}$$

where $d_{com,1}$ and $d_{com,2}$ are coefficients of penalty terms for violating interactive constraints and physical constraints of compressor, respectively, β_{com} is a gradually decreasing coefficient of compressor energy consumption.

$$K_{com,i} = \left(T_{com,r,o} - T_{c,r,i}\right)^2 + \left(T_{com,r,i} - T_{e,r,o}\right)^2 + \left(P_{com,c} - P_{c,c}\right)^2 + \left(P_{com,e} - P_{e,e}\right)^2 + \left(\dot{Q}_e - \dot{Q}_{req}\right)^2 \tag{156}$$

and

$$
\begin{aligned}
K_{com,o} = & \frac{1}{F_{max}}\left\{\max\left[\max\left(F_{min}-F,0\right),\max\left(F-F_{max},0\right)\right]\right\}^2 + \\
& + \frac{1}{\dot{m}_{r,max}}\left\{\max\left[\max\left(\dot{m}_{r,min}-\dot{m}_{com,r},0\right),\max\left(\dot{m}_{com,r}-\dot{m}_{r,max},0\right)\right]\right\}^2 + \\
& + \frac{1}{P_{com,c,max}}\left\{\max\left[\max\left(P_{com,c,min}-P_{com,c},0\right),\max\left(P_{com,c}-P_{com,c,max},0\right)\right]\right\}^2 + \\
& + \frac{1}{P_{com,e,max}}\left\{\max\left[\max\left(P_{com,e,min}-P_{com,e},0\right),\max\left(P_{com,e}-P_{com,e,max},0\right)\right]\right\}^2 + \\
& + \left\{\max\left[\max\left(-A_v,0\right),\max\left(A_v-1,0\right)\right]\right\}^2
\end{aligned}
\tag{157}
$$

The corresponding structure is as follows:

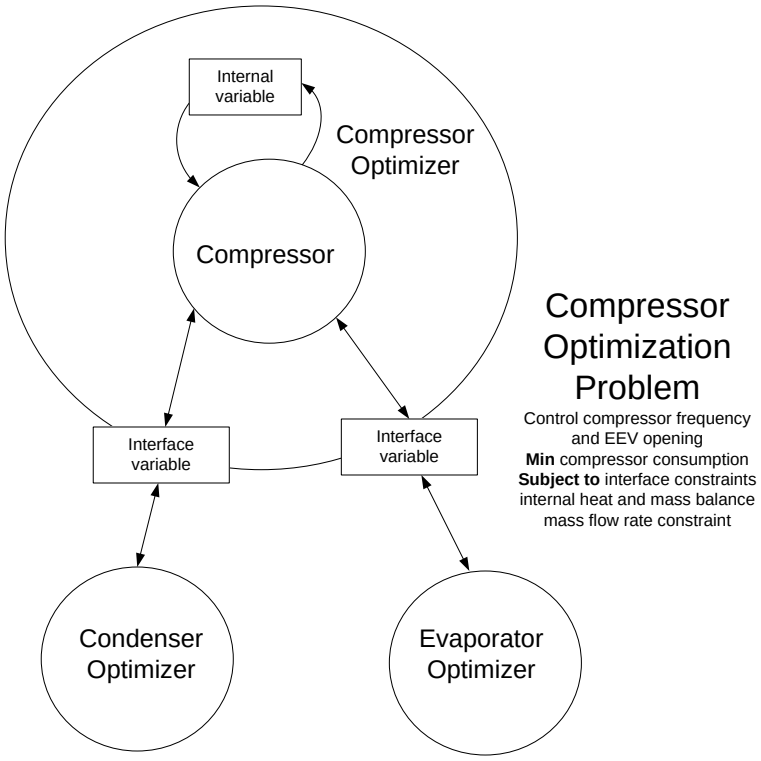

Figure 78 Decentralized optimization problem of compressor

7.4 Optimization algorithm

A sequential optimization scheme is adopted in each optimization cycle, that is, for the results obtained from other two subsystems; the subsystem under optimization optimizes its own cost function with local selection of energy consumption coefficient, and sends the solution to other subsystems. Detailed procedures are given as following:

1. Coefficients Initialization: For each subsystem, there are maximum four parameters, i.e., $d_{\bullet,1}$ $d_{\bullet,2}$, $d_{\bullet,3}$ and $\beta_{\bullet}$. Since violation of physical constraints cause

damage to system, the corresponding coefficients $d_{\bullet,2}$ and $d_{\bullet,3}$ should have much larger values than that of $d_{\bullet,1}$ (in the factor of 5 is recommended), while $\beta_{\bullet}$ corresponding to the power consumption whose initial value should be 10 times larger than that of $d_{\bullet,2}$ or $d_{\bullet,3}$ to find the optimal solution without much consideration of other constraints at first.

2. Operating State Initialization: The typical operation states will be used to initialize the states of the three subsystems.
3. Update: At each step, the states of all the subsystems are used to update interactive constraints. Then coefficients of energy consumption terms $\beta_{\bullet}$'s are updated by

$$\beta_{\bullet,k+1}=\gamma\beta_{\bullet,k} \quad 0<\gamma<1 \tag{158}$$

where γ is the updating coefficient.

4. Optimization: Line search Newton's method with Hessian modification is used to find the optimal states by [112]

$$x_{k+1} = x_k - \alpha_k M_k^{-1}\nabla f_k \tag{159}$$

where α_k , x_k , M_k and ∇f_k are the step length, state vector to be optimized, Cholesky factorization of Hessian Matrix (see Appendix F for its procedure) of the cost function and gradient vector of cost function, respectively.

5. Termination: the optimization will be terminated if: 1) the coefficients $\beta_{\bullet}$ of energy consumption terms in cost function is smaller than a predefined value ε (say 10^{-5}); or 2) the maximum number of predetermined generations is reached. Otherwise, return to step 3.

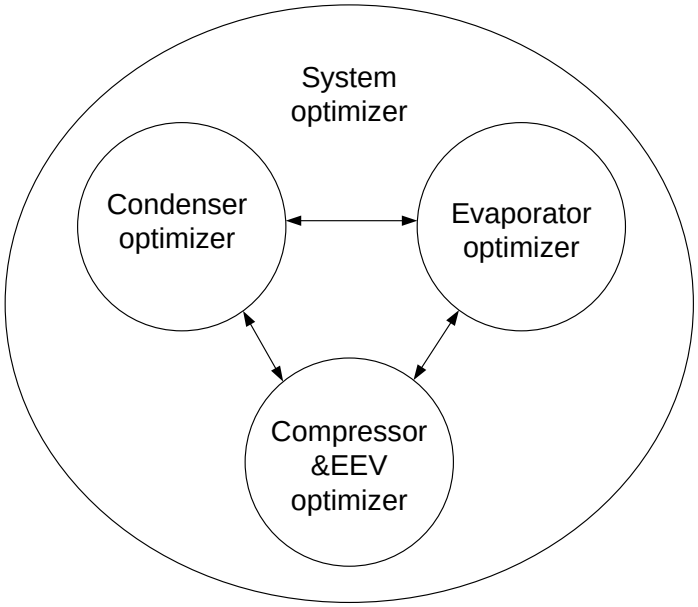

Figure 79 Decentralized Optimizer of whole system

Remark 1: The choice of the parameter γ is a trade-off between the number of steps in each cycle and total number of cycles required. If γ is large, the coefficients β only decrease slightly, leading to small number of Newton steps for current cycle. On the other hand, if γ is small, bigger reduction will result β after each cycle. The converged point from last cycle may not be a good starting point for the current one; much more computation load of Newton method is expected in each cycle. The recommended value of γ is in between 0.1 to 0.3 [113].

Remark 2: The choice of α_k is to result a big cost function reduction in each cycle yet to keep the procedure simple. Here line search algorithm is utilized to try a series of potential candidates of α_k until the Wolfe conditions are satisfied (see Appendix E for details).

Remark 3: Different from the standard Newton method, modified Cholesky factorization rather than the original form of Hessian matrix is used in this work to ensure the search resulting in a lower cost. Moreover, contrast with Cholesky factorization, the modified form guarantees the existence and bound of Cholesky factors (see Appendix F for details) [112].

In summary, the outline of original decentralized optimization proposed by Inalhan is as follows [103, 104]:

1. Separate the system to several subsystems
2. Formulate the objective function and constraints of each subsystem.
3. Each subsystem searches its own optimal solution under the constraints.
4. If subsystem B has a constraint involving subsystem A, update this constraint according to the value of A's optimal solution as soon as A finishes its optimization.
5. Stop if the predetermined termination criterion is met, otherwise go back to step 4.

The relation between solutions for centralized and decentralized optimization problems was given by Inalhan [102, 104]:

1. decentralized and centralized optimization have identical feasible solutions;
2. decentralized optimal solutions equivalent to the Nash equilibrium of the global optimization problem.

Since VCC has numerous feasible operating states, there exists a set of feasible solutions which can be classified as the decentralized optimization solution set if they meet the constraint conditions, as shown in the left side circle of Figure 80.

On the other hand, the global problem can be reckoned as multi-subsystem optimization which is to minimize the total costs of the whole system as well as to satisfy all the constraints from each subsystem (Pareto Optimality) [114]. If each subsystem has determined its own states and no subsystem can benefit by changing its own solution while other subsystems keep their states unchanged, these states reach their Nash Equilibrium [102, 103]. The relation between Pareto optimal and Nash Equilibrium is given in the right side circle of Figure 80.

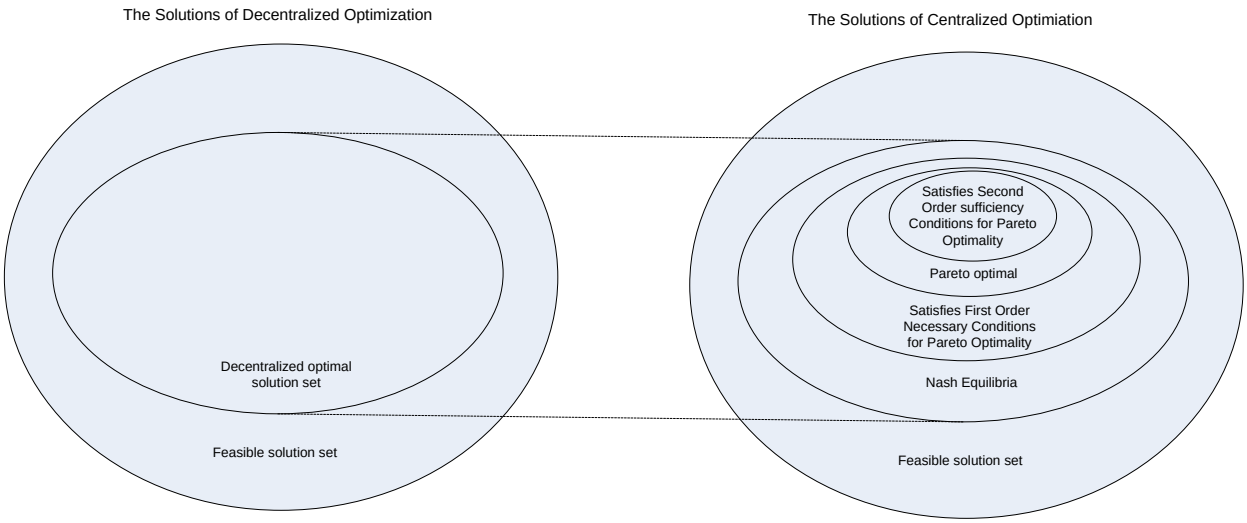

Figure 80 Relations between decentralized and centralized optimal solutions

7.5 Simulation and experiment results

The simulated model was built upon the measured data from lab scale pilot plant. All the coefficients of hybrid models derive from fitting the measured data. These constraints follow the system physical limits listed as in Table 5.

The cooling capacity requirement for simulation is based on a sample of one day temperature in Singapore, as shown in Figure 81:

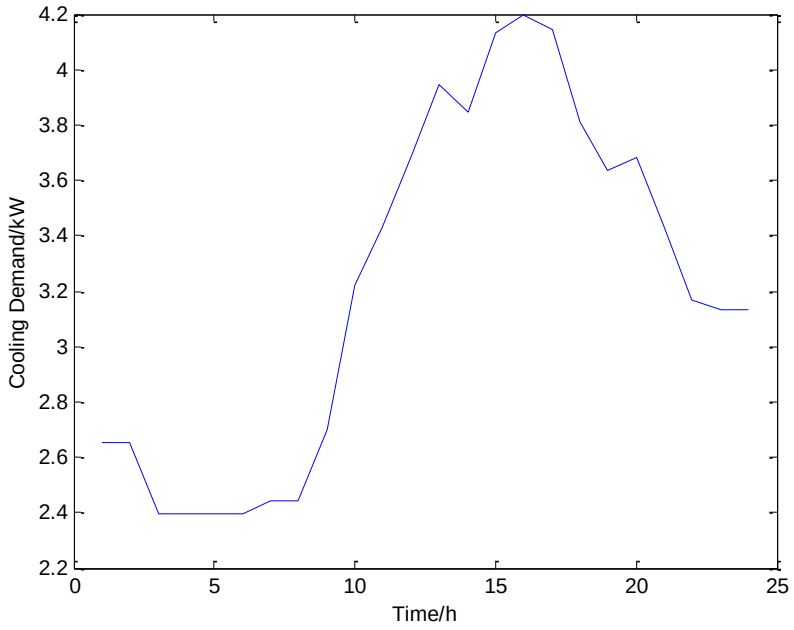

Figure 81 Sample cooling load of Singapore [115]

For the lab scale pilot plant model, energy consumption under different cooling load with decentralized optimization (MDA), centralized optimization (MGA) based on genetic algorithm and on-off control are illustrated as in Figure 82:

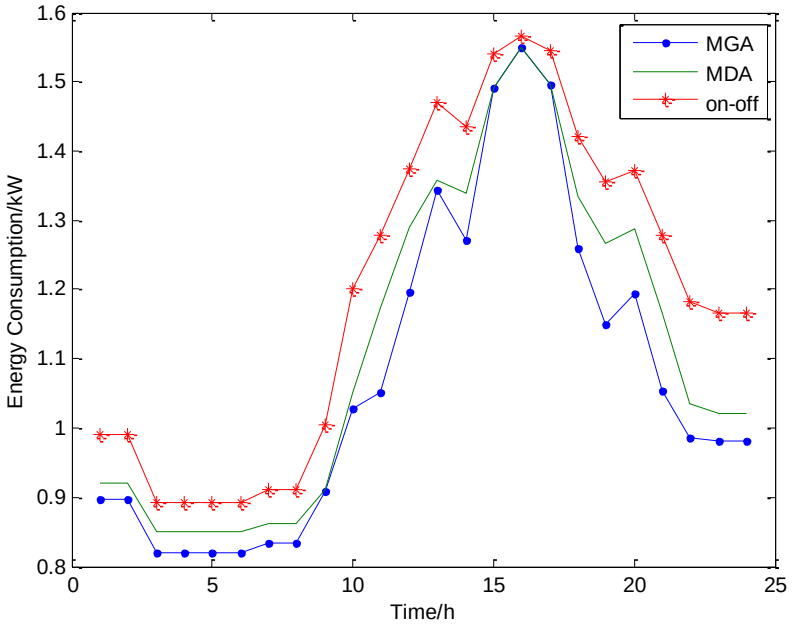

Figure 82 Simulated Energy Consumption of MGA, MDA and on-off

The simulated results shown in Figure 82 indicate that the energy saving effect of genetic and decentralized optimization algorithms are quite close, especially when cooling load approaches its upper bound. Numerical analysis reveals that the overall energy consumption difference between of MDA and MGA during daytime is only 3.47%, and the energy saving effect of MDA compared with on-off control is 7.16%. However, MDA saves considerable computational time; the whole algorithm only takes 6.85s compared with MGA of 669s, as listed in Table 6.

Table 6 Computation times of decentralized and genetic algorithms

Time (h) Algorithm (s)	Decentralized Algorithm (s)	Genetic
1	7.03	664
2	6.92	646
3	6.73	643
4	6.78	655
5	6.89	633

6	6.75	673
7	6.94	671
8	6.83	680
9	6.83	699
10	6.79	705
11	6.87	682
12	6.75	659
13	6.94	649
14	6.88	662
15	7.01	634
16	6.77	692
17	6.86	687
18	6.78	649
19	6.81	703
20	6.80	667
21	6.95	676
22	6.84	642
23	6.78	681
24(0)	6.83	695

The proposed MDA is tested with the experiment system described in Chapter 5. Under the temperature scheme shown in Figure 81, the experiment results of MDA, MGA and genetic algorithm and on-off control under are as following:

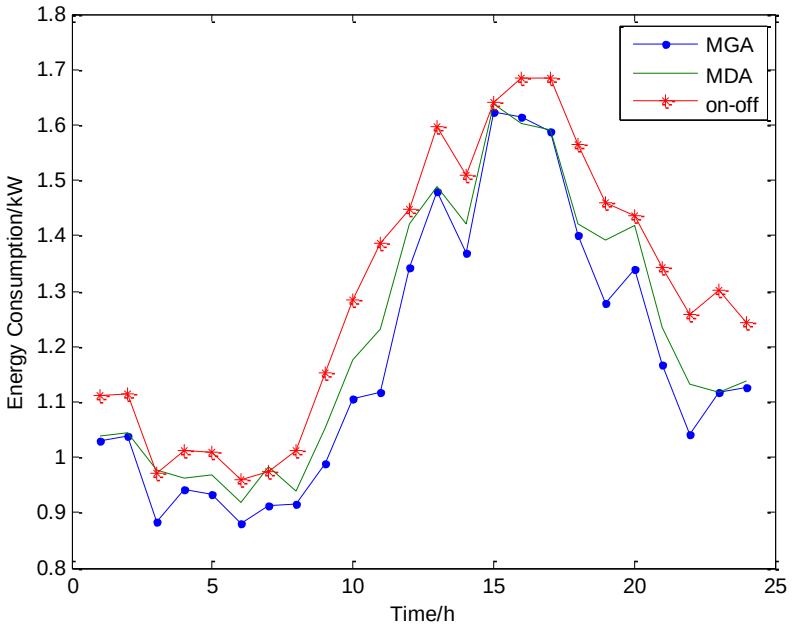

Figure 83 Experiment results

The testing results show that the energy consumptions of optimizing algorithms are smaller than that of on-off control all the time. The overall energy saving effect of MDA is 6.5% compared with on-off control, while MGA is only 3.12% better than MDA. For the time period (9 to 18), the difference between MGA and MDA is only 1.05%. It is also noted that energy consumption of MDA in certain periods is smaller than of MGA which may be caused by the fluctuation of incoming air temperature and humidity, both of which are unavoidable in the testing environment.

7.6 Summary

In this chapter, the optimization problem for vapor compression cycle is divided into three subsystem optimization problems which subject to mechanical limitations and components interaction. Modified decentralized optimization algorithm was proposed for solving these subsystem optimization problems so that to obtain suboptimal solutions for different operating conditions. The experimental results showed that the suboptimal results calculated by MDA can reduce energy consumption compared with traditional on-off control by 6.5% for a typical day, and is larger than that of genetic algorithm by only 1.05% during the working hours. Furthermore, the average difference between simulated and experimental results for energy consumptions is 3.43%, which demonstrated the effectiveness of the proposed method. The high convergence rate of decentralized optimization suits loosely interconnected systems, an interesting topic along this direction is to study the its application in whole heating, ventilating and air conditioning systems to realize its online optimization.

Chapter 8 Conclusions and Future Work

8.1 Conclusion

In this thesis, several optimization methodologies for the VCC's modeling and state prediction have been developed. The fundamentals of vapor compression cycle have been presented in Chapter 1. The neural network based intelligent modeling and training methods, including the feedforward neural networks, the back-propagation, the support vector machine, the extreme learning machine, and the genetic algorithms, have been discussed in Chapter 2. Chapter 3 focused on the modeling of the major components of VCCs. A novel SLFN based modeling approach, trained with the ELM, for VCCs has been proposed in Chapter 4 with the results that the neural model is robust against the system uncertainties and disturbance and the accurate prediction of the system states can be achieved. In Chapter 5, the optimization method for VCC together with SLFN classifier based on black box model was then developed. Through modeling the relation between system control variable state and energy consumption, the optimization problem is solved by a grid search algorithm. With the models introduced in Chapter 3, the centralized optimization problem was formulated and solved by a modified genetic algorithm combined with equation solving procedure for varying cooling load demands and changing ambient environments in Chapter 6. The suboptimal set points of system under different cooling loads and varied ambient environment were computed by the decentralized optimization algorithm in Chapter 7.

8.2 Future work

The intention of this research work is to establish several systematic methodologies to control the operation of VCC with minimal energy consumption under acceptable the indoor air quality requirement. However, more efforts are needed to realize the VCC online optimization in practice, including:

1. The analysis of robustness of centralized and decentralized algorithms suggests various areas to be explored in development of VCC optimization. It would be interesting how much sensitive the coefficients of components should be, for the optimization to be robust, i.e. what are the allowable bounds for the variation in the parameter adaptation of components' hybrid model?

2. An integrated framework that can jointly perform decentralized with centralized optimization for VCC would be very useful tool. The centralized optimization based on the searching results from decentralized optimization can significantly reduce the search space, therefore, the speed of convergence. Consequently, the approach can achieve global optimization with fast convergence.
3. Since ELM has shown good performance in VCC modeling, introducing ELM and self-optimizing control scheme into vapor compression refrigeration cycle control has good prospect. The traditional self-optimizing method focus on few states and highly relies on experience, the combination of ELM and self-optimizing control can reduce the limitation on variable choice and give better online performance since ELM can be updated easily and quickly. It is worthwhile to develop more reliable self-optimizing control scheme based on theoretical model to improve universality.
4. So far, all the proposed method is for vapor compression cycle systems without considering the energy storage effect of building or house. If the systems energy storage effect is evaluated and considered, the formulation of the optimization problem should be re-considered and the optimization procedure may become more complicated since it may include prediction of future load. How to determine the optimal set points for the VCC systems with energy storage needs to be further studied in the future.

Appendix A Calculation of State Penalty Functions

Following procedures are used to calculate penalty for individual system state variable (dependent variable):

Step 1: for the assigned independent variables P_c, P_e and ω, $\dot{m}_r$ and A_v are determined by Eqs. (5) and (8), respectively, where ρ is a linear function of P_c and $T_{c,r,o}$

$$\rho = f_\rho(P_c, T_{c,r,o}) = a_\rho P_c + b_\rho T_{c,r,o} + c_\rho \tag{160}$$

and the coefficients a_ρ, b_ρ, c_ρ can be obtained by curve fitting for give refrigerant.

Step 2: $\dot{Q}_{com}$ and $\dot{Q}_c$ are determined by Eqs. (7) and (9), respectively.

Step 3: for $H_{e,r,o}$ and $H_{c,r,o}$ determined through

$$H_{e,r,o} = f_{He,r,o}(P_e, T_{e,r,o}) = a_{He,r,o} P_e + b_{He,r,o} T_{e,r,o} + c_{He,r,o} \tag{161}$$

and

$$H_{c,r,o} = f_{Hc,r,o}(P_c, T_{c,r,o}) = a_{Hc,r,o} P_c + b_{Hc,r,o} T_{c,r,o} + c_{Hc,r,o} \tag{162}$$

respectively, where the coefficients $a_{He,r,o}$, $b_{He,r,o}$, $c_{He,r,o}$, $a_{Hc,r,o}$, $b_{Hc,r,o}$ and $c_{Hc,r,o}$ can be obtained by curve fitting for the given refrigerant. $T_{e,r,o}$ can then be solved by

$$T_{e,r,o} = \left(H_{e,r,o} - c_{He,r,o} - a_{He,r,o} P_e\right) / b_{He,r,o} \tag{163}$$

where $H_{e,r,o} = \dot{Q}_e / \dot{m}_r + H_{e,r,i}$ and $H_{e,r,i} = H_{c,r,o}$

Step 4: for the $H_{c,r,i}$ determined through

$$H_{c,r,i} = f_{Hc,r,i}(P_c, T_{c,r,i}) = a_{Hc,r,i} P_c + b_{Hc,r,i} T_{c,r,i} + c_{Hc,r,i} \tag{164}$$

where the coefficients $a_{Hc,r,i}$, $b_{Hc,r,i}$ and $c_{Hc,r,i}$ can be obtained by curve fitting for the given refrigerant. $T_{c,r,i}$ can then be determined by

$$T_{c,r,i} = (H_{c,r,i} - a_{Hc,r,i} H_{c,r,i} - c_{Hc,r,i}) / b_{Hc,r,i} \tag{165}$$

where $H_{c,r,i} = \dot{Q}_c / \dot{m}_r + H_{c,r,o}$

Step 5: for $H_{e,fg}$, $T_{e,r,sat}$, $H_{c,fg}$ and $T_{c,r,sat}$ expressed by

$$H_{e,fg} = f_{He,fg}\left(P_e\right) = a_{He,fg} P_e^2 + b_{He,fg} P_e + c_{He,fg} \tag{166}$$

$$T_{e,r,sat} = f_{Te,r,sat}\left(P_e\right) = a_{Te,r,sat}P_e^2 + b_{Te,r,sat}P_e + c_{Te,r,sat} \tag{167}$$

$$H_{c,fg} = f_{Hc,fg}\left(P_c\right) = a_{Hc,fg}P_c^2 + b_{Hc,fg}P_c + c_{Hc,fg} \tag{168}$$

and

$$T_{c,r,sat} = f_{Tc,r,sat}\left(P_c\right) = a_{Tc,r,sat}P_c^2 + b_{Tc,r,sat}P_c + c_{Tc,r,sat} \tag{169}$$

respectively, the coefficients $a_{He,fg}$, $b_{He,fg}$, $c_{He,fg}$, $a_{Te,r,sat}$, $b_{Te,r,sat}$, $c_{Te,r,sat}$, $a_{Hc,fg}$, $b_{Hc,fg}$, $c_{Hc,fg}$, $a_{Tc,r,sat}$, $b_{Tc,r,sat}$, $c_{Tc,r,sat}$ can be obtained by curve fitting for the given refrigerant and operating conditions. Then $\dot{m}_{e,air}$ and $\dot{m}_{c,air}$ are determined through Eq. (1) and Eq. (3), respectively.

Appendix B Levenberg-Marquart method

In Levenberg-Marquart method, the downhill iteration direction can be obtained by solving:

$$(J^{(k)^T}(c)J^{(k)}(c)+\lambda^{(k)}I)P^{(k)}(c)=-J^{(k)^T}(c)r^{(k)}(c) \tag{170}$$

$$r(c)=\begin{bmatrix} r_1(c) & r_2(c) & \cdots & r_N(c) \end{bmatrix}^T$$

The addition of $\lambda^{(k)}I$ is to ensure the left matrix is positive definite and reduce singularity effect. $J^{(k)T}$ represents Jacobian matrix which can be calculated as

$$J=\begin{bmatrix} \frac{\partial r_1}{\partial c_1} & \frac{\partial r_1}{\partial c_2}\cdots\frac{\partial r_1}{\partial c_n} \\ \frac{\partial r_2}{\partial c_1} & \frac{\partial r_2}{\partial c_2}\cdots\frac{\partial r_2}{\partial c_n} \\ \vdots & \vdots \quad \vdots \\ \frac{\partial r_N}{\partial c_1} & \frac{\partial r_N}{\partial c_2}\cdots\frac{\partial r_N}{\partial c_n} \end{bmatrix}$$

After obtaining the downhill iteration direction, coefficients are updated by

$$c^{(k+1)}=c^{(k)}+P^{(k)} \tag{171}$$

The iteration continues until $|c^{(k+1)}-c^{(k)}|<\mu$, where μ is a predefined positive number(1×10^{-7})

Appendix C Moore Penrose Generalized Inverse

The resolution of a general linear system $Ax = y$, where A may be singular and may even not be square, can be made very simple by the use of the Moore–Penrose generalized inverse.

Definition B.1 [15]. A matrix G of order $n \times m$ is the Moore–Penrose generalized inverse of matrix A of order $m \times n$, if

$$AGA = A \quad GAG = G \quad \left(AG\right)^T = AG \quad \left(GA\right)^T = GA \tag{172}$$

For the sake of convenience, the Moore–Penrose generalized inverse of matrix ***A*** will be denoted by A^+.

Theorem B.1[15]: Let there exist a matrix **G** such that **G**y is a minimum norm least-squares solution of a linear system $Ax = y$. Then it is necessary and sufficient that $G = A^+$, the Moore–Penrose generalized inverse of matrix A.

Appendix D Definition of State Penalty Functions

Condenser Air Mass Flow Rate Penalty:

$$K_1 = \begin{cases} 0 & if\ \dot{m}_{c,air,min} \le \dot{m}_{c,air} \le \dot{m}_{c,air,max} \\ \left|(\dot{m}_{c,air,min} - \dot{m}_{c,air}) / \dot{m}_{c,air}\right| & if\ \dot{m}_{c,air,min} > \dot{m}_{c,air} \\ \left|(\dot{m}_{c,air,max} - \dot{m}_{c,air}) / \dot{m}_{c,air}\right| & if\ \dot{m}_{c,air} > \dot{m}_{c,air,max} \end{cases} \quad (173)$$

Evaporator Air Mass Flow Rate Penalty:

$$K_2 = \begin{cases} 0 & if\ \dot{m}_{e,air,min} \le \dot{m}_{e,air} \le \dot{m}_{e,air,max} \\ \left|(\dot{m}_{e,air,min} - \dot{m}_{e,air}) / \dot{m}_{e,air}\right| & if\ \dot{m}_{e,air,min} > \dot{m}_{e,air} \\ \left|(\dot{m}_{e,air,max} - \dot{m}_{e,air}) / \dot{m}_{e,air}\right| & if\ \dot{m}_{e,air} > \dot{m}_{e,air,max} \end{cases} \quad (174)$$

Condensing Saturated Temperature Penalty:

$$K_3 = \begin{cases} 0 & if\ T_{c,r,o} \le T_{c,r,sat} \le T_{c,r,i} \\ \left|(T_{c,r,i} - T_{c,r,sat}) / T_{c,r,sat}\right| & if\ T_{c,r,i} < T_{c,r,sat} \end{cases} \quad (175)$$

Evaporating Saturated Temperature Penalty:

$$K_4 = \begin{cases} 0 & if\ T_{e,r,sat} \le T_{e,air,i} \\ \left|(T_{e,r,sat} - T_{e,air,i}) / T_{e,r,sat}\right| & if\ T_{e,r,sat} > T_{e,air,i} \end{cases} \quad (176)$$

Superheat Penalty:

$$K_5 = \begin{cases} 0 & if\ T_{e,r,sat} + 7 \le T_{e,r,o} \le T_{e,r,sat} + 25 \\ \left|(T_{e,r,o} - T_{e,r,sat}) / T_{e,r,o}\right| & if\ T_{e,r,o} < T_{e,r,sat} + 7 \\ \left|\left(T_{e,r,o} - T_{e,r,sat}\right) / T_{e,r,sat}\right| & if\ T_{e,r,o} > T_{e,r,sat} + 25 \end{cases} \quad (177)$$

Subcool Penalty:

$$K_6 = \begin{cases} 0 & if\ T_{c,r,o} \le T_{c,r,sat} \\ \left|(T_{c,r,o} - T_{c,r,sat}) / T_{c,r,sat}\right| & if\ T_{c,r,o} > T_{c,r,sat} \end{cases} \quad (178)$$

Refrigerant Mass flow Rate Penalty:

$$K_7 = \begin{cases} 0 & if\ \dot{m}_{r,min} \le \dot{m}_r \le \dot{m}_{r,max} \\ \left|(\dot{m}_{r,min} - \dot{m}_r)/\dot{m}_r\right| & if\ \dot{m}_{r,min} > \dot{m}_r \\ \left|(\dot{m}_{r,max} - \dot{m}_r)/\dot{m}_r\right| & if\ \dot{m}_r > \dot{m}_{r,max} \end{cases} \quad (179)$$

EEV Opening Percentage Penalty:

$$K_8 \begin{cases} 0 & 0 \le A_v \le 1 \\ 1 & A_v < 0 \\ \left|(A_v - 1)/A_v\right| & A_v > 1 \end{cases} \quad (180)$$

Appendix E Wolfe Condition:

The step length of optimization must follow Wolfe condition to tradeoff substantial reduction of objective function and time expenditure. The specific form of Wolfe condition applied to the experiment system is

$$\begin{aligned} f(x_k + \alpha_k p_k) &\le f(x_k) + 10^{-3}\alpha_k \nabla f_k^T p_k \\ \nabla f(x_k + \alpha_k p_k)^T p_k &\ge 0.8 \nabla f_k^T p_k \end{aligned} \tag{181}$$

where $p_k = -M_k^{-1}\nabla f_k$.

Appendix F Modified Cholesky Factorization

The pseudo-code of modified Cholesky factorization is given as following:

$g = \max_{1 \le i \le n} |a_{ii}|$

$l = \max_{i \ne k} |a_{ik}|$

$M = 10^{-6} * \max(g + l, 1)$

$N = \max(g, \frac{l}{\sqrt{n^2 - 1}}, 10^{-6})^{0.5}$

for $i = 1$ to n

$c_{ii} = a_{ii}$

end for

for $j = 1$ to n

for $v = 1$ to $j - 1$

$l_{jv} = c_{jv} / d_v$

end for

for k = $j + 1, \ldots, n$

$c_{kj} = a_{kj} - \sum_{v=1}^{j-1} l_{jv} c_{kv};$

end for

$\theta_j = 0$

if $j \le n$

then $\theta_j = \max_{j < s \le n} |c_{sj}|$

end if

$d_j = \max\left\{|c_{jj}|, \left(\theta_j / N\right)^2, M\right\};$

if $j < n$

then for $s = j + 1$ to n

$c_{ss} = c_{ss} - c_{sj}^2 / d_j;$

end for

end if

end for

where *c*, *a* and *n* are elements of the modified Cholesky matrix and original matrix, and length of them, respectively.

Author's publication

1. Lei Zhao, Wen-Jian Cai*, Xudong Ding and Weichung Chang, *Model Based Optimization For Vapor Compression Refrigeration Cycle*, *Energy*, Energy, accepted.
2. Lei Zhao, Wen-Jian Cai*, Xudong Ding and Weichung Chang, *Decentralized optimization for vapor compression refrigeration cycle.* Applied Thermal Engineering, 2013. **51**(1–2): p. 753-763.
3. Lei Zhao, Wen-Jian Cai*, Zhihong Man, *Neural Modeling of Vapor Compression Refrigeration Cycle with Extreme Learning Machine*, Neurocomputing: Special Issue on Extreme Learning Machine: Theory and Applications, accepted.
4. Lei Zhao, Wen-Jian Cai*, Zhi-Hong Man, Guang-Bin Huang, Wei-Chung Chang, *Vapor Compression Refrigeration Cycle Optimization Based on Extreme Learning Machine*, Applied Energy, submitted.
5. Lei Zhao, Wenjian Cai, Xudong Ding, *A Modified Hybrid Model of Heat Exchanger Based on Fouling Effect*, in 2009 6th IEEE Conference on Industrial Electronics and Applications, ICIEA 2009.
6. Lei Zhao, Wenjian Cai, Xudong Ding, *Optimization of Vapor Compression Cycle Based on Genetic Algorithm*, in 2012 The 10th International Power and Energy Conference, IPEC 2012
7. Lei Zhao, Wenjian Cai, Zhihong Man, Weichung Chang, *Model of Vapor Compression Refrigeration Cycle Based on Modified Extreme Learning Machine*, in 2012 The International Symposium on Extreme Learning Machines, ISELM 2012

Reference

[1] R. J. Dossat and T. J. Horan, *Principles of refrigeration*, 5th ed. Upper Saddle River, N.J.,U.S.A: Prentice Hall, 2002.

[2] W. B. Gosney, *Principles of refrigeration*. Cambridge [Cambridgeshire] ; New York: Cambridge University Press, 1982.

[3] *Green Building Design Guide*. Singapore: Building & Construction Authority, 2007.

[4] W. F. Stoecker, *Industrial refrigeration handbook*. New York, U.S.A: McGraw-Hill, 1998.

[5] G. Dreyfus and SpringerLink (Online service). (2005). *Neural Networks Methodology and Applications*.

[6] S. S. Haykin, *New directions in statistical signal processing : from systems to brain*. Cambridge, Mass.: MIT Press, 2007.

[7] S. S. Haykin, *Neural networks : a comprehensive foundation*, 2nd ed. Upper Saddle River, NJ: Prentice Hall, 1999.

[8] S. S. Haykin, *Neural networks and learning machines*, 3rd ed. New York: Prentice Hall, 2009.

[9] V. N. Vapnik, *Statistical learning theory*. New York: Wiley, 1998.

[10] V. N. Vapnik, *The nature of statistical learning theory*, 2nd ed. New York: Springer, 2000.

[11] B. H. Boyle, *Support vector machines : data analysis, machine learning, and applications / Brandon H. Boyle, editor*: New York : Nova Science Publishers, c2011., 2011.

[12] F. Fogelman-Souli é and P. Gallinari, *Industrial applications of neural networks*. Singapore ; River Edge, NJ: World Scientific, 1998.

[13] G.-B. Huang, Q.-Y. Zhu, and C.-K. Siew, "Extreme learning machine: a new learning scheme of feedforward neural networks," in *2004 IEEE International Joint Conference on Neural Networks, 25-29 July 2004*, Piscataway, NJ, USA, 2004, pp. 985-90.

[14] G.-B. Huang, Q.-Y. Zhu, and C.-K. Siew, "Extreme learning machine: Theory and applications," *Neurocomputing*, vol. 70, pp. 489-501, 2006.

[15] D. Serre and SpringerLink (Online service). (2010). *Matrices Theory and Applications*.

[16] C. A. Hooker, *Adaptation in Natural and Artificial Systems - Holland,Jh*.

[17] D. E. Goldberg, *Genetic algorithms in search, optimization, and machine learning*. Reading, Mass, U.S.A: Addison-Wesley Pub. Co., 1989.

[18] D. E. Goldberg, *The design of innovation : lessons from and for competent genetic algorithms*. Boston: Kluwer Academic Publishers, 2002.

[19] R. B. Hollstien, "Artificial genetic adaptation in computer control systems," University Microfilms, Ann Arbor, MI, 1971.

[20] J. Schiffmann and D. Favrat, "Design, experimental investigation and multi-objective optimization of a small-scale radial compressor for heat pump applications," *Energy*, vol. 35, pp. 436-450, 2010.

[21] W. Li, "Simplified steady-state modeling for hermetic compressors with focus on extrapolation," *International Journal of Refrigeration,* vol. 35, pp. 1722-1733, 2012.
[22] X. Q. Kong, D. Zhang, Y. Li, and Q. M. Yang, "Thermal performance analysis of a direct-expansion solar-assisted heat pump water heater," *Energy,* vol. 36, pp. 6830-6838, 2011.
[23] H. Wang and S. Touber, "Distributed and non-steady-state modelling of an air cooler," *International Journal of Refrigeration,* vol. 14, pp. 98-111, 1991.
[24] X. Jia, C. P. Tso, P. Jolly, and Y. W. Wong, "Distributed steady and dynamic modelling of dry-expansion evaporators," *International Journal of Refrigeration,* vol. 22, pp. 126-136, 1999.
[25] C. P. Tso, Y. C. Cheng, and A. C. K. Lai, "Dynamic behavior of a direct expansion evaporator under frosting condition. Part I. Distributed model," *International Journal of Refrigeration,* vol. 29, pp. 611-623, 2006.
[26] M. W. Browne and P. K. Bansal, "An elemental NTU- model for vapour-compression liquid chillers," *International Journal of Refrigeration,* vol. 24, pp. 612-627, 2001.
[27] N. H. S. Tay, M. Belusko, and F. Bruno, "An effectiveness-NTU technique for characterising tube-in-tank phase change thermal energy storage systems," *Applied Energy,* vol. 91, pp. 309-319, 2012.
[28] A. Hasan, "Going below the wet-bulb temperature by indirect evaporative cooling: Analysis using a modified ε-NTU method," *Applied Energy,* vol. 89, pp. 237-245, 2012.
[29] C.-Q. Ren, "Corrections to the simple effectiveness-NTU method for counterflow cooling towers and packed bed liquid desiccant–air contact systems," *International Journal of Heat and Mass Transfer,* vol. 51, pp. 237-245, 2008.
[30] L. A. Sphaier and W. M. Worek, "Parametric analysis of heat and mass transfer regenerators using a generalized effectiveness-NTU method," *International Journal of Heat and Mass Transfer,* vol. 52, pp. 2265-2272, 2009.
[31] M. Adamski, "Heat transfer correlations and NTU number for the longitudinal flow spiral recuperators," *Applied Thermal Engineering,* vol. 29, pp. 591-596, 2009.
[32] G. N. Xie, Q. W. Wang, M. Zeng, and L. Q. Luo, "Heat transfer analysis for shell-and-tube heat exchangers with experimental data by artificial neural networks approach," *Applied Thermal Engineering,* vol. 27, pp. 1096-1104, 2007.
[33] H. Peng and X. Ling, "Neural networks analysis of thermal characteristics on plate-fin heat exchangers with limited experimental data," *Applied Thermal Engineering,* vol. 29, pp. 2251-2256, 2009.
[34] C. K. Tan, J. Ward, S. J. Wilcox, and R. Payne, "Artificial neural network modelling of the thermal performance of a compact heat exchanger," *Applied Thermal Engineering,* vol. 29, pp. 3609-3617, 2009.
[35] Y.-W. Wang, W.-J. Cai, and Y.-C. Soh, "A simplified modeling of cooling coils for control and optimization of HVAC systems," *Energy Conversion and Management,* vol. 45, pp. 2915-2930, 2004.

[36] W.-J. Cai, G.-Y. Jin, L. Lu, E. L. Lee, and A. Chiang, "A simplified modeling of mechanical cooling tower for control and optimization of HVAC systems," *Energy Conversion and Management*, vol. 48, pp. 355-65, 2007.
[37] X. Ding, W. Cai, and L. Jia, "Evaporator modeling - A hybrid approach," *Applied Energy*, vol. 86, pp. 81-8, 2009.
[38] X. Ding, W. Cai, and L. Jia, "A hybrid condenser model for real-time applications in performance monitoring, control and optimization," *Energy Conversion and Management*, vol. 50, pp. 1513-21, 2009.
[39] J. Nocedal, S. J. Wright, and SpringerLink (Online service). (2006). *Numerical Optimization (Second Edition. ed.)*.
[40] J. F. Bonnans, *Numerical optimization : theoretical and practical aspects*, 2nd ed. Berlin ; New York: Springer, 2006.
[41] X. Ding, L. Jia, and W. Cai, "A hybrid modeling for the real-time control and optimization of compressors," in *2009 4th IEEE Conference on Industrial Electronics and Applications, ICIEA 2009, May 25, 2009 - May 27, 2009*, Xi'an, China, 2009, pp. 3256-3261.
[42] C. P. Arora, *Refrigeration and air conditioning*, 2nd ed. New Delhi, India: Tata McGraw-Hill, 2000.
[43] P. C. Koelet and T. B. Gray, *Industrial refrigeration : principles, design, and applications*. New York: M. Dekker, 1992.
[44] J. F. Kreider, A. Rabl, and P. Curtiss, *Heating and cooling of buildings : design for efficiency*. New York: McGraw-Hill, 1994.
[45] S. L. Dixon, *Fluid mechanics and thermodynamics of turbomachinery*, 4th ed. Boston, U.S.A: Butterworth-Heinemann, 1998.
[46] S. L. Dixon and C. Hall, *Fluid Mechanics and Thermodynamics of Turbomachinery*, 6th ed. Burlington: Elsevier, 2010.
[47] D. Hasson, M. Avriel, W. Resnick, T. Rozenman, and S. Windreich, "Mechanism of calcium carbonate scale deposition on heat-transfer surfaces," *Industrial and Engineering Chemistry -- Fundamentals*, vol. 7, pp. 59-65, 1968.
[48] N. Andritsos, M. Kontopoulou, A. J. Karabelas, and P. G. Koutsoukos, "Calcium carbonate deposit formation under isothermal conditions," *Canadian Journal of Chemical Engineering*, vol. 74, pp. 911-919, 1996.
[49] S. M. Zubair, A. K. Sheikh, M. O. Budair, M. U. Haq, A. Quddus, and O. A. Ashiru, "Statistical aspects of CaCO3 fouling in AISI 316 stainless-steel tubes," *Transactions of the ASME. Journal of Heat Transfer*, vol. 119, pp. 581-96, 1997.
[50] M. Sultan Khan, S. M. Zubair, M. O. Budair, A. K. Sheikh, and A. Quddus, "Fouling resistance model for prediction of CaCO3 scaling in AISI 316 tubes," *Heat and Mass Transfer*, vol. 32, pp. 73-9, 1996.
[51] E. F. C. Somerscales and M. Kassemi, "Fouling due to corrosion products formed on a heat transfer surface," *Transactions of the ASME. Journal of Heat Transfer*, vol. 109, pp. 267-71, 1987.
[52] H. Muller-Steinhagen, F. Reif, N. Epstein, and A. P. Watkinson, "Influence of operating conditions on particulate fouling," *Canadian Journal of Chemical Engineering*, vol. 66, pp. 42-50, 1988.

[53] B. Bansal and H. Muller-Steinhagen, "Crystallization fouling in plate heat exchangers," *Transactions of the ASME. Journal of Heat Transfer,* vol. 115, pp. 584-91, 1993.
[54] S. M. Zubair, A. K. Sheikh, M. Younas, and M. O. Budair, "A risk based heat exchanger analysis subject to fouling. I. Performance evaluation," *Energy,* vol. 25, pp. 427-43, 2000.
[55] D. P. Bertsekas, *Nonlinear programming*, 2nd ed. Belmont, Mass.: Athena Scientific, 1999.
[56] M. W. Browne and P. K. Bansal, "Challenges in modeling vapor-compression liquid chillers," in *Proceedings of the 1998 ASHRAE Winter Meeting. Part 1 (of 2), January 18, 1998 - January 21, 1998*, San Francisco, CA, USA, 1998, pp. 474-486.
[57] M. Hosoz and H. M. Ertunc, "Artificial neural network analysis of a refrigeration system with an evaporative condenser," *Applied Thermal Engineering,* vol. 26, pp. 627-35, 2006.
[58] S. Yilmaz and K. Atik, "Modeling of a mechanical cooling system with variable cooling capacity by using artificial neural network," *Applied Thermal Engineering*, vol. 27, pp. 2308-2313, 2007.
[59] J. Navarro-Esbrí V. Berbegall, G. Verdu, R. Cabello, and R. Llopis, "A low data requirement model of a variable-speed vapour compression refrigeration system based on neural networks," *International Journal of Refrigeration,* vol. 30, pp. 1452-1459, 2007.
[60] R. Saidur, H. H. Masjuki, and M. Y. Jamaluddin, "A new approach to investigate the energy performance of a household refrigerator-freezer," *International Energy Journal*, vol. 7, pp. 13-23, 2006.
[61] G.-B. Huang, D. H. Wang, and Y. Lan, "Extreme learning machines: a survey," *International Journal of Machine Learning and Cybernetics*, vol. 2, pp. 107-22, 2011.
[62] X. Cai and T. C. Yeh, *Quantitative information fusion for hydrological sciences*. Berlin: Springer, 2008.
[63] G.-B. Huang, L. Chen, and C.-K. Siew, "Universal approximation using incremental constructive feedforward networks with random hidden nodes," *IEEE Transactions on Neural Networks*, vol. 17, pp. 879-92, 2006.
[64] Z. Man, K. Lee, D. Wang, Z. Cao, and C. Miao, "A new robust training algorithm for a class of single-hidden layer feedforward neural networks," *Neurocomputing,* vol. 74, pp. 2491-2501, 2011.
[65] H. Ricardo, *A modern introduction to linear algebra*. Boca Raton: CRC Press, 2010.
[66] G.-B. Huang, H. Zhou, X. Ding, and R. Zhang, "Extreme Learning Machine for Regression and Multiclass Classification," *IEEE Transactions on Systems, Man and Cybernetics, Part B (Cybernetics),* vol. 42, pp. 513-29, 2012.
[67] A. H. Nizar, Z. Y. Dong, and Y. Wang, "Power utility nontechnical loss analysis with extreme learning machine method," *IEEE Transactions on Power Systems,* vol. 23, pp. 946-55, 2008.
[68] Z.-L. Sun, T.-M. Choi, K.-F. Au, and Y. Yu, "Sales forecasting using extreme learning machine with applications in fashion retailing," *Decision Support Systems*, vol. 46, pp. 411-19, 2008.

[69] J. Kim, H. S. Shin, K. Shin, and M. Lee, "Robust algorithm for arrhythmia classification in ECG using extreme learning machine," *Biomedical Engineering OnLine,* vol. 10, p. 31 (12 pp.), 2009.
[70] R. Minhas, A. Baradarani, S. Seifzadeh, and Q. M. J. Wu, "Human Action Recognition Using Non-separable Oriented 3D Dual-Tree Complex Wavelets," in *Computer Vision - ACCV 2009. 9th Asian Conference on Computer Vision, 23-27 Sept. 2009*, Berlin, Germany, 2009, pp. 226-35.
[71] American Society of Heating Refrigerating and Air-Conditioning Engineers. and Knovel (Firm). (2009). *2009 ASHRAE handbook fundamentals (SI ed.)*.
[72] American Society of Heating Refrigerating and Air-Conditioning Engineers. and Knovel (Firm). (2008). *2008 ASHRAE handbook heating, ventilating, and air-conditioning systems and equipment (Inch-Pound ed.)*.
[73] N. Liang, S. Shao, C. Tian, and Y. Y. Yan, "Two-phase flow instabilities in horizontal straight tube evaporator," *Applied Thermal Engineering,* vol. 31, pp. 181-187, 2011.
[74] J. A. Boure, A. E. Bergles, and L. S. Tong, "Review of two-phase flow instability," *Nuclear Engineering and Design,* vol. 25, pp. 165-192, 1973.
[75] G. L. Wedekind, B. L. Bhatt, and B. T. Beck, "A system mean void fraction model for predicting various transient phenomena associated with two-phase evaporating and condensing flows," *International Journal of Multiphase Flow,* vol. 4, pp. 97-114, 1978.
[76] Z. R. Huelle, "How to avoid evaporator system hunting in practice," *Danfoss Journal,* vol. 26, pp. 3-8, 1971.
[77] P. Mithraratne and N. E. Wijeysundera, "An experimental and numerical study of hunting in thermostatic-expansion-valve-controlled evaporators," *International Journal of Refrigeration,* vol. 25, pp. 992-8, 2002.
[78] Y. Chen, S. Deng, X. Xu, and M. Chan, "A study on the operational stability of a refrigeration system having a variable speed compressor," *International Journal of Refrigeration,* vol. 31, pp. 1368-74, 2008.
[79] J. B. Jensen and S. Skogestad, "Optimal operation of simple refrigeration cycles: Part I: Degrees of freedom and optimality of sub-cooling," *Computers & Chemical Engineering,* vol. 31, pp. 712-721, 2007.
[80] R. Selbaş, Ö. Kızılkan, and A. Şencan, "Thermoeconomic optimization of subcooled and superheated vapor compression refrigeration cycle," *Energy,* vol. 31, pp. 2108-2128, 2006.
[81] H. Vidal and S. Colle, "Simulation and economic optimization of a solar assisted combined ejector–vapor compression cycle for cooling applications," *Applied Thermal Engineering,* vol. 30, pp. 478-486, 2010.
[82] R. Zhou, T. Zhang, J. Catano, J. T. Wen, G. J. Michna, Y. Peles, and M. K. Jensen, "The steady-state modeling and optimization of a refrigeration system for high heat flux removal," *Applied Thermal Engineering,* vol. 30, pp. 2347-2356, 2010.
[83] E. B. Ratts and J. S. Brown, "A generalized analysis for cascading single fluid vapor compression refrigeration cycles using an entropy generation minimization method," *International Journal of Refrigeration,* vol. 23, pp. 353-365, 2000.

[84] K. F. Fong, V. I. Hanby, and T. T. Chow, "System optimization for HVAC energy management using the robust evolutionary algorithm," *Applied Thermal Engineering,* vol. 29, pp. 2327-34, 2009.
[85] A. Kusiak, G. Xu, and F. Tang, "Optimization of an HVAC system with a strength multi-objective particle-swarm algorithm," *Energy,* vol. 36, pp. 5935-5943, 2011.
[86] A. Kusiak, F. Tang, and G. Xu, "Multi-objective optimization of HVAC system with an evolutionary computation algorithm," *Energy,* vol. 36, pp. 2440-2449, 2011.
[87] A. Kusiak and G. Xu, "Modeling and optimization of HVAC systems using a dynamic neural network," *Energy,* vol. 42, pp. 241-250, 2012.
[88] T. G. Hovgaard, L. F. S. Larsen, K. Edlund, and J. B. Jørgensen, "Model predictive control technologies for efficient and flexible power consumption in refrigeration systems," *Energy,* vol. 44, pp. 105-116, 2012.
[89] L. Lu and W. Cai, "Global optimization for overall HVAC systems - Part I problem formulation and analysis," *Energy Conversion and Management,* vol. 46, pp. 999-1014, 2005.
[90] L. Lu and W. Cai, "Global optimization for overall HVAC systems - Part II problem solution and simulations," *Energy Conversion and Management,* vol. 46, pp. 1015-1028, 2005.
[91] S. L. Dixon, *Fluid Mechanics and Thermodynamics of Turbomachinery*, 5th ed. Burlington: Elsevier, 2005.
[92] Y. A. Çengel and A. J. Ghajar, *Heat and mass transfer : fundamentals & applications / Yunus A. Çengel, Afshin A. Ghajar*: Boston : McGraw-Hill, 2010. 4th ed., 2010.
[93] C. J. L. Hermes, W. de Lima e Silva Jr, and F. A. G. de Castro, "Thermal-hydraulic design of fan-supplied tube-fin condensers for refrigeration cassettes aimed at minimum entropy generation," *Applied Thermal Engineering,* vol. 36, pp. 307-313, 2012.
[94] C. J. L. Hermes, "Thermodynamic design of condensers and evaporators: Formulation and applications," *International Journal of Refrigeration*.
[95] C. J. L. Hermes, "Conflation of ε-Ntu and EGM design methods for heat exchangers with uniform wall temperature," *International Journal of Heat and Mass Transfer,* vol. 55, pp. 3812-3817, 2012.
[96] E. Granryd, "Analytical expressions for optimum flow rates in evaporators and condensers of heat pumping systems," *International Journal of Refrigeration,* vol. 33, pp. 1211-1220, 2010.
[97] M. D. d'Accadia and L. Vanoli, "Thermoeconomic optimisation of the condenser in a vapour compression heat pump," *International Journal of Refrigeration,* vol. 27, pp. 433-441, 2004.
[98] P. Röytä, T. Turunen-Saaresti, and J. Honkatukia, "Optimising the refrigeration cycle with a two-stage centrifugal compressor and a flash intercooler," *International Journal of Refrigeration,* vol. 32, pp. 1366-1375, 2009.
[99] R. D. Braun, "Collaborative optimization: An architecture for large-scale distributed design," Ph.D. 9630279, Stanford University, United States -- California, 1996.

[100] R. D. Braun, R. W. Powell, R. A. Lepsch, D. O. Stanley, and I. M. Kroo, "Comparison of two multidisciplinary optimization strategies for launch-vehicle design," *Journal of Spacecraft and Rockets*, vol. 32, pp. 404-410, 1995.
[101] A. V. Miguel, "Two Decomposition Algorithms for Nonconvex Optimization Problems With Global Variables," *PhD thesis,Stanford University*, 2001.
[102] G. Inalhan, D. M. Stipanovic, and C. J. Tomlin, "Decentralized optimization, with application to multiple aircraft coordination," in *Proceedings of IEEE Conference on Decision and Control, 10-13 Dec. 2002*, Piscataway, NJ, USA, 2002, pp. 1147-55.
[103] G. Inalhan, *Decentralized Optimization with Independent Decision Makers* 2008.
[104] G. Inalhan, "Decentralized optimization across independent decision makers with incomplete models," Ph.D. 3145523, Stanford University, United States -- California, 2004.
[105] L. Zhao, W.-J. Cai, X.-d. Ding, and W.-c. Chang, "Decentralized optimization for vapor compression refrigeration cycle," *Applied Thermal Engineering*, vol. 51, pp. 753-763, 2013.
[106] A. M. Geoffrion, "Generalized Benders decomposition," *Journal of Optimization Theory and Applications*, vol. 10, pp. 237-260, 1972.
[107] K. Tammer, "The application of parametric optimization and embedding to the foundation and realization of a generalized primal decomposition approach," *Mathematical Research*, vol. 35, 1987.
[108] A. Moore, R. Braun, and P. R, "optimal technology investment strategies for a reusable launch vehicle," *Sixth AIAA/USAF/NASA/OAI Symposium on Multidisciplinary Analysis and Optimization*, pp. 96-4091, 1996.
[109] R. Braun, R. Powell, and R. Lepsch, "Multi-disciplinary Optimization Strategies for Launch Vehicle Design," *Fifth AIAA/USAF/NASA/OAI Symposium on Multidisciplinary Analysis*, pp. 94-4341, 1994.
[110] S. L. Dixon and C. A. Hall, *Fluid mechanics and thermodynamics of turbomachinery*, 6th ed. Burlington, MA: Butterworth-Heinemann/Elsevier, 2010.
[111] B. P. Rasmussen, "Dynamic modeling and advanced control of air conditioning and refrigeration systems," Ph.D. 3202157, University of Illinois at Urbana-Champaign, United States -- Illinois, 2005.
[112] J. Nocedal and S. J. Wright, *Numerical optimization*, 2nd ed. New York: Springer, 2006.
[113] D. P. Bertsekas, *Convex optimization theory*. Belmont, Mass.: Athena Scientific, 2009.
[114] T. J. Webster, *Introduction to game theory in business and economics*. Armonk, N.Y.: M.E. Sharpe, 2009.
[115] S. W. Data, "http://freemeteo.com/default.asp?pid=20&gid=1880252&la=1&sid=486980&md=0&ndate=16/06/2011&lc=5."